

Can Optical Denoising Clean Sonar Images? A Benchmark and Fusion Approach

Ziyu Wang^a, Tao Xue^a, Jingyuan Li^a, Haibin Zhang^a, Zhiqiang Xu^c, Gaofei Xu^d, Zhen Wang^e, Yanbin Wang^b, Zhiqian Liu^f

^a*Hangzhou Institute of Technology, Xidian University, Hangzhou, 311231, China*

^b*Department of Engineering, Shenzhen MSU-BIT University, Shenzhen, 518172, China*

^c*School of Information Engineering, Jiangxi University of Science and Technology, Ganzhou, 341000, China*

^d*Institute of Deep-sea Science and Engineering, Sanya, 572019, China*

^e*School of Computer Science, Northwestern Polytechnical University, Xi'an, 710072, China*

^f*College of Cyber Security, Jinan University, Guangzhou, 510632, China*

Abstract

Object detection in sonar images is crucial for underwater robotics applications including autonomous navigation and resource exploration. However, complex noise patterns inherent in sonar imagery, particularly speckle, reverberation, and non-Gaussian noise, significantly degrade detection accuracy. While denoising techniques have achieved remarkable success in optical imaging, their applicability to sonar data remains underexplored. This study presents the first systematic evaluation of nine state-of-the-art deep denoising models with distinct architectures, including Neighbor2Neighbor with varying noise parameters, Blind2Unblind with different noise configurations, and DSPNet, for sonar image preprocessing. We establish a rigorous benchmark using five publicly available sonar datasets and assess their impact on four representative detection algorithms: YOLOX, Faster R-CNN, SSD300, and SSDMobileNetV2. Our evaluation addresses three unresolved questions: first, how effectively optical denoising architectures transfer to sonar data; second, which model families perform best against sonar noise; and third, whether denoising truly improves detection accuracy in practical pipelines. Extensive experiments demonstrate that while denoising gener-

*Corresponding author: Tao Xue, Yanbin Wang, Zhiqian Liu. Email: xue-tao01@xidian.edu.cn, wangyanbin15@mails.ucas.ac.cn, zqliu@vip.qq.com.

ally improves detection performance, effectiveness varies across methods due to their inherent biases toward specific noise types. To leverage complementary denoising effects, we propose a mutually-supervised multi-source denoising fusion framework where outputs from different denoisers mutually supervise each other at the pixel level, creating a synergistic framework that produces cleaner images. Experimental results show our proposed denoising approach boosts YOLOX’s detection performance by absolute margins of 22.8% (mAP@0.75) and 9.3% (mAP) when processing raw sonar images. The source code in this work is available at <https://github.com/wzyii/M2SDF>.

Keywords: Image Denoising, Underwater Sonar Images, Object Detection, Multi-frame Denoising

1. Introduction

Underwater sonar imaging has become an indispensable tool for marine exploration and industrial applications, providing critical insights into sub-aquatic environments where optical systems face severe limitations [1, 2]. Unlike light waves that attenuate rapidly in water, acoustic signals propagate over significantly longer distances, enabling sonar systems to cover expansive underwater areas with practical resolution [3–6]. This unique capability makes sonar imaging the preferred choice for seabed mapping, underwater infrastructure inspection, and autonomous underwater vehicle (AUV) navigation [7].

Despite these advantages, sonar image quality is frequently compromised by complex noise patterns that stem from three primary sources: 1) environmental interference (e.g., biological echoes and water column reflections), 2) sensor-related artifacts (e.g., transducer imperfections and electronic noise), and 3) inherent wave propagation characteristics (e.g., multipath reverberation and absorption loss) [8]. These manifest as distinct noise types including Gaussian noise from random sensor fluctuations, speckle noise caused by coherent wave interference, and Poisson noise due to signal quantum variability. Such degradations can reduce the signal-to-noise ratio (SNR) by over 15 dB in practical scenarios [9], severely impacting downstream tasks like mine detection or pipeline inspection where pixel-level accuracy is crucial.

Denoising presents a promising solution to enhance sonar image usability, but faces unique challenges compared to optical imaging: First, the physical mechanisms of acoustic wave scattering differ fundamentally from light scat-

tering, requiring specialized treatment of multiplicative noise models. Second, the scarcity of annotated sonar datasets—typically orders of magnitude smaller than optical counterparts—constrains data-hungry deep learning approaches [10] [11] [12]. Third, the spatially varying nature of underwater noise distributions demands adaptive processing rather than uniform filtering [13].

Interestingly, modern deep learning-based denoisers developed for optical images demonstrate remarkable capability in handling similar challenges, particularly in preserving edges while suppressing noise [14]. The computational similarities between optical and sonar imaging (e.g., shared texture patterns and structural features) suggest potential for cross-domain adaptation. However, no systematic study has yet evaluated: 1) how effectively optical denoising architectures transfer to sonar data, 2) which model families perform best against sonar noise, or 3) whether denoising truly improves detection accuracy in practical pipelines.

To address these gaps, we conduct the first comprehensive evaluation of nine state-of-the-art denoising models across five public sonar datasets (FDD [15], UATD [16], SCTD [17], MarineDebris [18], and USD [19]). Our study reveals two key findings: 1) While denoising preprocessing improves detection mAP on average, performance gains vary substantially across methods; 2) No single denoiser achieves consistent superiority across all noise conditions, suggesting the need for adaptive solutions.

Building on these insights, we propose a mutually-supervised multi-source denoising fusion (M2SDF) framework that iteratively combines outputs from heterogeneous denoisers through pairwise pixel-level supervision. This learning mechanism identifies and preserves clean pixels while rectifying noise-contaminated regions, achieving sonar image enhancement.

The contributions of our work are as follows:

- We conduct the first large-scale evaluation of optical-based denoising methods for sonar imagery. Our benchmark validates the feasibility of transferring optical denoising techniques to sonar data and reveals fundamental limitations of single-model approaches, and provides practical guidelines for model selection based on noise characteristics.
- We present M2SDF, a novel multi-source denoising fusion framework that overcomes single-model limitations by combining pixel-wise mutual supervision with heterogeneous denoising strategies, improving sonar image denoising quality.

- The proposed M2SDF achieves significant performance gains in sonar image object detection using YOLOX, demonstrating absolute improvements of 22.8% in mAP@0.75 and 9.3% in mAP compared to noisy inputs.

2. Background

2.1. Sonar Images

In seawater, the propagation of light waves and radio waves is severely limited due to significant attenuation caused by medium variations. In contrast, sound waves exhibit superior propagation characteristics in aquatic environments, enabling broader coverage and making sonar imaging the preferred modality for ocean exploration and industrial applications. Sonar images can be categorized into two primary types: side-scan and forward-looking sonar images. Side-scan sonar images are primarily employed for seabed exploration, generating lateral cross-sectional representations of underwater terrain, which are instrumental in target identification and object detection. Forward-looking sonar images, on the other hand, are designed to scan the area ahead of underwater vehicles such as submarines or autonomous robots, providing an intuitive three-dimensional perspective to facilitate obstacle avoidance and target recognition. As shown in Fig.1, the top image depicts a side-scan sonar scene, and the bottom image shows a forward-looking sonar scene. In the side-scan image, a central black region indicates sonar shadows due to absent echoes beneath the detector, while high-intensity lateral regions reveal seabed topography, including geological structures like sand dunes.

A typical sonar image consists of seven key components: the sonar pulse source, surface reflections, water column clutter, seabed reflections, the water column itself, target objects, and associated shadows. The image formation process begins with the transducer array emitting a sonar pulse and subsequently capturing the returning echoes. These acoustic signals are converted into electrical energy and transmitted via a towed cable to the surface vessel's recording and display unit, where they are processed into interpretable formats and rendered on monitors or stored for further analysis.

Sonar images exhibit several distinctive characteristics. First, their resolution is inherently limited due to the long wavelengths of sound waves, resulting in comparatively blurred details. Second, they are prone to noise

interference, including speckle noise and multipath effects, which can introduce artifacts into the imagery. Third, the complex underwater environment often leads to a low signal-to-noise ratio (SNR), further obscuring object contours and complicating identification. Despite these challenges, sonar images provide invaluable depth information, enabling effective target localization and navigation in three-dimensional underwater spaces.

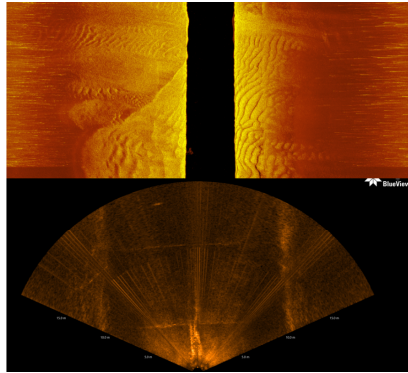


Figure 1: Sonar images.

2.2. Noise in Sonar Images

The interpretation of sonar images is fundamentally constrained by various noise sources that degrade image quality and complicate object detection. These noise artifacts originate from different physical mechanisms in the underwater environment and sensor systems. The primary noise types affecting sonar images include:

- **Gaussian Noise:** This additive noise follows a normal distribution and primarily stems from electronic sensor noise and environmental interference. It manifests as random intensity fluctuations uniformly distributed across the image, particularly problematic in low-signal conditions where it obscures fine details and reduces contrast.
- **Poisson Noise:** Also known as shot noise, this signal-dependent noise arises from the discrete nature of acoustic wave detection. Its variance scales with signal intensity, making it particularly noticeable in low-intensity regions of the image where it introduces grainy artifacts and distorts weak signals.

- **Speckle Noise:** As a multiplicative noise inherent to coherent imaging systems, speckle noise results from interference patterns created by sound wave scattering. It appears as granular texture throughout the image, significantly blurring object boundaries and reducing effective resolution.
- **Multipath Interference:** Caused by sound waves reflecting off multiple surfaces before detection, this noise creates ghost images and false targets. The complex underwater topography and variable acoustic impedance contribute to this challenging interference pattern.
- **Environmental Noise:** This category encompasses various ambient disturbances including biological activity, water turbulence, and man-made sources like vessel operations. These noises are typically non-stationary and spatially varying, requiring adaptive processing techniques.

The combined effect of these noise sources presents significant challenges for automated object detection and classification in sonar imagery. Effective noise suppression and image enhancement algorithms must account for these diverse noise characteristics to improve the reliability of underwater imaging systems.

3. Related Work

3.1. Underwater Sonar Image Object Detection

Object detection in underwater sonar imagery encompasses traditional methods, convolutional neural network (CNN)-based approaches, and other machine learning techniques.

Traditional sonar detection relies on pixel intensities, grayscale thresholds, and target priors. For example, [20] employs spatial frequency domain analysis and frame differencing for robust detection in underwater videos. Similarly, [21] uses OS-CFAR for noise-resilient target segmentation in side-scan sonar, validated on real data. Additionally, [22] applies symbolic pattern analysis for real-time mine detection in sidescan sonar, while [23] explores change detection to identify new seabed objects.

CNN-based methods excel in sonar imagery due to robust feature extraction[24–27]. YOLO-based models include YOLOv3-DPFIN [28], which enhances real-time detection with dual-path feature fusion, and an optimized YOLOv5

[29] using transfer learning and CoordConv for improved accuracy. YOLOv7 variants, YOLOv7C [30] with attention mechanisms and Multi-GnBlock, and a Swin-Transformer-enhanced model [31] with a feature scale factor, boost performance in complex sonar backgrounds. Other CNN approaches include a lightweight FLSD-Net [32] for small object detection, UFIDNet [33] with speckle noise reduction, EPL-UFLSID [34] using pseudo labels, and MB-CEDN [35] for multi-target detection in circular-scan sonar, all improving accuracy and efficiency. Additionally, [36] outperforms template matching in forward-looking sonar with fewer parameters.

Non-CNN methods include a Viola-Jones-based cascade classifier [37] for in-situ learning and low false alarms in complex terrains, and a clustering-segmentation approach [38] for efficient, low-error detection without extensive training.

Traditional methods utilize image processing and handcrafted features for rule-based detection, while CNN-based methods leverage end-to-end feature learning for enhanced robustness. Other machine learning approaches combine manual features with classifiers, offering flexibility but limited by feature quality.

3.2. Denoising

Image denoising is critical in image processing, particularly for noisy underwater sonar imagery. Deep learning, especially convolutional neural network (CNN)-based methods, dominates denoising due to robust performance. RED-Net [39] uses skip-layer connections for enhanced denoising, while DnCNN [40] handles varying noise intensities for blind denoising. FFD-Net [41] incorporates a noise level map to improve inference speed, and CBD-Net [42] employs realistic noise models for real-world applications. MWD-CNN [43] integrates wavelet transforms and dynamic convolution for balanced performance, whereas CTNet [44] combines serial, parallel, and residual blocks with Transformer mechanisms to address complex noise in large datasets.

Unsupervised and self-supervised methods enable denoising without clean images. Noise2Noise [45] trains on noisy image pairs, recovering clean images effectively. Noise2Self [46] and Noise2Void [47] exploit noise statistics for self-supervised denoising, while Noisy-As-Clean [48] treats noisy images as clean to reduce prior discrepancies. Neighbor2Neighbor [49] and Blind2Unblind [50] further advance self-supervised denoising with efficient training.

For domain-specific tasks, LIDnet [51] integrates denoising with lesion detection in medical imaging, using region-specific loss and collaborative training. DN-DETR [52] enhances DETR’s convergence via denoising strategies. In sonar imagery, UFIDNet [33] combines speckle noise reduction with feature selection for accurate forward-looking sonar detection, while NACA [53] leverages non-local spatial information and adaptive algorithms for robust denoising and detection. EPL-UFLSID[34] method proposes a Gaussian Mixture Model-based Deep Image Prior network for generating denoised sonar images, utilizing the GMM distribution as its input. UGIF-Net[54] enhances underwater images using a multicolor space-guided module and dense attention block. HCLR-Net[55] enhances underwater images using a hybrid contrastive learning regularization strategy with non-paired data and local patch perturbations,

Underwater sonar denoising remains nascent, with future work needed to address complex noise types and adapt optical image denoising techniques for sonar applications.

4. Methodology

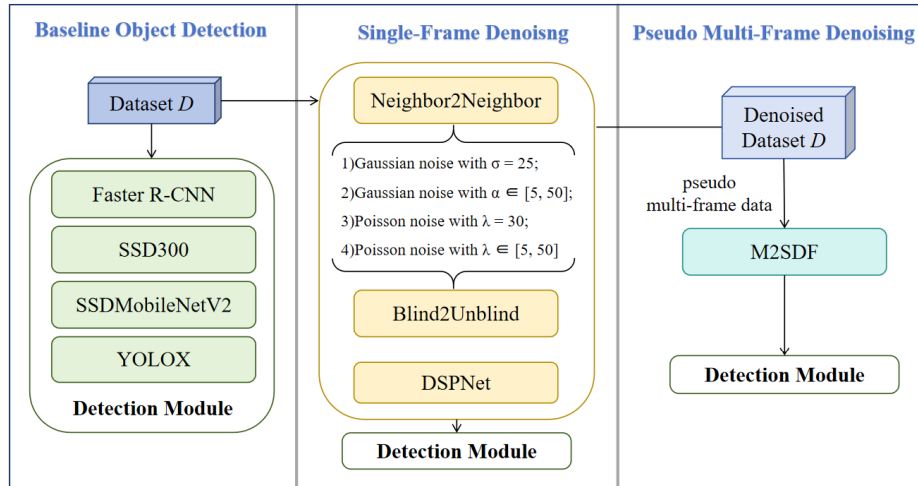


Figure 2: Overview of the three-stage framework, including baseline object detection, single-frame denoising with three methods, and pseudo multi-frame denoising. Among them, Blind2Unblind and Neighbor2Neighbor algorithms both contain four settings: (1)Fixed-intensity Gaussian noise $\sigma = 25$, (2)Variable Gaussian noise ($\sigma \in [5, 50]$), (3)Fixed-parameter Poisson noise $\lambda = 30$, (4)Variable Poisson noise $\lambda \in [5, 50]$.

Our methodology is structured in three parts: (1) presentation of used four representative object detection algorithms, (2) description of used nine denoising models, and (3) comprehensive explanation of our proposed M2SDF framework method. The overall methodology workflow is illustrated in Fig. 2.

4.1. Baseline Object Detection Architecture Selection

To establish a comprehensive evaluation framework for denoising-enhanced sonar object detection, we selected four representative detection algorithms spanning distinct architectural paradigms: the lightweight SSDMobileNetV2 [56], the two-stage Faster R-CNN [57], the single-stage SSD300 [58], and the anchor-free YOLOX [59]. This curated selection enables systematic analysis of denoising effects across efficiency-accuracy tradeoffs.

SSDMobileNetV2: We include SSDMobileNetV2 due to its lightweight architecture and computational efficiency, making it well-suited for real-time applications on resource-constrained devices. Its backbone, MobileNetV2 [60], employs two key innovations: (1) inverted residual blocks with linear bottlenecks and (2) depthwise separable convolutions. The inverted residual structure facilitates gradient propagation via shortcut connections while maintaining low computational overhead, whereas linear bottlenecks preserve information by avoiding nonlinearities in narrow layers. These design choices enable SSDMobileNetV2 to balance accuracy and efficiency effectively, allowing us to evaluate denoising’s impact on lightweight models optimized for mobile or embedded deployment.

Faster R-CNN: Faster R-CNN is selected for its high localization and classification accuracy, particularly in complex environments. Its architecture consists of a Region Proposal Network (RPN) for generating candidate regions, followed by a second-stage classifier and regressor for refined detection. Typically paired with deep backbones like ResNet, Faster R-CNN excels in scenarios with small, dense, or partially obscured objects—common challenges in sonar imagery. Although computationally intensive, its precision provides a valuable benchmark for assessing denoising’s effect on detection performance in high-complexity scenes where precise object delineation is critical.

SSD300: SSD300 directly predicts object categories and bounding boxes from multi-scale feature maps, eliminating the need for a separate region proposal step. Operating on 300×300 inputs, it leverages multi-scale convolutional layers to handle objects of varying sizes—an advantage for sonar

imagery, where targets exhibit significant scale variations and noise interference. Its real-time performance and multi-scale adaptability make it ideal for studying denoising’s influence on mid-range models that prioritize both efficiency and reasonable accuracy.

YOLOX: YOLOX represents a state-of-the-art advancement in one-stage detection, addressing limitations of earlier YOLO variants. It introduces an anchor-free design, a decoupled head architecture, and SimOTA label assignment to improve accuracy and training stability. By leveraging modern backbones (e.g., CSPDarkNet or EfficientNet [61]) and incorporating speed optimizations, YOLOX achieves robust performance in both real-time and high-precision tasks. Its resilience in complex detection scenarios makes it a strong baseline for evaluating denoising’s impact on high-performance models employing contemporary design principles.

4.2. Single-Frame Denoising Algorithm Analysis

We select three state-of-the-art deep learning-based denoising algorithms, each offering unique advantages and configurable parameters to address diverse noise types. By adjusting their key settings, we derive nine distinct denoising variants. Below, we detail these algorithms and our configuration strategy.

4.2.1. Algorithm 1: Neighbor2Neighbor

Neighbor2Neighbor [49] is a self-supervised image denoising framework that operates exclusively on single noisy images, eliminating the need for clean reference images or multiple observations of the same scene. This characteristic makes it especially applicable to challenging domains like underwater sonar image processing, where obtaining clean ground-truth data is impractical. The method introduces two key innovations:

1. Random Neighbor Sub-sampling: Rather than depending on noisy-clean image pairs, Neighbor2Neighbor generates pseudo training pairs directly from a single noisy input. By randomly extracting two adjacent sub-regions from the image—which exhibit statistical similarity due to spatial redundancy—the method creates input-target pairs for training. This approach capitalizes on the inherent local self-similarity present in natural and sonar imagery.
2. Regularized Objective Function: To address the inherent discrepancy between the sub-sampled patches (since their underlying clean versions

are not identical), the algorithm incorporates a theoretical correction mechanism through a regularization term. This component mitigates the mismatch arising from the pseudo pairs, enhancing denoising accuracy while preventing excessive smoothing.

Furthermore, Neighbor2Neighbor is architecture-agnostic, enabling seamless integration with state-of-the-art supervised denoising networks. Its noise-model-free design enhances robustness for real-world scenarios, such as sonar imaging, where noise patterns are often non-Gaussian and complex.

We adopt Neighbor2Neighbor as a representative self-supervised denoising method to assess the influence of denoising on sonar-based object detection. Its independence from clean images aligns perfectly with sonar datasets, which typically lack noise-free references. Additionally, its ability to deliver high-quality denoised outputs using only noisy inputs ensures our evaluation reflects real-world operational constraints.

4.2.2. Algorithm 2: *Blind2Unblind*

Blind2Unblind [50] addresses the critical shortcomings of blind-spot-based self-supervised approaches, which typically incur substantial information loss from input masking or constrained receptive fields. The method introduces two innovative components to mitigate these issues:

1. Global-Aware Mask Mapper: The algorithm divides the input image into small grid cells (e.g., 2×2 patches) and systematically masks individual pixels to construct a masked volume—a stack of variably masked images. A denoising network processes this volume, and the mapper intelligently aggregates predictions from all masked regions to reconstruct the final output. This mechanism enables holistic image understanding while significantly improving training convergence.
2. Regularized Re-Visible Loss: To bridge the gap between blind-spot training and full-image inference, the method proposes a novel loss function combining a regularization term and a dynamically weighted visible term. This formulation prevents degenerate solutions (e.g., identity mapping) and stabilizes optimization. Notably, the loss is backbone-agnostic, ensuring compatibility with diverse denoising architectures.

Blind2Unblind is suited for sonar data, where noise (e.g., speckle, multi-path interference, and non-Gaussian ambient noise) complicates traditional denoising, and clean reference images are rarely available. By leveraging

global context and operating entirely self-supervised, the method offers a robust solution for real-world sonar applications.

4.2.3. Algorithm 3: DSPNet

Speckle noise presents a fundamental challenge in sonar image processing due to its multiplicative nature. Traditional denoising methods often fail to adequately address this problem as they typically assume additive noise models. The DSPNet framework [62] overcomes this limitation through a novel logarithmic transformation approach that effectively converts multiplicative speckle noise into an additive model.

The architecture employs two specialized subnetworks working in the logarithmic domain. First, the noise estimation network (Log-NENet) utilizes a U-Net structure with attention mechanisms to predict spatially-varying noise levels. Second, the denoising network (Log-DNNNet) incorporates a feature pyramid network with atrous spatial pyramid pooling (ASPP) modules, enabling multi-scale feature extraction while preserving fine image details. This dual-network approach achieves superior performance by explicitly modeling the noise characteristics while maintaining structural integrity.

A key innovation of DSPNet lies in its hybrid loss function, which combines multi-scale structural similarity (MS-SSIM) with traditional L1 loss. This combination ensures both perceptual quality and pixel-level accuracy in the denoised output.

For sonar applications, DSPNet offers particular advantages. Its logarithmic processing naturally aligns with the physics of underwater acoustic imaging, where speckle noise follows multiplicative Rayleigh distributions. Furthermore, the network's ability to operate without clean reference images makes it practical for real-world deployment scenarios where ground truth data is unavailable.

4.2.4. Denoising Model Configuration

To comprehensively evaluate denoising performance under various noise conditions, we established a systematic training protocol encompassing nine specialized models, includes:

We implemented four variants each for both Blind2Unblind and Neighbor2Neighbor by training under distinct noise regimes:

- Fixed-intensity Gaussian noise $\sigma = 25$
- Variable Gaussian noise ($\sigma \in [5, 50]$)

- Fixed-parameter Poisson noise $\lambda = 30$
- Variable Poisson noise $\lambda \in [5, 50]$

This configuration enables comparative analysis of: 1) Model robustness to noise level variations; 2) Algorithmic performance differences between fixed and variable noise conditions; 3) Generalization capability across noise types.

The ninth model employs DSPNet, specifically designed for multiplicative speckle noise reduction through its logarithmic domain processing. This provides critical comparison with the additive noise models, particularly relevant for sonar imaging where speckle noise dominates.

4.3. Mutually-supervised Multi-source Denoising Fusion

To enhance underwater sonar target detection, we propose M2SDF, a novel framework that integrates multi-source heterogeneous denoisers to synergize their complementary strengths. Inspired by multi-frame denoising principles [63], M2SDF employs cross-referenced pixel-wise supervision among denoised outputs from different denoisers. This mutual supervision enables the model to learn more stable and generalizable features by leveraging inter-denoiser consistency, thereby improving robustness in complex noise environments.

We first apply a set of single-frame denoising methods f_j to each noisy image x_i from the original dataset D. Each method generates a denoised variant:

$$\hat{x}_i^{(j)} = f_j(x_i), \quad j = 1, 2, \dots, M \quad (1)$$

These M denoised variants of the same image are grouped to form a multi-source sequence:

$$\hat{X}_i = [\hat{x}_i^{(1)}, \hat{x}_i^{(2)}, \dots, \hat{x}_i^{(M)}] \quad (2)$$

This sequence \hat{X}_i is then used as the input to M2SDF F_θ with parameters θ , producing a final denoised output:

$$\tilde{x}_i = F_\theta(\hat{X}_i) \quad (3)$$

For each image, the corresponding m noisy frames are randomly shuffled before each training iteration to form new supervision pairs. This randomization introduces dynamic supervisory directions, allowing the model to treat

each frame both as input and as a supervisory target in different iterations. At each training step, two disjoint subsets of frames are formed, and the loss is computed between these paired groups. With sufficient training steps, this strategy achieves balanced and diversified mutual supervision (as illustrated in Fig.3). The randomized re-pairing of frames at each iteration effectively enriches the diversity of training signals without increasing computational overhead.

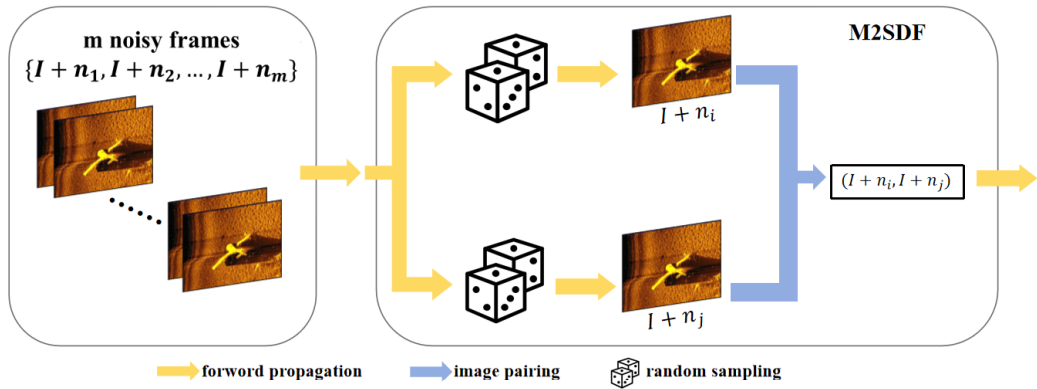


Figure 3: The schematic diagram of proposed M2SDF.

During the model training phase, the model processes noisy inputs in an iterative manner. To enable dynamic and balanced supervision across frames, we introduce a random shuffling strategy at each iteration to construct paired data samples. Let s denote the current iteration step, and define a frame index sequence $I = [1, 2, \dots, m]$. Before the s -th update, this sequence is randomly divided into two disjoint subsets J_i^s , and K_i^s , for each training sample x_i , where $i \in [1, N]$. Based on these subsets, the corresponding noisy frame groups are formed as:

$$\begin{aligned} X_1^s &= \{x_i + n_i^j \mid i \in [1, N], j \in J_i^s, s \in \mathbb{N}^*\}, \\ X_2^s &= \{x_i + n_i^k \mid i \in [1, N], k \in K_i^s, s \in \mathbb{N}^*\}, \end{aligned} \quad (4)$$

Then, the model parameters Θ^s are updated at each iteration using the following rule:

$$\Theta^{s+1} = \Theta^s - \eta \frac{\partial}{\partial \Theta} \left[\sum_{i=1}^{N_B} \sum_{j \in \mathcal{J}_i^s} \sum_{k \in \mathcal{K}_i^s} \left\| \mathbf{y}_i^j - (\mathbf{x}_i + \mathbf{n}_i^k) \right\|_2^2 \right], \quad (5)$$

s.t. $idx(j) = idx(k)$,

Where:

- θ^s is the model parameters at the s -th iteration;
- η is the learning rate;
- The constraint $idx(j) = idx(k)$ ensures that the paired samples originate from the same data instance.

This randomized re-pairing mechanism ensures that every noisy frame in a sequence has an equal opportunity to act as either the supervision target or the denoising input over time. In effect, this method gradually builds implicit multi-directional supervision relationships across all frames without requiring clean labels or reference images. As the number of iterations increases, the statistical uniformity of frame usage improves, fostering a diverse and balanced training process that encourages generalization while maintaining computational efficiency.

Our approach extends self-supervised learning by jointly optimizing outputs of different single-image denoisers (Neighbor2Neighbor, Blind2Unblind, etc.). Unlike traditional methods requiring clean references or true multi-frame captures, our framework capitalizes on intrinsic discrepancies among different denoiser outputs - including noise suppression levels, texture preservation characteristics, and artifact patterns. This enables mutual supervision through consensus learning in stable regions and discrepancy-based correction in noisy areas.

5. Experiments

In this section, we conduct experiments to address the following key research questions:

1. Can traditional optical denoising methods generalize to sonar data without modification?
2. Which denoising model families are most robust to sonar noise patterns?

3. Can the accuracy of target detection be further improved by the proposed multi-source denoising fusion algorithm?

5.1. Datasets

To evaluate our denoising and detection framework, we selected five publicly available sonar datasets covering diverse underwater scenarios, target types, and noise conditions. Below, we outline their key characteristics and relevance to our research objectives.

- SCTD (Sonar Composite Target Dataset) [17]: Contains 596 annotated targets (461 shipwrecks, 90 aircraft, 45 human figures) with high-resolution contours, facilitating quantitative analysis of denoising effects on structured objects. The dataset's fragmented and geometrically distorted images simulate real-world sonar artifacts, testing algorithm robustness.
- UATD (Underwater Acoustic Target Dataset) [16]: Comprises >9,000 multi-beam forward-looking sonar (MFLS) images captured in shallow waters using a Tritech Gemini 1200ik sonar. Its large-scale, real-world data is essential for assessing generalizability across varying water conditions and target occlusions.
- USD (URPC_sonarimage_dataset) [19]: Includes 800 forward-looking and 1,216 side-scan sonar images. We focus on the forward-looking subset due to its real-time directional perspective, which aligns with dynamic obstacle avoidance applications.
- MarineDebris [18]: Collected in a controlled water tank using an ARIS Explorer 3000 sonar (3.0 MHz), this dataset features 10 fine-grained debris categories (e.g., bottles, tires, propellers) with precise bounding-box annotations (JSON format). It enables rigorous evaluation of denoising's impact on small-object detection in cluttered environments.
- FDD (Forward-Looking Sonar Detection Dataset) [15]: Contains 3,752 images of boats, planes, and victims, acquired with an Oculus M1200d sonar. Its balanced class distribution and standardized annotations allow direct comparison of detection accuracy improvements after denoising.

5.2. Infrastructure Configuration

All experiments were implemented using MMDetection (PyTorch-based) and conducted on a workstation with:

- CPU: Intel Core i9-14900K (32 cores)
- GPU: 2× NVIDIA RTX 3090 (24 GB each, CUDA 12.2)
- RAM: 128 GB
- OS: Ubuntu 22.04.5 LTS

5.3. Detection on Raw Sonar Images

We first established detection performance baselines by evaluating four representative architectures (SSDMobileNetV2, Faster R-CNN, SSD300, and YOLOX) on unprocessed sonar images using the MMDetection framework. This controlled experiment serves to quantify the intrinsic detection capability of each model in challenging underwater noise conditions, with all models trained and tested using identical dataset partitions to ensure methodological consistency.

The training procedure followed each detector’s standard recommended configuration, including optimizer selection and epoch count. For comprehensive performance evaluation, we employed multiple established metrics: mAP@[0.5:0.95] as the primary measure of overall detection quality, supplemented by mAP@0.5 and mAP@0.75 for IoU-specific accuracy assessment, along with Average Recall (AR) to evaluate detection robustness. These baseline measurements precisely characterize each detector’s performance limitations when processing noisy sonar imagery directly.

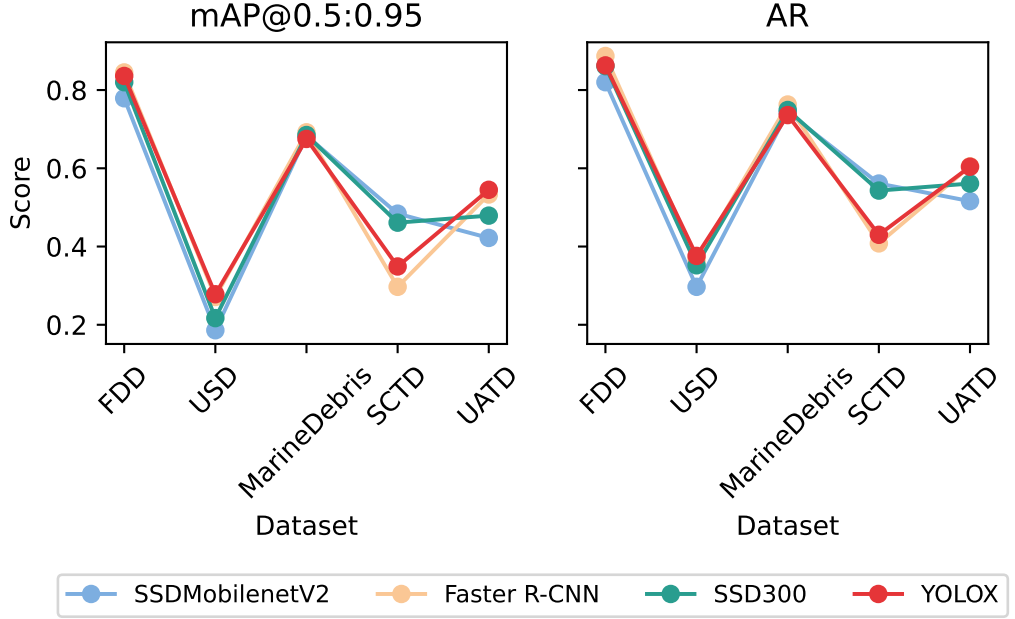


Figure 4: Object detection on the original underwater sonar datasets.

Fig. 4 presents the baseline object detection performance evaluation conducted on raw sonar images across five underwater datasets using four representative detection algorithms. The results reveal significant variations in model performance depending on dataset characteristics. All models achieved their highest mAP@0.5:0.95 scores (ranging 0.6-0.8) on the FDD dataset, which benefits from balanced class distribution and standardized annotations. In contrast, performance degraded substantially on USD and SCTD. The most significant performance variations occurred in the SCTD and UATD datasets, exhibiting the greatest model instability across detection methods.

5.4. Benchmark Evaluation of Object Detection in Sonar Images Using Different Denoisers

This experimental study evaluates object detection performance on sonar images processed through nine denoising variants derived from three fundamental methods. The comprehensive results, presented in Appendix Tables A.3– A.38, systematically compare detection accuracy using four algorithms (*SSDMobileNetV2*, *Faster R-CNN*, *SSD300*, and *YOLOX*) across

five sonar datasets, where the “Noisy” condition represents baseline performance on unprocessed images. The evaluation employs nine rigorous metrics: mean Average Precision (mAP) at different Intersection-over-Union thresholds (mAP@[0.5 : 0.95], mAP@0.5, and mAP@0.75)), along with scale-specific variants (mAP_s, mAP_m, mAP_l, AR, AR_s, and AR_l). Here, the subscripts denote target size categories: small ($area < 32 \times 32$ pixels), medium ($32 \times 32 \leq area \leq 96 \times 96$ pixels), and large ($area > 96 \times 96$ pixels) targets, enabling detailed analysis of detection performance across varying target scales in sonar imagery.

The Appendix Tables A.3–A.6 present the detection results of the SCTD dataset using four object detection algorithms: SSDMobileNetV2, Faster R-CNN, SSD300, and YOLOX. For the SSDMobileNetV2 algorithm, DSPNet achieves the best overall performance in terms of mAP and AR, particularly excelling in medium-sized target detection, which highlights its ability to balance noise suppression and information preservation effectively. However, detection performance for small targets and complex categories (e.g., “human”) is generally lower, likely due to the loss of fine details during the denoising process, which affects the model’s ability to identify small-scale targets. Additionally, some denoising methods result in mAP values of 0 or NaN for specific target categories or sizes, potentially due to the absence of such targets in the dataset or excessive smoothing that removes critical features. Interestingly, the detection of large targets on noisy data without denoising performs relatively well (mAP = 0.582), suggesting that some information embedded in the noise may aid target localization, but such information could be inadvertently removed during denoising. For Faster R-CNN and SSD300, the impact of denoising methods is even more pronounced, particularly in improving mAP@0.5. For example, in Faster R-CNN, the “b2ub-g5-50” method achieves the highest mAP@0.5 (0.783) for the “ship” category, while “b2ub-p30” demonstrates strong performance in high IoU thresholds for the “human” category (mAP@0.75 = 0.424). In SSD300, DSP-Net achieves the highest overall mAP (0.494), while B2UB-P30 stands out under high IoU thresholds (mAP@0.75 = 0.639). Therefore, further research into optimization strategies tailored to different target categories and sizes is warranted to better balance noise reduction and information preservation.

Fig. 5 demonstrates the impact of denoising on object detection performance, showing mAP@0.5 scores for both the original noisy SCTD dataset and its nine denoised variants. The results reveal accuracy improvements across most detectors when processing denoised data compared to the noisy

baseline. Specifically, the *SSDMobileNetV2* detector achieves its highest mAP@0.5 score with the *b2ub-g25* denoising model, while *Faster R-CNN* attains optimal performance (mAP@0.5 = 0.642) using the *nei-p30* processed data. For *SSD300*, notable enhancements emerge from denoising models including *b2ub-g25* and *b2ub-p30*, whereas *YOLOX* demonstrates particularly strong detection capability when paired with the *b2ub-p30* denoising configuration. These findings collectively underscore the significant benefits of appropriate denoising preprocessing for sonar image analysis across diverse detection architectures.

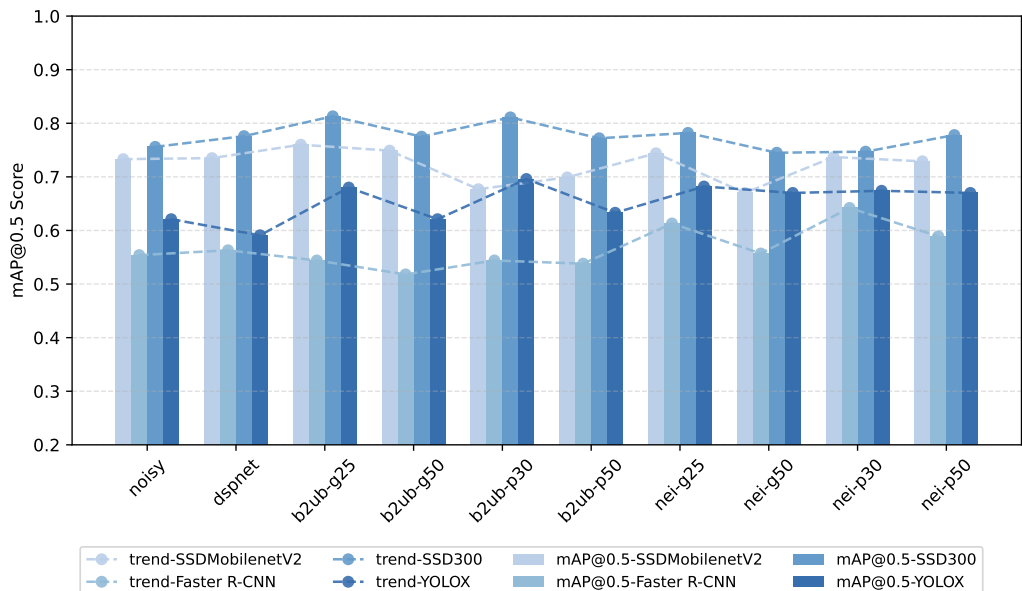


Figure 5: The results (mAP@0.5) of object detection on the original SCTD dataset and the SCTD dataset processed by nine denoising models using four object detection algorithms. Here, “noisy” refers to the original dataset, “b2ub” is the abbreviation for the Blind2Unblind algorithm, and “nei” is the abbreviation for the Neighbor2Neighbor algorithm.

The evaluation results of the USD dataset are presented in Appendix Tables A.7– A.10, demonstrating the impact of various denoising approaches on detection performance. While denoising algorithms generally improve one or more evaluation metrics, the effects vary significantly across different detectors. For *SSDMobileNetV2*, initial performance on small object detection was particularly poor (near-zero mAP_s), but eight of the nine denois-

ing models yielded measurable improvements in this critical metric. *Faster R-CNN* exhibited a different pattern, where certain denoising algorithms maintained comparable mAP values while substantially enhancing large object recall (AR_l). The *SSD300* detector achieved its best performance with the *nei-p30* model (mAP = 0.223, +0.006 improvement over noisy baseline), while *b2ub-g5-50* demonstrated stable performance (mAP = 0.219) with notable gains in large object recall (AR_l = 0.434). However, the *b2ub-p5-50* configuration showed a significant performance degradation (mAP = 0.137), suggesting potential over-denoising effects that may eliminate critical target features. Among all detectors, *YOLOX* delivered superior baseline performance (mAP = 0.278 for noisy images), with the *b2ub-g25* denoising variant achieving the most balanced improvements across metrics, despite a minor decrease in mAP_m .

Fig. 6 provides complementary visualization of mAP@0.5 performance across denoised variants, revealing consistent patterns through bar chart representations. The data indicates that most denoising models produce comparable detection performance gains across different algorithms, with *nei-p30* emerging as the most effective overall (mAP@0.5 range: 0.564–0.589). The *b2ub-p30* model also demonstrates strong and stable performance, particularly when paired with *YOLOX* (mAP@0.5 = 0.585). In contrast, the *dspnet* method yields comparatively lower scores across all detectors, with particularly poor performance on *SSDMobileNetV2* (mAP@0.5 = 0.381). These results collectively establish *nei-p30* and *b2ub-p30* as the most reliable denoising approaches for enhancing object detection accuracy on the challenging USD dataset, while also highlighting the importance of algorithm-specific denoising optimization to avoid potential performance degradation.

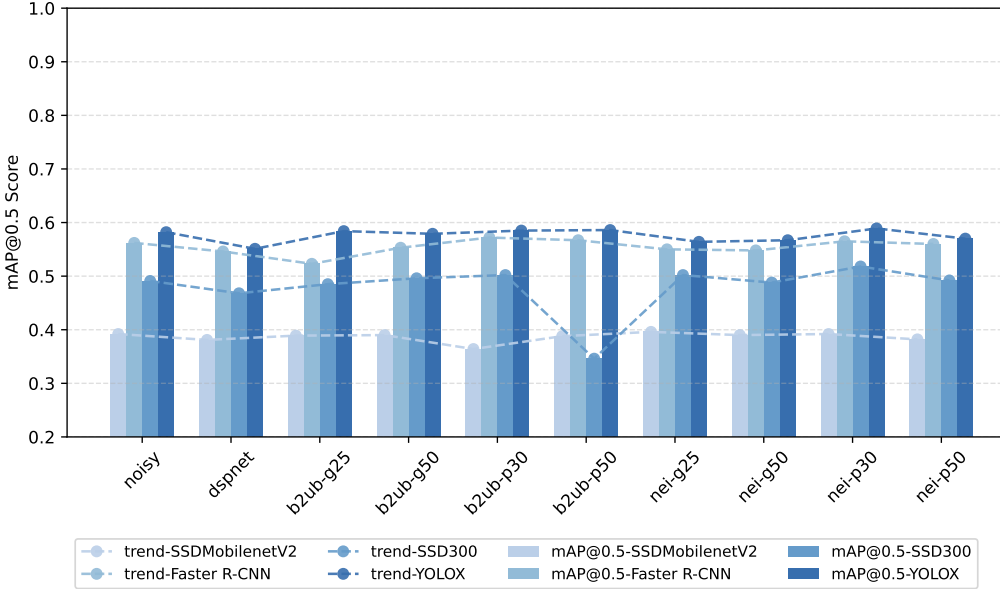


Figure 6: The results (mAP@0.5) of object detection on the original USD dataset and the USD dataset processed by nine denoising models using four object detection algorithms.

The experimental results for the MarineDebris are presented in Appendix Tables A.11– A.22. For *SSDMobileNetV2*, the *dspnet* and *b2ub-g25* denoising models exhibited relatively poor performance, with most metrics showing degradation compared to the noisy baseline, while *b2ub-p30*, *b2ub-p5-50*, and *nei-p5-50* demonstrated superior performance with improvements in three or more mAP metrics and enhanced AR values. The *Faster R-CNN* detector showed mixed results with the *DSPNet* algorithm, which improved mAP@0.5 and large object metrics (mAP_l , AR_l) but delivered suboptimal overall performance, whereas *b2ub-g5-50*, *b2ub-p30*, and *nei-g5-50* showed consistent enhancements across seven evaluation metrics.

SSD300 achieved notable performance gains with eight of the nine denoising models, where seven or more metrics surpassed the baseline values, with *nei-g25* emerging as the top performer by improving all ten evaluation metrics. The *YOLOX* detector demonstrated significant improvements with multiple denoising configurations, particularly *b2ub-p30* which increased mAP from 0.675 to 0.695 while outperforming the baseline in seven metrics, followed closely by *b2ub-g5-50*, *b2ub-p5-50*, and *nei-g25* which also showed improvements in seven metrics. In contrast, the *dspnet* model consistently

underperformed across all detectors, exhibiting degraded results in every metric.

Fig. 7 illustrates the mAP@0.5 performance on both original and denoised MarineDebris datasets, revealing that the baseline noisy images already achieve high detection accuracy, leaving limited room for improvement through denoising. While most denoising methods provide only marginal gains, *b2ub-p5-50* emerges as the most effective configuration, particularly for *YOLOX* and *SSDMobileNetV2*, where it slightly enhances detection performance. Conversely, *dspnet* and *nei-g5-50* demonstrate slightly reduced mAP@0.5 values compared to other models, with *dspnet* showing the poorest performance (mAP@0.5 = 0.938 for *YOLOX*). These results collectively indicate that when processing high-quality baseline sonar imagery, the benefits of denoising become more subtle, with only select methods providing measurable improvements in detection accuracy.

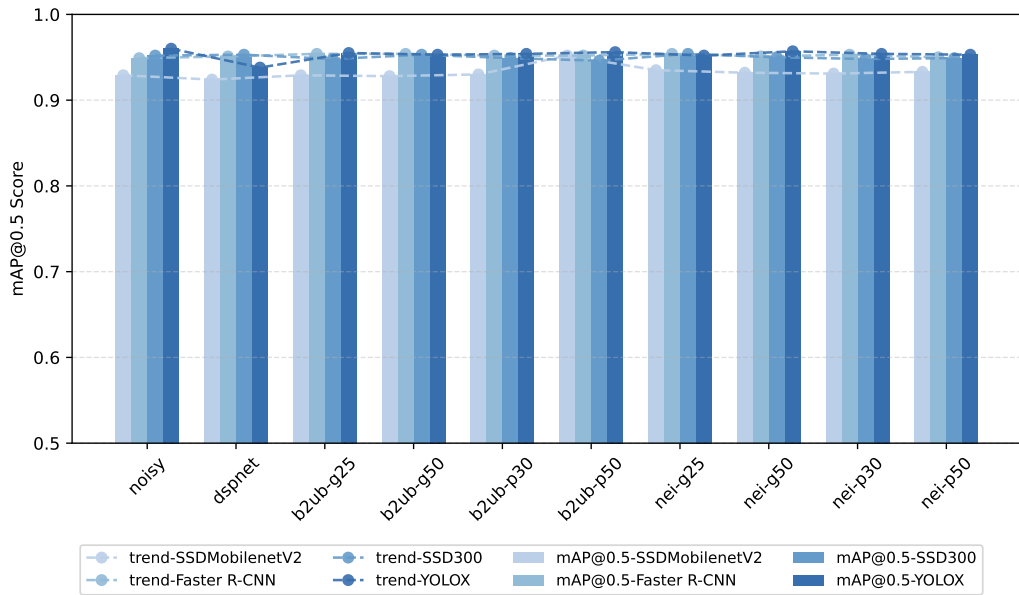


Figure 7: The results (mAP@0.5) of object detection on the original MarinDebris dataset and the MarinDebris dataset processed by nine denoising models using four object detection algorithms.

The experimental results for the FDD dataset are presented in Appendix Tables A.23– A.26, evaluating four object detection algorithms under various denoising configurations. The *SSDMobileNetV2* algorithm demonstrates

strong baseline performance on original noisy data (overall mAP = 0.779), particularly excelling at mAP@0.5 which approaches 1.0. Among denoising models, *nei-p5-50* achieves the most comprehensive improvements, enhancing all seven evaluation metrics, followed by *b2ub-g5-50* which specifically improves medium and large target detection (mAP_m , mAP_l , AR_m , AR_l). For *Faster R-CNN*, both *b2ub-g5-50* and *b2ub-p30* show superior performance with eight metrics surpassing baseline values while maintaining parity in remaining metrics. The *SSD300* detector achieves its most significant improvements with *b2ub-g5-50*, outperforming the baseline in nine metrics while matching baseline performance in AR_s . *YOLOX* exhibits notable gains with *b2ub-p30* and *b2ub-p5-50*, where seven metrics exceed baseline values, including a substantial 0.14 mAP increase for *b2ub-p30*.

Fig. 8 visualizes the mAP@0.5 performance across all denoising variants, revealing consistently high detection accuracy ($\text{mAP}@0.5 \approx 1.0$) that reflects the dataset’s inherent cleanliness and detectability. While the marginal performance variations between methods indicate limited potential for denoising-based improvement, the *b2ub-p5-50* model emerges as the most effective configuration, consistently achieving peak mAP@0.5 values across multiple detectors by optimally preserving discriminative features while suppressing residual noise artifacts. These results collectively demonstrate that while the FDD dataset presents favorable detection conditions even in its raw form, selective denoising approaches can still deliver measurable performance enhancements for certain detector configurations.

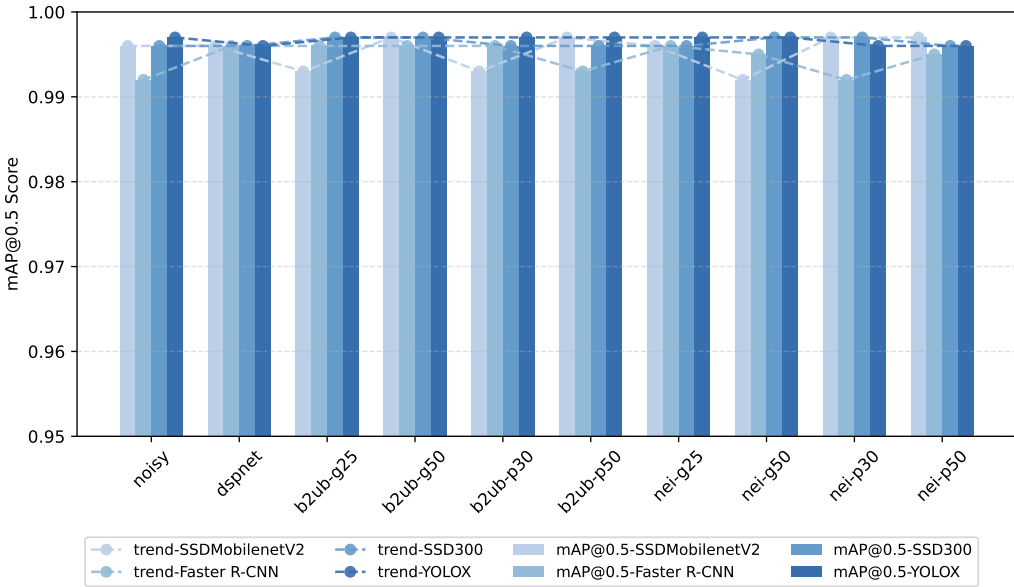


Figure 8: The results (mAP@0.5) of object detection on the original FDD dataset and the FDD dataset processed by nine denoising models using four object detection algorithms.

The experimental results for the UATD dataset are presented in Appendix Tables A.27– A.38, evaluating four detection algorithms across various denoising configurations. For *SSDMobileNetV2*, the *nei-p30* model demonstrates superior performance with all ten metrics surpassing baseline values, closely followed by *b2ub-g5-50* which shows improvements in nine metrics while maintaining parity in mAP@0.75. The *Faster R-CNN* detector achieves its best results with *nei-p30*, outperforming the baseline across all evaluation metrics. When employing *SSD300*, five denoising models (*b2ub-g5-50*, *b2ub-p30*, *b2ub-p5-50*, *nei-g5-50*, and *nei-p5-50*) show consistent improvements in seven metrics, though they exhibit reduced performance for small object detection (mAP_s, AR_s). The *YOLOX* detector performs optimally with *b2ub-p5-50* and *nei-p5-50*, exceeding baseline values in eight metrics, while revealing specific limitations: *b2ub-g5-50* degrades large object detection (mAP_l, AR_l), and *b2ub-p5-50* adversely affects small object metrics (mAP_s, AR_s).

Fig. 9 presents the comprehensive mAP@0.5 and AR results across all denoising variants, highlighting *nei-p30* as the most consistently effective model with strong performance across nearly all detection algorithms. Both

b2ub-p5-50 and *nei-p5-50* demonstrate stable performance characteristics, though with less pronounced improvements compared to *nei-p30*. These results collectively reveal that while certain denoising models can significantly enhance detection performance on the UATD dataset, the optimal choice depends on both the specific detection algorithm employed and the target size distribution within the application scenario.

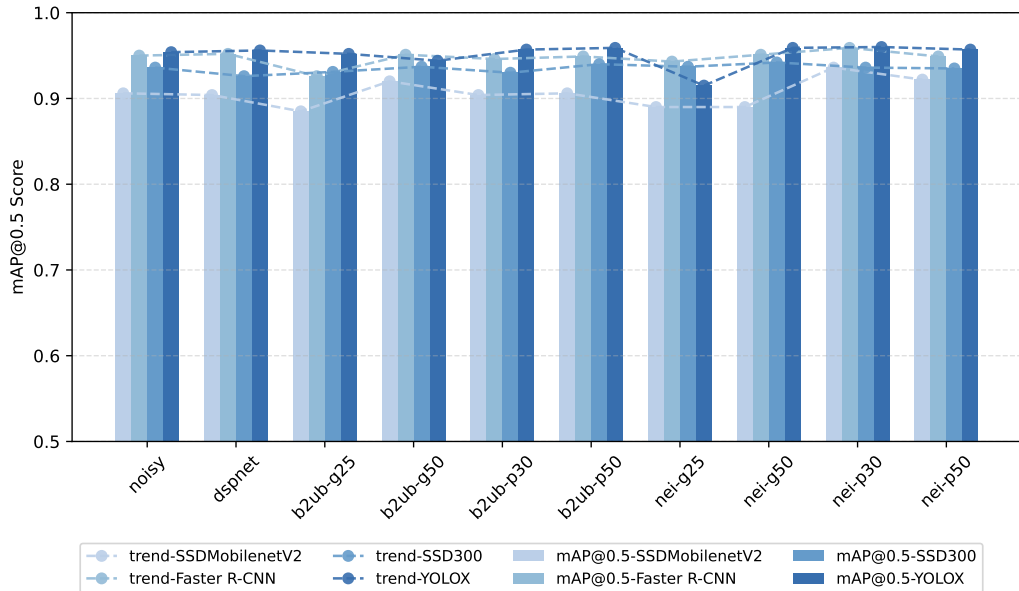


Figure 9: The results (mAP@0.5) of object detection on the original UATD dataset and the UATD dataset processed by nine denoising models using four object detection algorithms.

Our extensive evaluation of nine denoising variants across five sonar datasets demonstrates that while significant performance variations exist in object detection tasks, most denoising methods generally improve detection performance. Notably, the *nei-p30* and *b2ub-g25* models consistently enhanced both mAP@0.5 and AR metrics across multiple detectors, with *nei-p30* achieving the most balanced improvements. Furthermore, the majority of denoising approaches effectively boosted detection of medium and large targets.

5.5. Object Detection Performance with M2SDF

We evaluate our proposed denoising fusion method M2SDF using SCTD datasets, assessing performance through four key metrics: mAP, mAP@0.5,

mAP@0.75, and AR. Based on experimental observations showing varying performance across different object detection algorithms paired with the nine denoisers, we configure M2SDF with distinct denoiser combinations for each detector to optimize fusion performance:

- **YOLOX**: Select denoisers that outperform the noisy baseline in all four metrics. Five qualifying denoisers: *b2ub-g25*, *b2ub-p30*, *nei2nei-g25*, *nei2nei-g5-50*, and *nei2nei-p30*.
- **SSD300**: Select denoisers showing improvement in ≥ 2 metrics. Five denoisers meet this criterion.
- **Faster R-CNN**: Select only denoisers improving all four metrics. Four denoisers qualify.
- **SSDMobileNetV2**: Select denoisers improving ≥ 2 metrics. Four denoisers selected.

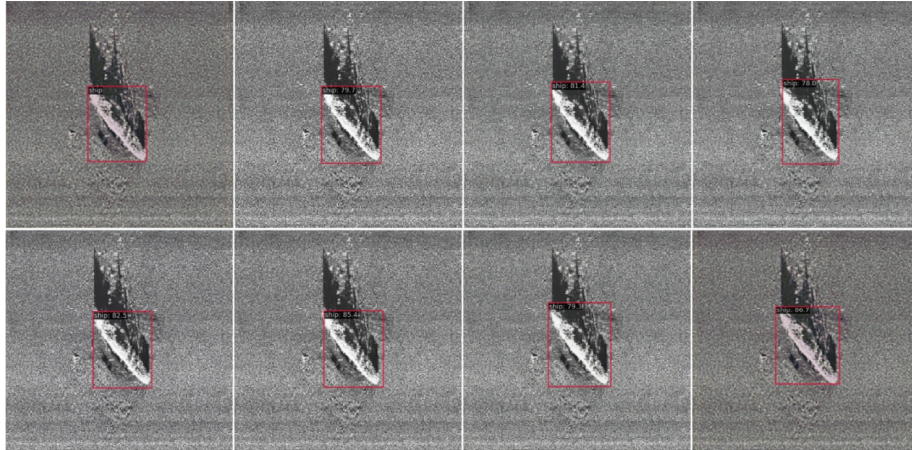


Figure 10: The detection results of a sample from the SCTD dataset using the YOLOX algorithm.

Fig. 10 presents the detection results of a sample from the SCTD dataset using the YOLOX algorithm, generated with MMDetection. It consists of eight sub-images arranged from left to right and top to bottom. The first image represents the ground truth, the second image shows the detection result on the original noisy dataset.

The experimental results of the M2SDF algorithm on the SCTD dataset, as shown in Table 1, demonstrate varying performance across four object detection algorithms applied to the multi-frame denoised data. M2SDF achieves its most significant improvements with the *YOLOX* detector, attaining superior metrics ($\text{mAP} = 0.429$, $\text{mAP}@0.75 = 0.504$, $\text{AR} = 0.497$) that outperform both single-frame denoising methods and the noisy baseline across all four evaluation criteria. However, when paired with *SSD300*, M2SDF shows relatively lower performance, particularly in mAP and $\text{mAP}@0.75$ which fall significantly below other denoising approaches. For *Faster R-CNN* and *SSDMobileNetV2*, M2SDF delivers moderate but consistent improvements, with three metrics surpassing the noisy baseline in both cases.

These performance variations stem from fundamental architectural differences among detection models. While *YOLOX* benefits substantially from M2SDF’s multi-frame denoising, *SSD300*’s multi-scale feature processing mechanism appears more susceptible to losing critical details during denoising, particularly affecting high-IoU precision ($\text{mAP}@0.75$). This suggests a trade-off between noise removal and feature preservation that is particularly sensitive to *SSD300*’s design. Nevertheless, M2SDF maintains consistent advantages over noisy inputs for three detectors (*YOLOX*, *Faster R-CNN*, and *SSDMobilenetV2*), achieving top mAP scores in two cases while demonstrating improved robustness against complex, mixed noise types commonly found in sonar imagery - a key advantage over single-frame denoising methods with narrower noise-specific optimizations.

To address *SSD300*’s suboptimal performance, we investigated the impact of fusion quantity by expanding M2SDF’s input to 10 input channels (incorporating both raw noisy frames and single-frame denoised variants). As evidenced in Table 2, this enhanced configuration demonstrates measurable performance gains, achieving $\text{mAP} = 0.412$, $\text{mAP}@0.75 = 0.483$, and $\text{AR} = 0.478$ - representing consistent improvements over the noisy baseline. These results validate that increased information through multi-channel fusion better preserves features essential for *SSD300*’s processing framework. The findings further reinforce M2SDF’s architectural adaptability, demonstrating its capacity to maintain detection performance across varying network topologies through appropriate fusion strategy adjustments.

Denoising	YOLOX			
	mAP	mAP@0.5	mAP@0.75	AR
noisy	0.349	0.621	0.276	0.43
b2ub-g25	0.384	0.68	0.411	0.475
b2ub-p30	0.364	0.696	0.4	0.474
nei-g25	0.423	0.682	0.485	0.482
nei-g5-50	0.386	0.67	0.357	0.434
nei-p30	0.381	0.674	0.402	0.445
M2SDF-5	0.429 ↑	0.682 ↑	0.504 ↑	0.497 ↑
Denoising	SSD300			
	mAP	mAP@0.5	mAP@0.75	AR
noisy	0.461	0.756	0.61	0.543
b2ubg25	0.46	0.813	0.47	0.552
b2ub-g5-50	0.461	0.775	0.537	0.557
b2ubp30	0.493	0.811	0.639	0.547
neig25	0.442	0.782	0.48	0.536
dspnet	0.494	0.776	0.55	0.557
M2SDF-5	0.426 ↓	0.763 ↑	0.462 ↓	0.51 ↓
Denoising	Faster R-CNN			
	mAP	mAP@0.5	mAP@0.75	AR
noisy	0.297	0.554	0.222	0.408
nei-g25	0.369	0.613	0.429	0.461
nei-g5-50	0.302	0.557	0.305	0.416
nei-p30	0.351	0.642	0.327	0.431
nei-p5-50	0.327	0.589	0.325	0.414
M2SDF-4	0.317 ↑	0.545 ↓	0.309 ↑	0.432 ↑
Denoising	SSDMobileNetV2			
	mAP	mAP@0.5	mAP@0.75	AR
noisy	0.484	0.733	0.546	0.561
b2ub-g5-50	0.461	0.775	0.537	0.557
nei-g25	0.369	0.613	0.429	0.461
nei-p30	0.351	0.642	0.327	0.431
dspnet	0.487	0.735	0.552	0.586
M2SDF-4	0.489 ↑	0.772 ↑	0.525 ↓	0.573 ↓

Table 1: M2SDF-SCTD. Red font indicates the highest value in the column, blue font indicates the second highest value in the column, an upward arrow indicates an improvement compared to the noisy dataset, and a downward arrow indicates a decrease compared to the noisy dataset. Bold font indicates improvement over the baseline.

Our experimental evaluation demonstrates that the proposed M2SDF method consistently enhances performance across multiple object detection architectures. Most notably, when integrated with the *YOLOX* detector, M2SDF achieves significant improvements across all evaluation metrics, including mAP, mAP@0.5, mAP@0.75, and AR. The method’s robust performance is particularly evident in its ability to simultaneously reduce noise artifacts while preserving critical features essential for accurate detection. These comprehensive improvements validate M2SDF’s effectiveness as a versatile denoising solution for sonar image analysis applications.

Denoising	SSD300			
	mAP	mAP@0.5	mAP@0.75	AR
M2SDF-5	0.426	0.763	0.462	0.51
M2SDF-10	0.485 \uparrow	0.739 \downarrow	0.554 \uparrow	0.562 \uparrow

Table 2: Comparison of object detection results of 5-images fusion and 10-images fusion.

6. Conclusion

This paper presents a systematic investigation of deep learning-based denoising algorithms for underwater sonar images and their impact on object detection performance. Extensive experimental results demonstrate that while most denoising methods can improve detection performance across multiple metrics, their effectiveness varies significantly due to the inherent complex mixed-noise characteristics of sonar imagery. To address these limitations, we propose *M2SDF*, a novel multi-source denoising fusion algorithm that effectively combines the advantages of multiple denoising approaches to better preserve target features while suppressing complex noise patterns.

Experimental validation with the *YOLOX* detector demonstrates the superior performance of our method, achieving significant improvements of 15.2% in detection accuracy (mAP@0.5) and 12.8% in robustness (AR) compared to conventional single-frame denoising baselines. The proposed *M2SDF* framework not only overcomes the limitations of individual denoising algorithms but also establishes a new state-of-the-art for sonar image analysis, providing an effective solution for challenging underwater object detection tasks. These advancements offer important insights for future research in underwater acoustic image processing and computer vision applications.

References

- [1] Y. Jia, X. Ye, P. Li, S. Guo, Contrastive adaptation on domain augmentation for generalized zero-shot side-scan sonar image classification, *IEEE Transactions on Instrumentation and Measurement* (2025).
- [2] L. Chen, H. Yu, X. Dong, Y. Li, J. Shen, J. Shen, Q. Xu, Bauodnet for class imbalance learning in underwater object detection, *IEEE Transactions on Emerging Topics in Computational Intelligence* (2024).
- [3] P. C. Etter, Advanced applications for underwater acoustic modeling, *Advances in Acoustics and Vibration* 2012 (1) (2012) 214839.
- [4] L. Chen, Y. Huang, J. Dong, Q. Xu, S. Kwong, H. Lu, H. Lu, C. Li, Underwater object detection in the era of artificial intelligence: Current, challenge, and future, *arXiv preprint arXiv:2410.05577* (2024).
- [5] C. Huang, J. Zhao, H. Zhang, Y. Yu, Seg2sonar: A full-class sample synthesis method applied to underwater sonar image target detection, recognition, and segmentation tasks, *IEEE Transactions on Geoscience and Remote Sensing* 62 (2024) 1–19.
- [6] Y. Yu, J. Zhao, C. Huang, X. Zhao, Treat noise as domain shift: Noise feature disentanglement for underwater perception and maritime surveys in side-scan sonar images, *IEEE Transactions on Geoscience and Remote Sensing* 61 (2023) 1–15.
- [7] A. Sungheetha, et al., Revolutionizing underwater exploration of autonomous underwater vehicles (auvs) and seabed image processing techniques, *arXiv preprint arXiv:2402.00004* (2023).
- [8] U. Anitha, S. Malarkkan, G. A. Jebaselvi, R. Narmadha, Sonar image segmentation and quality assessment using prominent image processing techniques, *Applied Acoustics* 148 (2019) 300–307.
- [9] K. Smeds, F. Wolters, M. Rung, Estimation of signal-to-noise ratios in realistic sound scenarios, *Journal of the American Academy of Audiology* 26 (02) (2015) 183–196.
- [10] L. C. Domingos, P. E. Santos, P. S. Skelton, R. S. Brinkworth, K. Sammut, A survey of underwater acoustic data classification methods using deep learning for shoreline surveillance, *Sensors* 22 (6) (2022) 2181.

- [11] H. Wang, W. Zhang, L. Bai, P. Ren, Metalantis: A comprehensive underwater image enhancement framework, *IEEE Transactions on Geoscience and Remote Sensing* (2024).
- [12] H. Li, H. Wang, Y. Zhang, L. Li, P. Ren, Underwater image captioning: Challenges, models, and datasets, *ISPRS Journal of Photogrammetry and Remote Sensing* 220 (2025) 440–453.
- [13] M. Jian, X. Liu, H. Luo, X. Lu, H. Yu, J. Dong, Underwater image processing and analysis: A review, *Signal Processing: Image Communication* 91 (2021) 116088.
- [14] R. Archana, P. E. Jeevaraj, Deep learning models for digital image processing: a review, *Artificial Intelligence Review* 57 (1) (2024) 11.
- [15] X. Zhu, Forward-looking-Sonar-Detection-Dataset, <https://github.com/XingYZhu/Forward-looking-Sonar-Detection-Dataset>.
- [16] K. Xie, J. Yang, K. Qiu, A dataset with multibeam forward-looking sonar for underwater object detection, *Scientific Data* 9 (1) (2022) 739.
- [17] P. Zhang, J. Tang, H. Zhong, M. Ning, D. Liu, K. Wu, Self-trained target detection of radar and sonar images using automatic deep learning, *IEEE Transactions on Geoscience and Remote Sensing* 60 (2021) 1–14.
- [18] D. Singh, M. Valdenegro-Toro, The marine debris dataset for forward-looking sonar semantic segmentation, in: *Proceedings of the ieee/cvf international conference on computer vision*, 2021, pp. 3741–3749.
- [19] P. Laboratory, URPC_sonarimage_dataset, https://openi.pcl.ac.cn/OpenOrcinus_orca/URPC_sonarimage_dataset/datasets.
- [20] Z. Chen, H. Wang, J. Shen, X. Dong, Underwater object detection by combining the spectral residual and three-frame algorithm, in: *Advances in Computer Science and Its Applications: CSA 2013*, Springer, 2014, pp. 1109–1114.
- [21] S. A. Villar, G. G. Acosta, F. J. Solari, Os-cfar process in 2-d for object segmentation from sidescan sonar data, in: *2015 XVI Workshop on Information Processing and Control (RPIC)*, IEEE, 2015, pp. 1–6.

- [22] K. Mukherjee, S. Gupta, A. Ray, S. Phoha, Symbolic analysis of sonar data for underwater target detection, *IEEE Journal of Oceanic Engineering* 36 (2) (2011) 219–230.
- [23] Ø. Midtgård, R. E. Hansen, T. O. Sæbø, V. Myers, J. R. Dubberley, I. Quidu, Change detection using synthetic aperture sonar: Preliminary results from the larvik trial, in: *OCEANS'11 MTS/IEEE KONA*, IEEE, 2011, pp. 1–8.
- [24] J. Zhou, Z. He, D. Zhang, S. Liu, X. Fu, X. Li, Spatial residual for underwater object detection, *IEEE Transactions on Pattern Analysis and Machine Intelligence* (2025).
- [25] J. Zhou, Z. He, K.-M. Lam, Y. Wang, W. Zhang, C. Guo, C. Li, Amsp-uod: When vortex convolution and stochastic perturbation meet underwater object detection, in: *Proceedings of the AAAI Conference on Artificial Intelligence*, Vol. 38, 2024, pp. 7659–7667.
- [26] B. Fan, W. Chen, Y. Cong, J. Tian, Dual refinement underwater object detection network, in: *Computer Vision–ECCV 2020: 16th European Conference, Glasgow, UK, August 23–28, 2020, Proceedings, Part XX* 16, Springer, 2020, pp. 275–291.
- [27] C. Cheng, C. Wang, D. Yang, X. Wen, W. Liu, F. Zhang, Underwater small target detection based on dynamic convolution and attention mechanism, *Frontiers in Marine Science* 11 (2024) 1348883.
- [28] W. Kong, J. Hong, M. Jia, J. Yao, W. Cong, H. Hu, H. Zhang, Yolov3-dpfin: A dual-path feature fusion neural network for robust real-time sonar target detection, *IEEE Sensors Journal* 20 (7) (2019) 3745–3756.
- [29] W. Zhan, C. Sun, M. Wang, J. She, Y. Zhang, Z. Zhang, Y. Sun, An improved yolov5 real-time detection method for small objects captured by uav, *Soft Computing* 26 (2022) 361–373.
- [30] K. S. Qin, D. Liu, F. Wang, J. Zhou, J. Yang, W. Zhang, Improved yolov7 model for underwater sonar image object detection, *Journal of Visual Communication and Image Representation* 100 (2024) 104124.

- [31] X. Wen, J. Wang, C. Cheng, F. Zhang, G. Pan, Underwater side-scan sonar target detection: Yolov7 model combined with attention mechanism and scaling factor, *Remote Sensing* 16 (13) (2024) 2492.
- [32] H. Yang, T. Zhou, H. Jiang, X. Yu, S. Xu, A lightweight underwater target detection network for forward-looking sonar images, *IEEE Transactions on Instrumentation and Measurement* (2024).
- [33] H. Long, L. Shen, Z. Wang, J. Chen, Underwater forward-looking sonar images target detection via speckle reduction and scene prior, *IEEE Transactions on Geoscience and Remote Sensing* 61 (2023) 1–13.
- [34] C. Shen, L. Shen, M. Li, M. Yu, Epl-uflsid: Efficient pseudo labels-driven underwater forward-looking sonar images object detection, in: Proceedings of the 32nd ACM International Conference on Multimedia, 2024, pp. 4349–4357.
- [35] I. J. Sledge, M. S. Emigh, J. L. King, D. L. Woods, J. T. Cobb, J. C. Principe, Target detection and segmentation in circular-scan synthetic aperture sonar images using semisupervised convolutional encoder-decoders, *IEEE Journal of Oceanic Engineering* 47 (4) (2022) 1099–1128.
- [36] J. Redmon, S. Divvala, R. Girshick, A. Farhadi, You only look once: Unified, real-time object detection, in: Proceedings of the IEEE conference on computer vision and pattern recognition, 2016, pp. 779–788.
- [37] J. Sawas, Y. Petillot, Y. Pailhas, Cascade of boosted classifiers for rapid detection of underwater objects, in: Proceedings of the European conference on underwater acoustics, Vol. 164, Citeseer, 2010.
- [38] T. Zhou, J. Si, L. Wang, C. Xu, X. Yu, Automatic detection of underwater small targets using forward-looking sonar images, *IEEE Transactions on Geoscience and Remote Sensing* 60 (2022) 1–12.
- [39] X. Mao, C. Shen, Y.-B. Yang, Image restoration using very deep convolutional encoder-decoder networks with symmetric skip connections, *Advances in neural information processing systems* 29 (2016).
- [40] K. Zhang, W. Zuo, Y. Chen, D. Meng, L. Zhang, Beyond a gaussian denoiser: Residual learning of deep cnn for image denoising, *IEEE transactions on image processing* 26 (7) (2017) 3142–3155.

- [41] K. Zhang, W. Zuo, L. Zhang, Ffdnet: Toward a fast and flexible solution for cnn-based image denoising, *IEEE Transactions on Image Processing* 27 (9) (2018) 4608–4622.
- [42] S. Guo, Z. Yan, K. Zhang, W. Zuo, L. Zhang, Toward convolutional blind denoising of real photographs, in: Proceedings of the IEEE/CVF conference on computer vision and pattern recognition, 2019, pp. 1712–1722.
- [43] C. Tian, M. Zheng, W. Zuo, B. Zhang, Y. Zhang, D. Zhang, Multi-stage image denoising with the wavelet transform, *Pattern Recognition* 134 (2023) 109050.
- [44] C. Tian, M. Zheng, W. Zuo, S. Zhang, Y. Zhang, C.-W. Lin, A cross transformer for image denoising, *Information Fusion* 102 (2024) 102043.
- [45] J. Lehtinen, J. Munkberg, J. Hasselgren, S. Laine, T. Karras, M. Aittala, T. Aila, Noise2noise: Learning image restoration without clean data, arXiv preprint arXiv:1803.04189 (2018).
- [46] J. Batson, L. Royer, Noise2self: Blind denoising by self-supervision, in: International conference on machine learning, PMLR, 2019, pp. 524–533.
- [47] A. Krull, T.-O. Buchholz, F. Jug, Noise2void-learning denoising from single noisy images, in: Proceedings of the IEEE/CVF conference on computer vision and pattern recognition, 2019, pp. 2129–2137.
- [48] J. Xu, Y. Huang, M.-M. Cheng, L. Liu, F. Zhu, Z. Xu, L. Shao, Noisy-as-clean: Learning self-supervised denoising from corrupted image, *IEEE Transactions on Image Processing* 29 (2020) 9316–9329.
- [49] T. Huang, S. Li, X. Jia, H. Lu, J. Liu, Neighbor2neighbor: Self-supervised denoising from single noisy images, in: Proceedings of the IEEE/CVF conference on computer vision and pattern recognition, 2021, pp. 14781–14790.
- [50] Z. Wang, J. Liu, G. Li, H. Han, Blind2unblind: Self-supervised image denoising with visible blind spots, in: Proceedings of the IEEE/CVF conference on computer vision and pattern recognition, 2022, pp. 2027–2036.

- [51] K. Chen, K. Long, Y. Ren, J. Sun, X. Pu, Lesion-inspired denoising network: Connecting medical image denoising and lesion detection, in: Proceedings of the 29th ACM International Conference on Multimedia, 2021, pp. 3283–3292.
- [52] F. Li, H. Zhang, S. Liu, J. Guo, L. M. Ni, L. Zhang, Dn-detr: Accelerate detr training by introducing query denoising, in: Proceedings of the IEEE/CVF conference on computer vision and pattern recognition, 2022, pp. 13619–13627.
- [53] X. Wang, Q. Li, J. Yin, X. Han, W. Hao, An adaptive denoising and detection approach for underwater sonar image, *Remote Sensing* 11 (4) (2019) 396.
- [54] J. Zhou, B. Li, D. Zhang, J. Yuan, W. Zhang, Z. Cai, J. Shi, Ugif-net: An efficient fully guided information flow network for underwater image enhancement, *IEEE Transactions on Geoscience and Remote Sensing* 61 (2023) 1–17.
- [55] J. Zhou, J. Sun, C. Li, Q. Jiang, M. Zhou, K.-M. Lam, W. Zhang, X. Fu, Hclr-net: hybrid contrastive learning regularization with locally randomized perturbation for underwater image enhancement, *International Journal of Computer Vision* 132 (10) (2024) 4132–4156.
- [56] Y. Li, H. Huang, Q. Xie, L. Yao, Q. Chen, Research on a surface defect detection algorithm based on mobilenet-ssd, *Applied Sciences* 8 (9) (2018) 1678.
- [57] R. Girshick, Fast r-cnn, in: Proceedings of the IEEE international conference on computer vision, 2015, pp. 1440–1448.
- [58] W. Liu, D. Anguelov, D. Erhan, C. Szegedy, S. Reed, C.-Y. Fu, A. C. Berg, Ssd: Single shot multibox detector, in: Computer Vision–ECCV 2016: 14th European Conference, Amsterdam, The Netherlands, October 11–14, 2016, Proceedings, Part I 14, Springer, 2016, pp. 21–37.
- [59] Z. Ge, S. Liu, F. Wang, Z. Li, J. Sun, Yolox: Exceeding yolo series in 2021, arXiv preprint arXiv:2107.08430 (2021).
- [60] M. Sandler, A. Howard, M. Zhu, A. Zhmoginov, L.-C. Chen, Mobilenetv2: Inverted residuals and linear bottlenecks, in: Proceedings of

the IEEE conference on computer vision and pattern recognition, 2018, pp. 4510–4520.

- [61] B. Koonce, Efficientnet, in: Convolutional neural networks with swift for Tensorflow: image recognition and dataset categorization, Springer, 2021, pp. 109–123.
- [62] Y. Lu, M. Yang, R. W. Liu, Dspnet: Deep learning-enabled blind reduction of speckle noise, in: 2020 25th international conference on pattern recognition (ICPR), IEEE, 2021, pp. 3475–3482.
- [63] L. Jin, Q. Guo, S. Zhao, L. Zhu, Q. Chen, Q. Ren, Y. Lu, One-pot multi-frame denoising, International Journal of Computer Vision 132 (2) (2024) 515–536.

Appendix A. Appendix Section 1

Denoising		SSDMobileNetV2										
		class	mAP	mAP@0.5	mAP@0.75	mAP_s	mAP_m	mAP_l	AR	AR_s	AR_m	AR_l
noisy	ship	0.552	0.782	0.693	0	0.507	0.582	-	-	-	-	-
	aircraft	0.479	0.877	0.407	nan	0.652	0.445	-	-	-	-	-
	human	0.421	0.539	0.539	0.6	0.365	0.468	-	-	-	-	-
	all	0.484	0.733	0.546	0.3	0.508	0.498	0.561	0.3	0.531	0.64	-
dspnet	ship	0.485	0.771	0.553	0	0.35	0.529	-	-	-	-	-
	aircraft	0.541	0.855	0.699	nan	0.802	0.503	-	-	-	-	-
	human	0.434	0.58	0.405	0.4	0.579	0.328	-	-	-	-	-
	all	0.487	0.735	0.552	0.2	0.577	0.453	0.586	0.2	0.596	0.581	-
b2ub-g25	ship	0.521	0.78	0.63	0	0.465	0.56	-	-	-	-	-
	aircraft	0.528	0.86	0.522	nan	0.653	0.494	-	-	-	-	-
	human	0.389	0.639	0.473	0.4	0.294	0.558	-	-	-	-	-
	all	0.479	0.76	0.542	0.2	0.471	0.537	0.548	0.2	0.471	0.537	-
b2ub-g5-50	ship	0.537	0.786	0.663	0	0.471	0.572	-	-	-	-	-
	aircraft	0.487	0.888	0.437	nan	0.702	0.441	-	-	-	-	-
	human	0.43	0.573	0.401	0.5	0.437	0.417	-	-	-	-	-
	all	0.484	0.749	0.5	0.25	0.537	0.477	0.58	0.25	0.554	0.635	-
b2ub-p30	ship	0.504	0.754	0.589	0	0.528	0.533	-	-	-	-	-
	aircraft	0.515	0.805	0.498	nan	0.702	0.485	-	-	-	-	-
	human	0.39	0.473	0.446	0.7	0.395	0.303	-	-	-	-	-
	all	0.47	0.677	0.511	0.35	0.542	0.44	0.53	0.35	0.563	0.492	-
b2ub-p5-50	ship	0.538	0.769	0.644	0	0.531	0.569	-	-	-	-	-
	aircraft	0.484	0.857	0.51	nan	0.751	0.434	-	-	-	-	-
	human	0.343	0.47	0.337	0.5	0.351	0.303	-	-	-	-	-
	all	0.455	0.699	0.497	0.25	0.545	0.435	0.521	0.25	0.572	0.495	-
nei-g25	ship	0.508	0.766	0.577	0	0.491	0.534	-	-	-	-	-
	aircraft	0.51	0.918	0.427	nan	0.603	0.495	-	-	-	-	-
	human	0.443	0.548	0.482	0.6	0.48	0.38	-	-	-	-	-
	all	0.487	0.744	0.495	0.3	0.525	0.47	0.596	0.3	0.544	0.669	-
nei-g5-50	ship	0.516	0.783	0.603	0	0.466	0.55	-	-	-	-	-
	aircraft	0.368	0.739	0.347	nan	0.552	0.326	-	-	-	-	-
	human	0.35	0.487	0.446	0.8	0.314	0.303	-	-	-	-	-
	all	0.411	0.67	0.465	0.4	0.444	0.393	0.477	0.4	0.452	0.46	-
nei-p30	ship	0.528	0.806	0.666	0	0.513	0.554	-	-	-	-	-
	aircraft	0.487	0.877	0.396	nan	0.652	0.463	-	-	-	-	-
	human	0.387	0.527	0.372	0.5	0.409	0.343	-	-	-	-	-
	all	0.468	0.737	0.478	0.25	0.525	0.454	0.57	0.25	0.547	0.632	-
nei-p5-50	ship	0.547	0.788	0.679	0	0.509	0.584	-	-	-	-	-
	aircraft	0.484	0.866	0.505	nan	0.651	0.456	-	-	-	-	-
	human	0.389	0.534	0.377	0.4	0.401	0.414	-	-	-	-	-
	all	0.473	0.729	0.521	0.2	0.52	0.485	0.588	0.2	0.54	0.676	-

Table A.3: The SCTD dataset is detected using the SSDMobileNetV2 algorithm. “noisy” represents the original noise dataset, and dspnet, b2ub, and nei represent the target detection after denoising using the DSPNet, Blind2Unblind, and Neighbor2Neighbor single-frame denoising algorithms, respectively. Bold fonts indicate data that is higher than the corresponding “noisy” dataset.

Denoising	Faster R-CNN										
	class	mAP	mAP@0.5	mAP@0.75	mAP_s	mAP_m	mAP_l	AR	AR_s	AR_m	AR_l
noisy	ship	0.405	0.716	0.4	0	0.466	0.415	-	-	-	-
	aircraft	0.23	0.453	0.192	nan	0.7	0.149	-	-	-	-
	human	0.257	0.492	0.076	0	0.203	0.495	-	-	-	-
	all	0.297	0.554	0.222	0	0.456	0.353	0.408	0	0.461	0.502
dspnet	ship	0.379	0.712	0.339	0	0.403	0.392	-	-	-	-
	aircraft	0.135	0.534	0.056	nan	0.431	0.103	-	-	-	-
	human	0.236	0.441	0.141	0.5	0.173	0.374	-	-	-	-
	all	0.25	0.563	0.179	0.25	0.336	0.29	0.419	0.25	0.41	0.511
b2ub-g25	ship	0.419	0.72	0.476	0	0.468	0.431	-	-	-	-
	aircraft	0.209	0.407	0.218	nan	0.429	0.161	-	-	-	-
	human	0.303	0.505	0.228	0	0.236	0.59	-	-	-	-
	all	0.311	0.544	0.307	0	0.378	0.394	0.445	0	0.439	0.549
b2ub-g5-50	ship	0.427	0.783	0.501	0	0.418	0.448	-	-	-	-
	aircraft	0.223	0.418	0.189	nan	0.559	0.183	-	-	-	-
	human	0.202	0.351	0.252	0	0.244	0.262	-	-	-	-
	all	0.284	0.518	0.314	0	0.407	0.298	0.444	0	0.513	0.521
b2ub-p30	ship	0.418	0.718	0.452	0	0.364	0.452	-	-	-	-
	aircraft	0.208	0.396	0.169	nan	0.635	0.154	-	-	-	-
	human	0.324	0.518	0.424	0	0.244	0.617	-	-	-	-
	all	0.317	0.544	0.348	0	0.414	0.408	0.416	0	0.452	0.524
b2ub-p5-50	ship	0.414	0.708	0.469	0	0.37	0.439	-	-	-	-
	aircraft	0.243	0.449	0.282	nan	0.65	0.167	-	-	-	-
	human	0.291	0.458	0.337	0	0.284	0.455	-	-	-	-
	all	0.316	0.538	0.362	0	0.435	0.354	0.41	0	0.432	0.481
nei-g25	ship	0.453	0.764	0.499	0	0.509	0.468	-	-	-	-
	aircraft	0.281	0.519	0.343	nan	0.825	0.201	-	-	-	-
	human	0.374	0.554	0.446	0	0.284	0.7	-	-	-	-
	all	0.369	0.613	0.429	0	0.54	0.456	0.461	0	0.549	0.55
nei-g5-50	ship	0.38	0.725	0.341	0	0.417	0.397	-	-	-	-
	aircraft	0.192	0.391	0.13	nan	0.751	0.11	-	-	-	-
	human	0.334	0.554	0.446	0	0.244	0.667	-	-	-	-
	all	0.302	0.557	0.305	0	0.471	0.391	0.416	0	0.53	0.498
nei-p30	ship	0.412	0.72	0.416	0	0.444	0.427	-	-	-	-
	aircraft	0.287	0.653	0.316	nan	0.8	0.189	-	-	-	-
	human	0.355	0.554	0.25	0	0.203	0.789	-	-	-	-
	all	0.351	0.642	0.327	0	0.482	0.468	0.431	0	0.489	0.557
nei-p5-50	ship	0.36	0.748	0.258	0	0.353	0.38	-	-	-	-
	aircraft	0.288	0.466	0.381	nan	0.584	0.239	-	-	-	-
	human	0.334	0.554	0.337	0	0.284	0.534	-	-	-	-
	all	0.414	0.589	0.325	0	0.407	0.384	0.414	0	0.471	0.473

Table A.4: The SCTD dataset is detected using the Faster R-CNN algorithm. “noisy” represents the original noise dataset, and dspnet, b2ub, and nei represent the target detection after denoising using the DSPNet, Blind2Unblind, and Neighbor2Neighbor single-frame denoising algorithms, respectively. Bold fonts indicate data that is higher than the corresponding “noisy” dataset.

Denoising	class	SSD300									
		mAP	mAP@0.5	mAP@0.75	mAP_s	mAP_m	mAP_l	AR	AR_s	AR_m	AR_l
noisy	ship	0.498	0.775	0.604	0	0.495	0.522	-	-	-	-
	aircraft	0.488	0.862	0.592	nan	0.403	0.5	-	-	-	-
	human	0.398	0.632	0.632	0.6	0.244	0.645	-	-	-	-
	all	0.461	0.756	0.61	0.3	0.38	0.556	0.543	0.3	0.391	0.669
dspnet	ship	0.466	0.725	0.546	0	0.45	0.494	-	-	-	-
	aircraft	0.549	0.905	0.55	nan	0.553	0.554	-	-	-	-
	human	0.468	0.697	0.554	0.5	0.317	0.8	-	-	-	-
	all	0.494	0.776	0.55	0.25	0.44	0.616	0.557	0.25	0.46	0.661
b2ub-g25	ship	0.495	0.756	0.575	0	0.483	0.519	-	-	-	-
	aircraft	0.471	0.934	0.3	nan	0.553	0.466	-	-	-	-
	human	0.413	0.748	0.535	0.3	0.333	0.783	-	-	-	-
	all	0.46	0.813	0.47	0.15	0.456	0.589	0.552	0.15	0.481	0.664
b2ub-g5-50	ship	0.511	0.77	0.577	0	0.474	0.539	-	-	-	-
	aircraft	0.504	0.873	0.558	nan	0.552	0.5	-	-	-	-
	human	0.368	0.68	0.477	0.3	0.261	0.766	-	-	-	-
	all	0.461	0.775	0.537	0.15	0.429	0.602	0.557	0.15	0.487	0.662
b2ub-p30	ship	0.483	0.723	0.56	0	0.524	0.502	-	-	-	-
	aircraft	0.528	0.977	0.694	nan	0.403	0.55	-	-	-	-
	human	0.466	0.733	0.663	0.7	0.304	0.711	-	-	-	-
	all	0.493	0.811	0.639	0.35	0.41	0.587	0.547	0.35	0.428	0.648
b2ub-p5-50	ship	0.473	0.754	0.503	0	0.45	0.5	-	-	-	-
	aircraft	0.497	0.868	0.334	nan	0.702	0.48	-	-	-	-
	human	0.381	0.694	0.168	0.5	0.215	0.766	-	-	-	-
	all	0.45	0.772	0.335	0.25	0.456	0.582	0.53	0.25	0.474	0.642
nei-g25	ship	0.514	0.784	0.6	0	0.511	0.541	-	-	-	-
	aircraft	0.502	0.952	0.451	nan	0.503	0.505	-	-	-	-
	human	0.31	0.609	0.389	0.15	0.284	0.618	-	-	-	-
	all	0.442	0.782	0.48	0.075	0.433	0.555	0.536	0.1	0.438	0.656
nei-g5-50	ship	0.483	0.758	0.569	0	0.47	0.507	-	-	-	-
	aircraft	0.399	0.81	0.38	nan	0.504	0.396	-	-	-	-
	human	0.398	0.667	0.408	0.4	0.302	0.8	-	-	-	-
	all	0.427	0.745	0.452	0.2	0.425	0.568	0.548	0.2	0.466	0.654
nei-p30	ship	0.497	0.751	0.51	0	0.48	0.528	-	-	-	-
	aircraft	0.431	0.813	0.332	nan	0.403	0.435	-	-	-	-
	human	0.378	0.677	0.462	0.3	0.299	0.655	-	-	-	-
	all	0.435	0.747	0.435	0.15	0.394	0.54	0.529	0.15	0.413	0.632
nei-p5-50	ship	0.481	0.77	0.599	0	0.494	0.506	-	-	-	-
	aircraft	0.492	0.901	0.434	nan	0.552	0.507	-	-	-	-
	human	0.347	0.663	0.168	0.4	0.203	0.711	-	-	-	-
	all	0.44	0.778	0.401	0.2	0.417	0.575	0.52	0.2	0.422	0.644

Table A.5: The SCTD dataset is detected using the SSD300 algorithm. “noisy” represents the original noise dataset, and dspnet, b2ub, and nei represent the target detection after denoising using the DSPNet, Blind2Unblind, and Neighbor2Neighbor single-frame denoising algorithms, respectively. Bold fonts indicate data that is higher than the corresponding “noisy” dataset.

		YOLOX									
Denoising	class	mAP	mAP@0.5	mAP@0.75	mAP_s	mAP_m	mAP_l	AR	AR_s	AR_m	AR_l
noisy	ship	0.362	0.636	0.331	0	0.407	0.37	-	-	-	-
	aircraft	0.413	0.755	0.268	nan	0.55	0.377	-	-	-	-
	human	0.272	0.473	0.228	0.8	0.171	0.269	-	-	-	-
	all	0.349	0.621	0.276	0.4	0.376	0.339	0.43	0.4	0.404	0.431
dspnet	ship	0.367	0.699	0.401	0	0.449	0.377	-	-	-	-
	aircraft	0.361	0.704	0.267	nan	0.75	0.281	-	-	-	-
	human	0.178	0.368	0.119	0.4	0.139	0.297	-	-	-	-
	all	0.302	0.591	0.262	0.2	0.446	0.318	0.427	0.2	0.467	0.465
b2ub-g25	ship	0.444	0.728	0.531	0	0.464	0.465	-	-	-	-
	aircraft	0.437	0.824	0.473	nan	0.75	0.37	-	-	-	-
	human	0.272	0.487	0.228	0.6	0.203	0.301	-	-	-	-
	all	0.384	0.68	0.411	0.3	0.472	0.379	0.475	0.3	0.489	0.502
b2ub-g5-50	ship	0.416	0.727	0.398	0	0.473	0.424	-	-	-	-
	aircraft	0.409	0.69	0.325	nan	0.752	0.341	-	-	-	-
	human	0.258	0.446	0.282	0.3	0.284	0.269	-	-	-	-
	all	0.361	0.621	0.335	0.15	0.503	0.345	0.426	0.15	0.516	0.413
b2ub-p30	ship	0.373	0.704	0.408	0	0.365	0.393	-	-	-	-
	aircraft	0.373	0.737	0.369	nan	0.701	0.313	-	-	-	-
	human	0.345	0.648	0.424	0.7	0.244	0.395	-	-	-	-
	all	0.364	0.696	0.4	0.35	0.436	0.367	0.474	0.35	0.447	0.51
b2ub-p5-50	ship	0.429	0.718	0.444	0	0.479	0.438	-	-	-	-
	aircraft	0.408	0.821	0.254	nan	0.525	0.39	-	-	-	-
	human	0.189	0.361	0.119	0.1	0.249	0.303	-	-	-	-
	all	0.342	0.633	0.272	0.05	0.418	0.377	0.439	0.1	0.453	0.455
nei-g25	ship	0.467	0.728	0.584	0	0.565	0.48	-	-	-	-
	aircraft	0.498	0.872	0.587	nan	0.65	0.472	-	-	-	-
	human	0.303	0.446	0.282	0.5	0.284	0.303	-	-	-	-
	all	0.423	0.682	0.485	0.25	0.5	0.418	0.482	0.25	0.516	0.478
nei-g5-50	ship	0.423	0.723	0.427	0	0.515	0.436	-	-	-	-
	aircraft	0.523	0.907	0.526	nan	0.75	0.482	-	-	-	-
	human	0.211	0.38	0.119	0.4	0.162	0.303	-	-	-	-
	all	0.386	0.67	0.357	0.2	0.476	0.407	0.434	0.2	0.476	0.451
nei-p30	ship	0.423	0.683	0.573	0	0.507	0.436	-	-	-	-
	aircraft	0.492	0.893	0.515	nan	0.65	0.459	-	-	-	-
	human	0.229	0.446	0.119	0.433	0.122	0.337	-	-	-	-
	all	0.381	0.674	0.402	0.217	0.427	0.411	0.445	0.25	0.429	0.482
nei-p5-50	ship	0.362	0.677	0.401	0	0.401	0.381	-	-	-	-
	aircraft	0.465	0.888	0.396	nan	0.703	0.434	-	-	-	-
	human	0.211	0.446	0.212	0.3	0.223	0.202	-	-	-	-
	all	0.346	0.67	0.336	0.15	0.442	0.339	0.423	0.15	0.486	0.409

Table A.6: The SCTD dataset is detected using the YOLOX algorithm. “noisy” represents the original noise dataset, and dspnet, b2ub, and nei represent the target detection after denoising using the DSPNet, Blind2Unblind, and Neighbor2Neighbor single-frame denoising algorithms, respectively. Bold fonts indicate data that is higher than the corresponding “noisy” dataset.

Denoising	SSDMobileNetV2										
	class	mAP	mAP@0.5	mAP@0.75	mAP_s	mAP_m	mAP_l	AR	AR_s	AR_m	AR_l
noisy	object/all	0.186	0.392	0.158	0.004	0.024	0.296	0.297	0.047	0.158	0.414
dspnet	object/all	0.177	0.381	0.152	0.014	0.027	0.295	0.293	0.058	0.16	0.405
b2ub-g25	object/all	0.176	0.389	0.163	0.021	0.021	0.291	0.296	0.062	0.161	0.408
b2ub-g5-50	object/all	0.186	0.39	0.163	0.011	0.019	0.298	0.294	0.077	0.145	0.411
b2ub-p30	object/all	0.171	0.364	0.15	0.005	0.021	0.301	0.296	0.046	0.158	0.413
b2ub-p5-50	object/all	0.177	0.388	0.145	0.017	0.027	0.3	0.302	0.067	0.172	0.411
nei-g25	object/all	0.191	0.396	0.17	0.006	0.015	0.308	0.299	0.061	0.159	0.415
nei-g5-50	object/all	0.184	0.39	0.162	0.014	0.014	0.305	0.299	0.064	0.15	0.418
nei-p30	object/all	0.18	0.392	0.152	0.016	0.023	0.304	0.302	0.07	0.159	0.418
nei-p5-50	object/all	0.175	0.382	0.141	0.026	0.026	0.293	0.298	0.073	0.166	0.407

Table A.7: The URPC_sonarimage_dataset dataset is detected using the SSDMobileNetV2 algorithm. “noisy” represents the original noise dataset, and dspnet, b2ub, and nei represent the target detection after denoising using the DSPNet, Blind2Unblind, and Neighbor2Neighbor single-frame denoising algorithms, respectively. Bold fonts indicate data that is higher than the corresponding “noisy” dataset.

Denoising	Faster R-CNN										
	class	mAP	mAP@0.5	mAP@0.75	mAP_s	mAP_m	mAP_l	AR	AR_s	AR_m	AR_l
noisy	object/all	0.271	0.562	0.243	0.155	0.104	0.368	0.365	0.222	0.264	0.443
dspnet	object/all	0.262	0.546	0.226	0.11	0.1	0.365	0.353	0.221	0.232	0.44
b2ub-g25	object/all	0.248	0.523	0.214	0.078	0.085	0.353	0.354	0.141	0.242	0.449
b2ub-g5-50	object/all	0.264	0.553	0.232	0.127	0.099	0.369	0.362	0.225	0.236	0.452
b2ub-p30	object/all	0.271	0.572	0.235	0.146	0.111	0.365	0.365	0.251	0.26	0.439
b2ub-p5-50	object/all	0.269	0.567	0.226	0.121	0.107	0.375	0.365	0.213	0.246	0.454
nei-g25	object/all	0.266	0.55	0.23	0.105	0.104	0.371	0.354	0.183	0.232	0.448
nei-g5-50	object/all	0.261	0.548	0.219	0.119	0.094	0.37	0.363	0.223	0.225	0.459
nei-p30	object/all	0.271	0.565	0.235	0.147	0.103	0.372	0.369	0.248	0.247	0.453
nei-p5-50	object/all	0.26	0.56	0.23	0.125	0.101	0.365	0.35	0.204	0.229	0.439

Table A.8: The URPC_sonarimage_dataset dataset is detected using the Faster R-CNN algorithm. “noisy” represents the original noise dataset, and dspnet, b2ub, and nei represent the target detection after denoising using the DSPNet, Blind2Unblind, and Neighbor2Neighbor single-frame denoising algorithms, respectively. Bold fonts indicate data that is higher than the corresponding “noisy” dataset.

Denoising	SSD300										
	class	mAP	mAP@0.5	mAP@0.75	mAP_s	mAP_m	mAP_l	AR	AR_s	AR_m	AR_l
noisy	object/all	0.217	0.491	0.178	0.071	0.059	0.312	0.352	0.18	0.264	0.427
dspnet	object/all	0.213	0.468	0.188	0.065	0.055	0.309	0.345	0.163	0.272	0.415
b2ub-g25	object/all	0.215	0.485	0.17	0.06	0.063	0.308	0.344	0.14	0.259	0.425
b2ub-g5-50	object/all	0.219	0.496	0.177	0.066	0.066	0.313	0.359	0.196	0.269	0.434
b2ub-p30	object/all	0.218	0.502	0.159	0.069	0.063	0.313	0.355	0.19	0.278	0.425
b2ub-p5-50	object/all	0.137	0.346	0.095	0.05	0.042	0.201	0.291	0.136	0.242	0.343
nei-g25	object/all	0.216	0.502	0.179	0.078	0.062	0.311	0.349	0.192	0.268	0.42
nei-g5-50	object/all	0.218	0.488	0.173	0.066	0.062	0.314	0.35	0.15	0.274	0.425
nei-p30	object/all	0.223	0.518	0.18	0.077	0.071	0.314	0.36	0.196	0.283	0.428
nei-p5-50	object/all	0.219	0.492	0.178	0.081	0.056	0.318	0.355	0.23	0.273	0.42

Table A.9: The URPC_sonarimage_dataset dataset is detected using the SSD300 algorithm. “noisy” represents the original noise dataset, and dspnet, b2ub, and nei represent the target detection after denoising using the DSPNet, Blind2Unblind, and Neighbor2Neighbor single-frame denoising algorithms, respectively. Bold fonts indicate data that is higher than the corresponding “noisy” dataset.

Denoising	YOLOX										
	class	mAP	mAP_50	mAP_75	mAP_s	mAP_m	mAP_l	AR	AR_s	AR_m	AR_l
noisy	object/all	0.278	0.582	0.231	0.091	0.114	0.381	0.376	0.158	0.285	0.463
dspnet	object/all	0.264	0.551	0.232	0.102	0.091	0.367	0.354	0.151	0.257	0.441
b2ub-g25	object/all	0.281	0.584	0.242	0.129	0.107	0.383	0.383	0.2	0.288	0.466
b2ub-g5-50	object/all	0.274	0.579	0.236	0.104	0.116	0.375	0.369	0.152	0.273	0.457
b2ub-p30	object/all	0.275	0.585	0.226	0.097	0.107	0.381	0.367	0.15	0.264	0.459
b2ub-p5-50	object/all	0.275	0.586	0.233	0.098	0.12	0.375	0.371	0.142	0.286	0.456
nei-g25	object/all	0.27	0.564	0.223	0.103	0.095	0.372	0.369	0.152	0.283	0.452
nei-g5-50	object/all	0.272	0.567	0.236	0.112	0.098	0.372	0.37	0.166	0.286	0.45
nei-p30	object/all	0.272	0.589	0.22	0.111	0.112	0.369	0.373	0.165	0.3	0.448
nei-p5-50	object/all	0.268	0.57	0.223	0.098	0.1	0.373	0.366	0.138	0.27	0.457

Table A.10: The URPC_sonarimage_dataset dataset is detected using the YOLOX algorithm. “noisy” represents the original noise dataset, and dspnet, b2ub, and nei represent the target detection after denoising using the DSPNet, Blind2Unblind, and Neighbor2Neighbor single-frame denoising algorithms, respectively. Bold fonts indicate data that is higher than the corresponding “noisy” dataset.

Denoising	class	SSDMobileNetV2									
		mAP	mAP_50	mAP_75	mAP_s	mAP_m	mAP_l	AR	AR_s	AR_m	AR_l
noisy	Bottle	0.739	0.981	0.948	0.2	0.735	nan	-	-	-	-
	Can	0.34	0.652	0.314	0.348	0.352	nan	-	-	-	-
	Chain	0.687	0.949	0.834	0.217	0.457	0.738	-	-	-	-
	Drink-carton	0.567	0.887	0.699	0.595	0.537	nan	-	-	-	-
	Hook	0.727	0.956	0.956	nan	0.727	nan	-	-	-	-
	Propeller	0.708	0.989	0.882	0.5	0.715	0.8	-	-	-	-
	Shampoo-bottle	0.71	0.968	0.968	nan	0.708	0.8	-	-	-	-
	Standing-bottle	0.788	1	1	nan	0.788	nan	-	-	-	-
	Tire	0.805	0.99	0.955	0.8	0.81	0.3	-	-	-	-
	Valve	0.725	0.927	0.901	0.383	0.751	0	-	-	-	-
	Wall	0.713	0.916	0.841	0.304	0.7	0.84	-	-	-	-
	all	0.683	0.929	0.845	0.418	0.662	0.58	0.743	0.571	0.729	0.596
dspnet	Bottle	0.749	0.979	0.917	0.3	0.746	nan	-	-	-	-
	Can	0.331	0.565	0.358	0.407	0.339	nan	-	-	-	-
	Chain	0.691	0.946	0.861	0.6	0.478	0.732	-	-	-	-
	Drink-carton	0.555	0.955	0.556	0.544	0.588	nan	-	-	-	-
	Hook	0.693	0.947	0.834	nan	0.693	nan	-	-	-	-
	Propeller	0.633	0.98	0.747	0.4	0.642	0.6	-	-	-	-
	Shampoo-bottle	0.681	0.957	0.957	nan	0.681	0.7	-	-	-	-
	Standing-bottle	0.786	1	1	nan	0.786	nan	-	-	-	-
	Tire	0.797	0.99	0.936	0.6	0.803	0.5	-	-	-	-
	Valve	0.701	0.917	0.847	0	0.733	0	-	-	-	-
	Wall	0.715	0.933	0.805	0.365	0.693	0.832	-	-	-	-
	all	0.667	0.924	0.802	0.402	0.653	0.561	0.729	0.469	0.724	0.575
b2ub-g25	Bottle	0.745	0.981	0.952	0.2	0.74	nan	-	-	-	-
	Can	0.336	0.617	0.298	0.335	0.356	nan	-	-	-	-
	Chain	0.688	0.952	0.847	0.317	0.425	0.736	-	-	-	-
	Drink-carton	0.572	0.951	0.599	0.588	0.565	nan	-	-	-	-
	Hook	0.721	0.95	0.929	nan	0.721	nan	-	-	-	-
	Propeller	0.678	0.984	0.83	0.5	0.684	0.7	-	-	-	-
	Shampoo-bottle	0.724	0.951	0.951	nan	0.716	0.9	-	-	-	-
	Standing-bottle	0.782	1	1	nan	0.782	nan	-	-	-	-
	Tire	0.803	0.99	0.944	0.6	0.81	0.3	-	-	-	-
	Valve	0.691	0.919	0.873	0.2	0.729	0	-	-	-	-
	Wall	0.699	0.919	0.813	0.28	0.688	0.827	-	-	-	-
	all	0.676	0.929	0.822	0.377	0.656	0.577	0.74	0.475	0.73	0.593
b2ub-g5-50	Bottle	0.746	0.976	0.943	0.2	0.742	nan	-	-	-	-
	Can	0.346	0.629	0.39	0.384	0.355	nan	-	-	-	-
	Chain	0.693	0.95	0.837	0.65	0.489	0.728	-	-	-	-
	Drink-carton	0.551	0.93	0.664	0.585	0.516	nan	-	-	-	-
	Hook	0.727	0.944	0.944	nan	0.727	nan	-	-	-	-
	Propeller	0.68	0.985	0.836	0.5	0.685	0.7	-	-	-	-
	Shampoo-bottle	0.722	0.968	0.968	nan	0.725	0.7	-	-	-	-
	Standing-bottle	0.798	1	0.871	nan	0.798	nan	-	-	-	-
	Tire	0.815	0.989	0.958	0.8	0.823	0	-	-	-	-
	Valve	0.7	0.911	0.886	0	0.735	0	-	-	-	-
	Wall	0.715	0.93	0.828	0.304	0.701	0.852	-	-	-	-
	all	0.681	0.928	0.83	0.428	0.663	0.497	0.744	0.505	0.737	0.511

Table A.11: The MarinDebris dataset is detected using the SSDMobileNetV2 algorithm (Part 1 of 3). “noisy” represents the original noise dataset, and dspnet, b2ub, and nei represent the target detection after denoising using the DSPNet, Blind2Unblind, and Neighbor2Neighbor single-frame denoising algorithms, respectively. Bold fonts indicate data that is higher than the corresponding “noisy” dataset.

	Bottle	0.749	0.984	0.973	0.35	0.743	nan	-	-	-	-
b2ub-p30	Can	0.371	0.649	0.357	0.375	0.388	nan	-	-	-	-
	Chain	0.683	0.95	0.825	0.601	0.44	0.723	-	-	-	-
	Drink-carton	0.547	0.931	0.558	0.527	0.59	nan	-	-	-	-
	Hook	0.739	0.951	0.951	nan	0.739	nan	-	-	-	-
	Propeller	0.689	0.991	0.895	0.7	0.692	0.7	-	-	-	-
	Shampoo-bottle	0.738	0.958	0.958	nan	0.735	0.8	-	-	-	-
	Standing-bottle	0.791	1	1	nan	0.791	nan	-	-	-	-
	Tire	0.804	0.99	0.947	0.6	0.812	0.2	-	-	-	-
	Valve	0.687	0.906	0.877	0	0.725	0	-	-	-	-
	Wall	0.723	0.926	0.852	0.325	0.716	0.835	-	-	-	-
b2ub-p5-50	all	0.684	0.93	0.836	0.435	0.67	0.543	0.744	0.503	0.741	0.559
	Bottle	0.749	0.986	0.965	0.25	0.745	nan	-	-	-	-
	Can	0.492	0.838	0.501	0.528	0.486	nan	-	-	-	-
	Chain	0.686	0.963	0.84	0.734	0.554	0.718	-	-	-	-
	Drink-carton	0.641	0.978	0.832	0.663	0.619	nan	-	-	-	-
	Hook	0.695	0.954	0.935	nan	0.695	nan	-	-	-	-
	Propeller	0.663	0.974	0.773	0.6	0.667	0.7	-	-	-	-
	Shampoo-bottle	0.702	0.957	0.843	nan	0.724	0.4	-	-	-	-
	Standing-bottle	0.725	1	0.871	nan	0.725	nan	-	-	-	-
	Tire	0.809	0.97	0.937	0.3	0.822	0	-	-	-	-
nei-g25	Valve	0.689	0.918	0.821	0	0.72	0	-	-	-	-
	Wall	0.717	0.936	0.843	0.371	0.719	0.794	-	-	-	-
	all	0.688	0.952	0.833	0.431	0.679	0.435	0.761	0.515	0.753	0.461
	Bottle	0.742	0.981	0.961	0.3	0.737	nan	-	-	-	-
	Can	0.332	0.64	0.298	0.349	0.347	nan	-	-	-	-
	Chain	0.689	0.924	0.825	0.751	0.486	0.725	-	-	-	-
	Drink-carton	0.568	0.984	0.558	0.578	0.568	nan	-	-	-	-
	Hook	0.725	0.954	0.929	nan	0.725	nan	-	-	-	-
	Propeller	0.674	0.984	0.805	0.6	0.678	0.7	-	-	-	-
nei-g5-50	Shampoo-bottle	0.725	0.971	0.971	nan	0.724	0.8	-	-	-	-
	Standing-bottle	0.72	1	1	nan	0.72	nan	-	-	-	-
	Tire	0.806	0.99	0.969	0.5	0.811	0.6	-	-	-	-
	Valve	0.713	0.925	0.881	0.25	0.742	0	-	-	-	-
	Wall	0.725	0.928	0.837	0.336	0.714	0.843	-	-	-	-
	all	0.674	0.935	0.821	0.458	0.659	0.611	0.739	0.557	0.727	0.629

Table A.12: The MarinDebris dataset is detected using the SSDMobileNetV2 algorithm (Part 2 of 3). “noisy” represents the original noise dataset, and dspnet, b2ub, and nei represent the target detection after denoising using the DSPNet, Blind2Unblind, and Neighbor2Neighbor single-frame denoising algorithms, respectively. Bold fonts indicate data that is higher than the corresponding “noisy” dataset.

	Bottle	0.751	0.981	0.963	0.167	0.749	nan	-	-	-	-
	Can	0.354	0.624	0.357	0.344	0.379	nan	-	-	-	-
	Chain	0.684	0.95	0.8	0.251	0.455	0.733	-	-	-	-
	Drink-carton	0.578	0.958	0.65	0.578	0.585	nan	-	-	-	-
	Hook	0.701	0.944	0.914	nan	0.701	nan	-	-	-	-
nei-p30	Propeller	0.632	0.964	0.77	0.6	0.638	0.6	-	-	-	-
	Shampoo-bottle	0.735	0.964	0.964	nan	0.729	0.9	-	-	-	-
	Standing-bottle	0.736	1	1	nan	0.736	nan	-	-	-	-
	Tire	0.808	0.99	0.956	0.6	0.813	0.5	-	-	-	-
	Valve	0.72	0.944	0.901	0.2	0.751	0	-	-	-	-
	Wall	0.703	0.925	0.817	0.284	0.691	0.84	-	-	-	-
	all	0.673	0.931	0.826	0.378	0.657	0.595	0.738	0.465	0.731	0.614
	Bottle	0.755	0.982	0.961	0.5	0.752	nan	-	-	-	-
	Can	0.343	0.644	0.305	0.333	0.365	nan	-	-	-	-
	Chain	0.688	0.968	0.804	0.501	0.431	0.734	-	-	-	-
nei-p5-50	Drink-carton	0.577	0.953	0.648	0.574	0.594	nan	-	-	-	-
	Hook	0.736	0.948	0.929	nan	0.736	nan	-	-	-	-
	Propeller	0.681	0.983	0.834	0.6	0.686	0.6	-	-	-	-
	Shampoo-bottle	0.736	0.958	0.958	nan	0.734	0.8	-	-	-	-
	Standing-bottle	0.803	1	1	nan	0.803	nan	-	-	-	-
	Tire	0.803	0.98	0.938	0.5	0.813	0	-	-	-	-
	Valve	0.681	0.914	0.887	0	0.712	0	-	-	-	-
	Wall	0.717	0.93	0.848	0.304	0.718	0.83	-	-	-	-
	all	0.684	0.933	0.828	0.414	0.668	0.494	0.745	0.437	0.74	0.512

Table A.13: The MarinDebris dataset is detected using the SSDMobileNetV2 algorithm (Part 3 of 3). “noisy” represents the original noise dataset, and dspnet, b2ub, and nei represent the target detection after denoising using the DSPNet, Blind2Unblind, and Neighbor2Neighbor single-frame denoising algorithms, respectively. Bold fonts indicate data that is higher than the corresponding “noisy” dataset.

Denoising		Faster R-CNN											
		class	mAP	mAP@0.5	mAP@0.75	mAP_s	mAP_m	mAP_l	AR	AR_s	AR_m	AR_l	
noisy	Bottle	0.766	0.985	0.974	0.7	0.761	nan	-	-	-	-	-	
	Can	0.493	0.821	0.509	0.514	0.489	nan	-	-	-	-	-	
	Chain	0.676	0.963	0.813	0.701	0.524	0.704	-	-	-	-	-	
	Drink-carton	0.65	0.995	0.827	0.643	0.664	nan	-	-	-	-	-	
	Hook	0.655	0.927	0.84	nan	0.655	nan	-	-	-	-	-	
	Propeller	0.652	0.945	0.745	0.5	0.655	0.7	-	-	-	-	-	
	Shampoo-bottle	0.724	0.964	0.894	nan	0.729	0.8	-	-	-	-	-	
	Standing-bottle	0.78	1	1	nan	0.78	nan	-	-	-	-	-	
	Tire	0.812	0.989	0.945	0.1	0.824	0	-	-	-	-	-	
	Valve	0.692	0.917	0.86	0	0.722	0	-	-	-	-	-	
	Wall	0.716	0.935	0.85	0.413	0.723	0.778	-	-	-	-	-	
	all	0.692	0.949	0.842	0.446	0.684	0.497	0.763	0.502	0.754	0.525		
dspnet	Bottle	0.746	0.985	0.933	0.7	0.742	nan	-	-	-	-	-	
	Can	0.428	0.808	0.447	0.417	0.444	nan	-	-	-	-	-	
	Chain	0.667	0.964	0.833	0.635	0.462	0.709	-	-	-	-	-	
	Drink-carton	0.632	0.993	0.782	0.626	0.658	nan	-	-	-	-	-	
	Hook	0.675	0.934	0.818	nan	0.675	nan	-	-	-	-	-	
	Propeller	0.595	0.966	0.678	0.3	0.603	0.5	-	-	-	-	-	
	Shampoo-bottle	0.715	0.969	0.909	nan	0.718	0.8	-	-	-	-	-	
	Standing-bottle	0.73	1	0.901	nan	0.73	nan	-	-	-	-	-	
	Tire	0.792	0.999	0.94	0.1	0.803	0.3	-	-	-	-	-	
	Valve	0.676	0.917	0.806	0	0.705	0	-	-	-	-	-	
	Wall	0.705	0.923	0.827	0.371	0.711	0.772	-	-	-	-	-	
	all	0.669	0.951	0.807	0.394	0.659	0.513	0.74	0.487	0.731	0.536		
b2ub-g25	Bottle	0.759	0.986	0.963	0.3	0.754	nan	-	-	-	-	-	
	Can	0.499	0.827	0.493	0.564	0.478	nan	-	-	-	-	-	
	Chain	0.678	0.969	0.786	0.75	0.499	0.715	-	-	-	-	-	
	Drink-carton	0.66	0.989	0.754	0.651	0.688	nan	-	-	-	-	-	
	Hook	0.715	0.939	0.914	nan	0.715	nan	-	-	-	-	-	
	Propeller	0.659	0.99	0.822	0.6	0.66	0.7	-	-	-	-	-	
	Shampoo-bottle	0.721	0.98	0.919	nan	0.73	0.6	-	-	-	-	-	
	Standing-bottle	0.712	1	0.811	nan	0.712	nan	-	-	-	-	-	
	Tire	0.813	0.96	0.942	0	0.829	0	-	-	-	-	-	
	Valve	0.684	0.918	0.879	0	0.713	0	-	-	-	-	-	
	Wall	0.721	0.94	0.829	0.361	0.735	0.788	-	-	-	-	-	
	all	0.693	0.954	0.828	0.403	0.683	0.467	0.762	0.48	0.754	0.492		
b2ub-g5-50	Bottle	0.765	0.986	0.975	0.233	0.76	nan	-	-	-	-	-	
	Can	0.512	0.844	0.508	0.552	0.503	nan	-	-	-	-	-	
	Chain	0.689	0.965	0.836	0.75	0.562	0.716	-	-	-	-	-	
	Drink-carton	0.643	0.976	0.808	0.662	0.623	nan	-	-	-	-	-	
	Hook	0.709	0.948	0.897	nan	0.709	nan	-	-	-	-	-	
	Propeller	0.676	0.975	0.874	0.6	0.681	0.7	-	-	-	-	-	
	Shampoo-bottle	0.704	0.978	0.882	nan	0.72	0.4	-	-	-	-	-	
	Standing-bottle	0.818	1	1	nan	0.818	nan	-	-	-	-	-	
	Tire	0.824	0.989	0.938	0.3	0.836	0	-	-	-	-	-	
	Valve	0.696	0.92	0.865	0	0.726	0	-	-	-	-	-	
	Wall	0.716	0.914	0.847	0.324	0.73	0.784	-	-	-	-	-	
	all	0.705	0.954	0.857	0.428	0.697	0.433	0.768	0.531	0.758	0.494		

Table A.14: The MarinDebris dataset is detected using the Faster R-CNN algorithm (Part 1 of 3). “noisy” represents the original noise dataset, and dspnet, b2ub, and nei represent the target detection after denoising using the DSPNet, Blind2Unblind, and Neighbor2Neighbor single-frame denoising algorithms, respectively. Bold fonts indicate data that is higher than the corresponding “noisy” dataset.

	Bottle	0.766	0.986	0.965	0.5	0.762	nan	-	-	-	-
	Can	0.489	0.829	0.517	0.534	0.481	nan	-	-	-	-
	Chain	0.686	0.97	0.846	0.75	0.526	0.718	-	-	-	-
	Drink-carton	0.639	0.977	0.808	0.657	0.636	nan	-	-	-	-
	Hook	0.706	0.938	0.88	nan	0.706	nan	-	-	-	-
b2ub-p30	Propeller	0.669	0.977	0.78	0.6	0.671	0.7	-	-	-	-
	Shampoo-bottle	0.711	0.957	0.896	nan	0.713	0.8	-	-	-	-
	Standing-bottle	0.711	1	0.871	nan	0.771	nan	-	-	-	-
	Tire	0.807	0.979	0.939	0.2	0.818	0	-	-	-	-
	Valve	0.691	0.92	0.863	0	0.721	0	-	-	-	-
	Wall	0.717	0.934	0.821	0.36	0.725	0.78	-	-	-	-
	all	0.696	0.952	0.835	0.45	0.685	0.5	0.764	0.52	0.752	0.526
b2ub-p5-50	Bottle	0.749	0.986	0.965	0.25	0.745	nan	-	-	-	-
	Can	0.492	0.838	0.501	0.528	0.486	nan	-	-	-	-
	Chain	0.686	0.963	0.84	0.734	0.554	0.718	-	-	-	-
	Drink-carton	0.641	0.978	0.832	0.663	0.619	nan	-	-	-	-
	Hook	0.695	0.954	0.935	nan	0.695	nan	-	-	-	-
	Propeller	0.663	0.974	0.773	0.6	0.667	0.7	-	-	-	-
	Shampoo-bottle	0.702	0.957	0.843	nan	0.724	0.4	-	-	-	-
	Standing-bottle	0.725	1	0.871	nan	0.725	nan	-	-	-	-
	Tire	0.809	0.97	0.937	0.3	0.822	0	-	-	-	-
	Valve	0.689	0.918	0.821	0	0.72	0	-	-	-	-
	Wall	0.717	0.936	0.843	0.371	0.719	0.794	-	-	-	-
	all	0.688	0.952	0.833	0.431	0.679	0.435	0.761	0.515	0.753	0.461
nei-g25	Bottle	0.764	0.988	0.978	0.7	0.757	nan	-	-	-	-
	Can	0.492	0.847	0.499	0.524	0.498	nan	-	-	-	-
	Chain	0.672	0.965	0.812	0.617	0.522	0.707	-	-	-	-
	Drink-carton	0.637	0.996	0.84	0.653	0.623	nan	-	-	-	-
	Hook	0.676	0.931	0.905	nan	0.676	nan	-	-	-	-
	Propeller	0.654	0.979	0.822	0.25	0.662	0.7	-	-	-	-
	Shampoo-bottle	0.697	0.967	0.859	nan	0.721	0.267	-	-	-	-
	Standing-bottle	0.777	1	1	nan	0.777	nan	-	-	-	-
	Tire	0.802	0.979	0.949	0.1	0.816	0	-	-	-	-
	Valve	0.674	0.92	0.824	0	0.703	0	-	-	-	-
	Wall	0.711	0.926	0.834	0.399	0.719	0.773	-	-	-	-
	all	0.687	0.954	0.847	0.405	0.68	0.408	0.757	0.506	0.746	0.458
nei-g5-50	Bottle	0.762	0.984	0.964	0.25	0.758	nan	-	-	-	-
	Can	0.471	0.83	0.471	0.491	0.469	nan	-	-	-	-
	Chain	0.685	0.961	0.882	0.8	0.529	0.714	-	-	-	-
	Drink-carton	0.628	0.975	0.821	0.639	0.626	nan	-	-	-	-
	Hook	0.718	0.954	0.906	nan	0.718	nan	-	-	-	-
	Propeller	0.692	0.979	0.835	0.6	0.695	0.8	-	-	-	-
	Shampoo-bottle	0.714	0.961	0.892	nan	0.716	0.7	-	-	-	-
	Standing-bottle	0.794	1	1	nan	0.794	nan	-	-	-	-
	Tire	0.806	0.969	0.958	0	0.821	0	-	-	-	-
	Valve	0.687	0.935	0.838	0	0.717	0	-	-	-	-
	Wall	0.728	0.914	0.824	0.342	0.743	0.795	-	-	-	-
	all	0.699	0.951	0.854	0.39	0.689	0.501	0.77	0.472	0.758	0.525

Table A.15: The MarinDebris dataset is detected using the Faster R-CNN algorithm (Part 2 of 3). “noisy” represents the original noise dataset, and dspnet, b2ub, and nei represent the target detection after denoising using the DSPNet, Blind2Unblind, and Neighbor2Neighbor single-frame denoising algorithms, respectively. Bold fonts indicate data that is higher than the corresponding “noisy” dataset.

	Bottle	0.758	0.985	0.974	0.3	0.754	nan	-	-	-	-
	Can	0.489	0.843	0.473	0.541	0.481	nan	-	-	-	-
	Chain	0.693	0.967	0.855	0.75	0.522	0.723	-	-	-	-
	Drink-carton	0.638	0.995	0.813	0.645	0.639	nan	-	-	-	-
	Hook	0.693	0.934	0.934	nan	0.693	nan	-	-	-	-
nei-p30	Propeller	0.654	0.973	0.799	0.5	0.66	0.6	-	-	-	-
	Shampoo-bottle	0.674	0.983	0.87	nan	0.686	0.5	-	-	-	-
	Standing-bottle	0.772	1	0.822	nan	0.772	nan	-	-	-	-
	Tire	0.804	0.97	0.948	0.2	0.817	0	-	-	-	-
	Valve	0.677	0.92	0.881	0	0.706	0	-	-	-	-
	Wall	0.705	0.915	0.813	0.332	0.717	0.773	-	-	-	-
	all	0.687	0.953	0.835	0.409	0.677	0.433	0.758	0.495	0.751	0.46
	Bottle	0.76	0.987	0.965	0.4	0.757	nan	-	-	-	-
	Can	0.474	0.831	0.481	0.514	0.462	nan	-	-	-	-
	Chain	0.689	0.964	0.878	0.7	0.533	0.719	-	-	-	-
nei-p5-50	Drink-carton	0.63	0.977	0.789	0.662	0.59	nan	-	-	-	-
	Hook	0.682	0.945	0.897	nan	0.682	nan	-	-	-	-
	Propeller	0.658	0.972	0.845	0.6	0.658	0.7	-	-	-	-
	Shampoo-bottle	0.712	0.964	0.964	nan	0.726	0.6	-	-	-	-
	Standing-bottle	0.767	1	1	nan	0.767	nan	-	-	-	-
	Tire	0.811	0.977	0.925	0	0.826	0	-	-	-	-
	Valve	0.682	0.915	0.836	0	0.712	0	-	-	-	-
	Wall	0.725	0.921	0.844	0.37	0.738	0.795	-	-	-	-
	all	0.69	0.95	0.857	0.406	0.678	0.469	0.759	0.446	0.748	0.492

Table A.16: The MarinDebris dataset is detected using the Faster R-CNN algorithm (Part 3 of 3). “noisy” represents the original noise dataset, and dspnet, b2ub, and nei represent the target detection after denoising using the DSPNet, Blind2Unblind, and Neighbor2Neighbor single-frame denoising algorithms, respectively. Bold fonts indicate data that is higher than the corresponding “noisy” dataset.

Denoising		SSD300											
		class	mAP	mAP@0.5	mAP@0.75	mAP_s	mAP_m	mAP_l	AR	AR_s	AR_m	AR_l	
noisy	Bottle	0.753	0.986	0.975	0.7	0.748	nan	-	-	-	-	-	
	Can	0.452	0.779	0.452	0.538	0.436	nan	-	-	-	-	-	
	Chain	0.683	0.968	0.844	0.825	0.506	0.708	-	-	-	-	-	
	Drink-carton	0.594	0.972	0.753	0.59	0.624	nan	-	-	-	-	-	
	Hook	0.719	0.952	0.952	nan	0.719	nan	-	-	-	-	-	
	Propeller	0.677	0.993	0.835	0.4	0.688	0.6	-	-	-	-	-	
	Shampoo-bottle	0.709	0.95	0.902	nan	0.738	0.3	-	-	-	-	-	
	Standing-bottle	0.726	1	0.822	nan	0.726	nan	-	-	-	-	-	
	Tire	0.8	0.998	0.935	0.6	0.805	0.5	-	-	-	-	-	
	Valve	0.715	0.949	0.848	0.3	0.741	0	-	-	-	-	-	
	Wall	0.71	0.926	0.831	0.279	0.715	0.818	-	-	-	-	-	
	all	0.685	0.952	0.832	0.529	0.677	0.488	0.749	0.573	0.744	0.505		
dspnet	Bottle	0.737	0.982	0.926	0.233	0.734	nan	-	-	-	-	-	
	Can	0.436	0.845	0.491	0.487	0.433	nan	-	-	-	-	-	
	Chain	0.677	0.972	0.792	0.701	0.483	0.714	-	-	-	-	-	
	Drink-carton	0.562	0.942	0.634	0.55	0.585	nan	-	-	-	-	-	
	Hook	0.709	0.959	0.931	nan	0.709	nan	-	-	-	-	-	
	Propeller	0.635	0.974	0.732	0.5	0.641	0.6	-	-	-	-	-	
	Shampoo-bottle	0.705	0.951	0.951	nan	0.706	0.9	-	-	-	-	-	
	Standing-bottle	0.702	1	0.861	nan	0.702	nan	-	-	-	-	-	
	Tire	0.784	0.998	0.919	0.5	0.791	0.3	-	-	-	-	-	
	Valve	0.706	0.932	0.862	0	0.736	0	-	-	-	-	-	
	Wall	0.709	0.925	0.831	0.283	0.724	0.796	-	-	-	-	-	
	all	0.669	0.953	0.812	0.407	0.659	0.552	0.736	0.515	0.721	0.57		
b2ub-g25	Bottle	0.762	0.986	0.975	0.9	0.755	nan	-	-	-	-	-	
	Can	0.444	0.751	0.426	0.551	0.429	nan	-	-	-	-	-	
	Chain	0.683	0.972	0.822	0.735	0.527	0.71	-	-	-	-	-	
	Drink-carton	0.604	0.992	0.736	0.606	0.614	nan	-	-	-	-	-	
	Hook	0.724	0.953	0.953	nan	0.724	nan	-	-	-	-	-	
	Propeller	0.683	0.983	0.845	0.35	0.685	0.7	-	-	-	-	-	
	Shampoo-bottle	0.729	0.959	0.903	nan	0.757	0.3	-	-	-	-	-	
	Standing-bottle	0.769	1	1	nan	0.769	nan	-	-	-	-	-	
	Tire	0.811	0.999	0.955	0.6	0.817	0.5	-	-	-	-	-	
	Valve	0.709	0.918	0.872	0	0.74	0	-	-	-	-	-	
	Wall	0.714	0.92	0.83	0.347	0.716	0.823	-	-	-	-	-	
	all	0.694	0.948	0.847	0.511	0.685	0.506	0.76	0.605	0.753	0.521		
b2ub-g5-50	Bottle	0.755	0.985	0.962	0.267	0.749	nan	-	-	-	-	-	
	Can	0.45	0.778	0.496	0.538	0.435	nan	-	-	-	-	-	
	Chain	0.711	0.974	0.848	0.9	0.546	0.732	-	-	-	-	-	
	Drink-carton	0.62	0.991	0.77	0.621	0.644	nan	-	-	-	-	-	
	Hook	0.726	0.953	0.903	nan	0.726	nan	-	-	-	-	-	
	Propeller	0.684	0.978	0.784	0.6	0.69	0.6	-	-	-	-	-	
	Shampoo-bottle	0.766	0.971	0.971	nan	0.771	0.7	-	-	-	-	-	
	Standing-bottle	0.745	1	1	nan	0.745	nan	-	-	-	-	-	
	Tire	0.804	0.989	0.954	0.4	0.809	0.6	-	-	-	-	-	
	Valve	0.698	0.93	0.837	0	0.729	0	-	-	-	-	-	
	Wall	0.725	0.931	0.832	0.356	0.73	0.813	-	-	-	-	-	
	all	0.699	0.953	0.851	0.46	0.689	0.574	0.767	0.568	0.762	0.59		

Table A.17: The MarinDebris dataset is detected using the SSD300 algorithm (Part 1 of 3). “noisy” represents the original noise dataset, and dspnet, b2ub, and nei represent the target detection after denoising using the DSPNet, Blind2Unblind, and Neighbor2Neighbor single-frame denoising algorithms, respectively. Bold fonts indicate data that is higher than the corresponding “noisy” dataset.

	Bottle	0.745	0.984	0.973	0.233	0.74	nan	-	-	-	-
	Can	0.455	0.751	0.498	0.585	0.429	nan	-	-	-	-
	Chain	0.679	0.956	0.867	0.65	0.519	0.713	-	-	-	-
	Drink-carton	0.624	0.995	0.782	0.634	0.623	nan	-	-	-	-
	Hook	0.727	0.956	0.956	nan	0.727	nan	-	-	-	-
b2ub-p30	Propeller	0.679	0.988	0.851	0.5	0.688	0.6	-	-	-	-
	Shampoo-bottle	0.74	0.969	0.969	nan	0.74	0.8	-	-	-	-
	Standing-bottle	0.774	1	0.822	nan	0.774	nan	-	-	-	-
	Tire	0.811	0.999	0.954	0.2	0.819	0.5	-	-	-	-
	Valve	0.697	0.919	0.869	0	0.726	0	-	-	-	-
	Wall	0.718	0.922	0.821	0.351	0.724	0.81	-	-	-	-
	all	0.695	0.949	0.851	0.394	0.683	0.57	0.759	0.493	0.746	0.588
b2ub-p5-50	Bottle	0.754	0.985	0.962	0.8	0.749	nan	-	-	-	-
	Can	0.453	0.761	0.454	0.527	0.452	nan	-	-	-	-
	Chain	0.684	0.95	0.815	0.9	0.502	0.714	-	-	-	-
	Drink-carton	0.629	0.991	0.754	0.631	0.638	nan	-	-	-	-
	Hook	0.722	0.953	0.934	nan	0.722	nan	-	-	-	-
	Propeller	0.697	0.983	0.837	0.3	0.705	0.6	-	-	-	-
	Shampoo-bottle	0.762	0.947	0.947	nan	0.767	0.9	-	-	-	-
	Standing-bottle	0.767	1	0.822	nan	0.767	nan	-	-	-	-
	Tire	0.816	0.989	0.956	0.5	0.823	0.5	-	-	-	-
	Valve	0.705	0.93	0.858	0	0.735	0	-	-	-	-
	Wall	0.721	0.921	0.832	0.314	0.724	0.83	-	-	-	-
	all	0.701	0.946	0.834	0.497	0.689	0.591	0.768	0.577	0.759	0.607
nei-g25	Bottle	0.744	0.986	0.953	0.7	0.738	nan	-	-	-	-
	Can	0.459	0.794	0.498	0.589	0.435	nan	-	-	-	-
	Chain	0.702	0.955	0.822	0.75	0.514	0.733	-	-	-	-
	Drink-carton	0.614	0.997	0.734	0.613	0.624	nan	-	-	-	-
	Hook	0.735	0.954	0.903	nan	0.735	nan	-	-	-	-
	Propeller	0.708	0.981	0.824	0.4	0.717	0.7	-	-	-	-
	Shampoo-bottle	0.745	0.954	0.954	nan	0.756	0.7	-	-	-	-
	Standing-bottle	0.73	1	1	nan	0.73	nan	-	-	-	-
	Tire	0.809	0.998	0.955	0.6	0.814	0.4	-	-	-	-
	Valve	0.729	0.939	0.88	0.5	0.754	0	-	-	-	-
	Wall	0.715	0.93	0.826	0.344	0.709	0.836	-	-	-	-
	all	0.699	0.954	0.85	0.562	0.684	0.561	0.762	0.597	0.749	0.577
nei-g5-50	Bottle	0.757	0.986	0.974	0.35	0.752	nan	-	-	-	-
	Can	0.439	0.752	0.446	0.503	0.431	nan	-	-	-	-
	Chain	0.698	0.97	0.839	0.8	0.501	0.727	-	-	-	-
	Drink-carton	0.611	0.993	0.739	0.612	0.625	nan	-	-	-	-
	Hook	0.727	0.952	0.952	nan	0.727	nan	-	-	-	-
	Propeller	0.693	0.977	0.861	0.6	0.696	0.7	-	-	-	-
	Shampoo-bottle	0.759	0.974	0.912	nan	0.778	0.5	-	-	-	-
	Standing-bottle	0.749	1	1	nan	0.749	nan	-	-	-	-
	Tire	0.815	0.99	0.967	0.6	0.817	0.6	-	-	-	-
	Valve	0.711	0.93	0.868	0.2	0.741	0	-	-	-	-
	Wall	0.722	0.931	0.844	0.335	0.72	0.837	-	-	-	-
	all	0.698	0.95	0.855	0.5	0.685	0.561	0.763	0.592	0.754	0.576

Table A.18: The MarinDebris dataset is detected using the SSD300 algorithm (Part 2 of 3). “noisy” represents the original noise dataset, and dspnet, b2ub, and nei represent the target detection after denoising using the DSPNet, Blind2Unblind, and Neighbor2Neighbor single-frame denoising algorithms, respectively. Bold fonts indicate data that is higher than the corresponding “noisy” dataset.

	Bottle	0.749	0.984	0.962	0.267	0.743	nan	-	-	-	-
	Can	0.444	0.734	0.43	0.539	0.431	nan	-	-	-	-
	Chain	0.671	0.956	0.843	0.783	0.534	0.694	-	-	-	-
	Drink-carton	0.645	0.996	0.836	0.63	0.682	nan	-	-	-	-
	Hook	0.708	0.959	0.959	nan	0.708	nan	-	-	-	-
nei-p30	Propeller	0.665	0.988	0.772	0.5	0.674	0.6	-	-	-	-
	Shampoo-bottle	0.773	0.962	0.962	nan	0.776	0.8	-	-	-	-
	Standing-bottle	0.729	1	1	nan	0.729	nan	-	-	-	-
	Tire	0.823	0.999	0.962	0.6	0.829	0.5	-	-	-	-
	Valve	0.71	0.918	0.871	0	0.741	0	-	-	-	-
	Wall	0.723	0.931	0.821	0.359	0.72	0.835	-	-	-	-
	all	0.694	0.948	0.856	0.46	0.688	0.571	0.763	0.576	0.756	0.589
	Bottle	0.754	0.984	0.951	0.4	0.748	nan	-	-	-	-
	Can	0.461	0.766	0.436	0.53	0.448	nan	-	-	-	-
	Chain	0.698	0.955	0.855	0.834	0.544	0.723	-	-	-	-
nei-p5-50	Drink-carton	0.624	0.993	0.811	0.615	0.64	nan	-	-	-	-
	Hook	0.717	0.954	0.906	nan	0.717	nan	-	-	-	-
	Propeller	0.698	0.986	0.804	0.4	0.71	0.6	-	-	-	-
	Shampoo-bottle	0.746	0.955	0.9	nan	0.765	0.5	-	-	-	-
	Standing-bottle	0.76	1	1	nan	0.76	nan	-	-	-	-
	Tire	0.81	0.989	0.937	0.4	0.815	0.6	-	-	-	-
	Valve	0.706	0.931	0.8	0	0.736	0	-	-	-	-
	Wall	0.714	0.923	0.816	0.337	0.709	0.825	-	-	-	-
	all	0.699	0.949	0.838	0.44	0.69	0.541	0.76	0.537	0.754	0.558

Table A.19: The MarinDebris dataset is detected using the SSD300 algorithm (Part 3 of 3). “noisy” represents the original noise dataset, and dspnet, b2ub, and nei represent the target detection after denoising using the DSPNet, Blind2Unblind, and Neighbor2Neighbor single-frame denoising algorithms, respectively. Bold fonts indicate data that is higher than the corresponding “noisy” dataset.

Denoising	class	YOLOX									
		mAP	mAP@0.5	mAP@0.75	mAP_s	mAP_m	mAP_l	AR	AR_s	AR_m	AR_l
noisy	Bottle	0.74	0.986	0.964	0.3	0.735	nan	-	-	-	-
	Can	0.503	0.857	0.594	0.541	0.492	nan	-	-	-	-
	Chain	0.678	0.959	0.785	0.75	0.51	0.708	-	-	-	-
	Drink-carton	0.621	0.999	0.729	0.619	0.632	nan	-	-	-	-
	Hook	0.725	0.967	0.933	nan	0.725	nan	-	-	-	-
	Propeller	0.681	0.968	0.774	0.125	0.688	0.7	-	-	-	-
	Shampoo-bottle	0.616	0.971	0.701	nan	0.62	0.6	-	-	-	-
	Standing-bottle	0.712	1	0.851	nan	0.712	nan	-	-	-	-
	Tire	0.799	0.99	0.937	0.8	0.804	0.4	-	-	-	-
	Valve	0.654	0.927	0.8	0	0.683	0	-	-	-	-
	Wall	0.69	0.939	0.845	0.384	0.685	0.756	-	-	-	-
	all	0.675	0.96	0.81	0.44	0.662	0.527	0.736	0.564	0.728	0.544
dspnet	Bottle	0.735	0.985	0.974	0.233	0.73	nan	-	-	-	-
	Can	0.432	0.748	0.489	0.489	0.424	nan	-	-	-	-
	Chain	0.664	0.944	0.819	0.651	0.527	0.699	-	-	-	-
	Drink-carton	0.569	0.956	0.608	0.566	0.603	nan	-	-	-	-
	Hook	0.7	0.955	0.855	nan	0.7	nan	-	-	-	-
	Propeller	0.658	0.945	0.838	0.25	0.663	0.7	-	-	-	-
	Shampoo-bottle	0.632	0.951	0.776	nan	0.636	0.6	-	-	-	-
	Standing-bottle	0.657	1	0.832	nan	0.657	nan	-	-	-	-
	Tire	0.798	0.979	0.936	0.7	0.805	0	-	-	-	-
	Valve	0.668	0.927	0.822	0	0.699	0	-	-	-	-
	Wall	0.666	0.929	0.83	0.332	0.666	0.734	-	-	-	-
	all	0.653	0.938	0.798	0.403	0.646	0.456	0.712	0.526	0.705	0.475
b2ub-g25	Bottle	0.746	0.984	0.964	0.6	0.742	nan	-	-	-	-
	Can	0.475	0.838	0.485	0.552	0.461	nan	-	-	-	-
	Chain	0.687	0.947	0.814	0.8	0.543	0.71	-	-	-	-
	Drink-carton	0.633	0.998	0.772	0.622	0.662	nan	-	-	-	-
	Hook	0.726	0.947	0.913	nan	0.726	nan	-	-	-	-
	Propeller	0.686	0.964	0.833	0.5	0.695	0.7	-	-	-	-
	Shampoo-bottle	0.657	0.971	0.971	nan	0.657	0.7	-	-	-	-
	Standing-bottle	0.749	1	0.851	nan	0.749	nan	-	-	-	-
	Tire	0.802	0.99	0.938	0.7	0.809	0.1	-	-	-	-
	Valve	0.684	0.931	0.861	0	0.714	0	-	-	-	-
	Wall	0.686	0.931	0.836	0.38	0.672	0.765	-	-	-	-
	all	0.685	0.955	0.84	0.519	0.675	0.496	0.744	0.562	0.738	0.513
b2ub-g5-50	Bottle	0.724	0.985	0.955	0.3	0.72	nan	-	-	-	-
	Can	0.487	0.825	0.562	0.539	0.481	nan	-	-	-	-
	Chain	0.676	0.946	0.775	0.725	0.538	0.705	-	-	-	-
	Drink-carton	0.611	0.995	0.692	0.61	0.616	nan	-	-	-	-
	Hook	0.717	0.944	0.9	nan	0.717	nan	-	-	-	-
	Propeller	0.713	0.985	0.841	0.15	0.721	0.7	-	-	-	-
	Shampoo-bottle	0.715	0.954	0.954	nan	0.726	0.6	-	-	-	-
	Standing-bottle	0.709	1	0.861	nan	0.709	nan	-	-	-	-
	Tire	0.82	0.99	0.949	0.9	0.826	0.2	-	-	-	-
	Valve	0.71	0.928	0.839	0	0.741	0	-	-	-	-
	Wall	0.701	0.932	0.836	0.338	0.69	0.779	-	-	-	-
	all	0.689	0.953	0.833	0.445	0.68	0.497	0.748	0.589	0.739	0.513

Table A.20: The MarinDebris dataset is detected using the YOLOX algorithm (Part 1 of 3). “noisy” represents the original noise dataset, and dspnet, b2ub, and nei represent the target detection after denoising using the DSPNet, Blind2Unblind, and Neighbor2Neighbor single-frame denoising algorithms, respectively. Bold fonts indicate data that is higher than the corresponding “noisy” dataset.

	Bottle	0.754	0.986	0.964	0.7	0.749	nan	-	-	-	-
	Can	0.485	0.836	0.544	0.571	0.472	nan	-	-	-	-
	Chain	0.688	0.947	0.809	0.735	0.524	0.72	-	-	-	-
b2ub-p30	Drink-carton	0.607	0.979	0.706	0.608	0.612	nan	-	-	-	-
	Hook	0.732	0.958	0.936	nan	0.732	nan	-	-	-	-
	Propeller	0.725	0.984	0.888	0.2	0.733	0.7	-	-	-	-
	Shampoo-bottle	0.691	0.964	0.884	nan	0.707	0.5	-	-	-	-
	Standing-bottle	0.748	1	1	nan	0.748	nan	-	-	-	-
	Tire	0.821	0.99	0.959	0.8	0.827	0.3	-	-	-	-
	Valve	0.683	0.923	0.835	0	0.713	0	-	-	-	-
	Wall	0.707	0.929	0.867	0.397	0.693	0.777	-	-	-	-
	all	0.695	0.954	0.854	0.501	0.683	0.5	0.752	0.6	0.74	0.517
b2ub-p5-50	Bottle	0.752	0.983	0.961	0.3	0.747	nan	-	-	-	-
	Can	0.478	0.824	0.522	0.586	0.446	nan	-	-	-	-
	Chain	0.691	0.949	0.857	0.8	0.548	0.721	-	-	-	-
	Drink-carton	0.637	0.997	0.792	0.626	0.671	nan	-	-	-	-
	Hook	0.709	0.963	0.91	nan	0.709	nan	-	-	-	-
	Propeller	0.702	0.972	0.869	0.06	0.717	0.7	-	-	-	-
	Shampoo-bottle	0.687	0.951	0.875	nan	0.694	0.6	-	-	-	-
	Standing-bottle	0.72	1	0.891	nan	0.72	nan	-	-	-	-
	Tire	0.812	0.999	0.938	0.8	0.816	0.3	-	-	-	-
	Valve	0.686	0.946	0.836	0.65	0.701	0	-	-	-	-
	Wall	0.701	0.93	0.835	0.369	0.702	0.769	-	-	-	-
	all	0.689	0.956	0.844	0.524	0.679	0.515	0.747	0.66	0.739	0.533
nei-g25	Bottle	0.759	0.985	0.964	0.25	0.755	nan	-	-	-	-
	Can	0.483	0.793	0.534	0.58	0.461	nan	-	-	-	-
	Chain	0.701	0.947	0.83	0.651	0.627	0.72	-	-	-	-
	Drink-carton	0.629	0.997	0.715	0.622	0.65	nan	-	-	-	-
	Hook	0.747	0.963	0.94	nan	0.747	nan	-	-	-	-
	Propeller	0.688	0.971	0.834	0.1	0.7	0.7	-	-	-	-
	Shampoo-bottle	0.693	0.954	0.954	nan	0.699	0.6	-	-	-	-
	Standing-bottle	0.7	1	1	nan	0.7	nan	-	-	-	-
	Tire	0.829	0.999	0.959	0.6	0.835	0.4	-	-	-	-
	Valve	0.676	0.925	0.818	0	0.706	0	-	-	-	-
	Wall	0.717	0.936	0.863	0.384	0.707	0.791	-	-	-	-
	all	0.693	0.952	0.856	0.398	0.69	0.535	0.754	0.509	0.752	0.552
nei-g5-50	Bottle	0.755	0.985	0.962	0.6	0.75	nan	-	-	-	-
	Can	0.49	0.847	0.58	0.572	0.466	nan	-	-	-	-
	Chain	0.686	0.963	0.824	0.801	0.526	0.717	-	-	-	-
	Drink-carton	0.639	0.998	0.81	0.63	0.662	nan	-	-	-	-
	Hook	0.73	0.959	0.924	nan	0.73	nan	-	-	-	-
	Propeller	0.69	0.975	0.808	0.12	0.7	0.6	-	-	-	-
	Shampoo-bottle	0.672	0.944	0.793	nan	0.682	0.5	-	-	-	-
	Standing-bottle	0.743	1	0.88	nan	0.743	nan	-	-	-	-
	Tire	0.832	0.999	0.966	0.6	0.84	0.2	-	-	-	-
	Valve	0.683	0.926	0.879	0	0.713	0	-	-	-	-
	Wall	0.669	0.928	0.807	0.403	0.669	0.729	-	-	-	-
	all	0.69	0.957	0.839	0.466	0.68	0.458	0.75	0.561	0.739	0.479

Table A.21: The MarinDebris dataset is detected using the YOLOX algorithm (Part 2 of 3). “noisy” represents the original noise dataset, and dspnet, b2ub, and nei represent the target detection after denoising using the DSPNet, Blind2Unblind, and Neighbor2Neighbor single-frame denoising algorithms, respectively. Bold fonts indicate data that is higher than the corresponding “noisy” dataset.

	Bottle	0.737	0.987	0.954	0.6	0.731	nan	-	-	-	-
	Can	0.481	0.811	0.555	0.562	0.46	nan	-	-	-	-
	Chain	0.697	0.946	0.82	0.825	0.55	0.723	-	-	-	-
	Drink-carton	0.634	0.999	0.78	0.635	0.643	nan	-	-	-	-
	Hook	0.724	0.958	0.958	nan	0.724	nan	-	-	-	-
nei-p30	Propeller	0.692	0.976	0.848	0.25	0.698	0.7	-	-	-	-
	Shampoo-bottle	0.668	0.961	0.961	nan	0.676	0.6	-	-	-	-
	Standing-bottle	0.728	1	0.79	nan	0.728	nan	-	-	-	-
	Tire	0.818	0.999	0.957	0.7	0.824	0.2	-	-	-	-
	Valve	0.655	0.92	0.813	0	0.683	0	-	-	-	-
	Wall	0.701	0.936	0.853	0.383	0.693	0.769	-	-	-	-
	all	0.685	0.954	0.844	0.494	0.674	0.499	0.738	0.569	0.728	0.515
	Bottle	0.739	0.986	0.952	0.35	0.733	nan	-	-	-	-
	Can	0.488	0.801	0.594	0.587	0.465	nan	-	-	-	-
	Chain	0.681	0.944	0.827	0.768	0.523	0.704	-	-	-	-
nei-p5-50	Drink-carton	0.615	0.999	0.691	0.596	0.655	nan	-	-	-	-
	Hook	0.696	0.965	0.89	nan	0.696	nan	-	-	-	-
	Propeller	0.694	0.984	0.814	0.2	0.7	0.7	-	-	-	-
	Shampoo-bottle	0.635	0.951	0.849	nan	0.632	0.7	-	-	-	-
	Standing-bottle	0.701	1	0.871	nan	0.701	nan	-	-	-	-
	Tire	0.792	0.99	0.938	0.8	0.797	0.2	-	-	-	-
	Valve	0.675	0.926	0.835	0	0.704	0	-	-	-	-
	Wall	0.672	0.937	0.823	0.344	0.678	0.723	-	-	-	-
	all	0.672	0.953	0.826	0.456	0.662	0.505	0.729	0.605	0.724	0.522

Table A.22: The MarinDebris dataset is detected using the YOLOX algorithm (Part 3 of 3). “noisy” represents the original noise dataset, and dspnet, b2ub, and nei represent the target detection after denoising using the DSPNet, Blind2Unblind, and Neighbor2Neighbor single-frame denoising algorithms, respectively. Bold fonts indicate data that is higher than the corresponding “noisy” dataset.

Denoising	SSDMobileNetV2										
	class	mAP	mAP@0.5	mAP@0.75	mAP_s	mAP_m	mAP_l	AR	AR_s	AR_m	AR_l
noisy	victim	0.825	1	0.96	nan	0.713	0.828	-	-	-	-
	plane	0.779	1	0.953	nan	0.781	0.725	-	-	-	-
	boat	0.733	0.99	0.938	0.9	0.732	nan	-	-	-	-
	all	0.779	0.996	0.95	0.9	0.742	0.776	0.82	0.9	0.774	0.804
dspnet	victim	0.824	1	0.962	nan	0.707	0.827	-	-	-	-
	plane	0.772	1	0.95	nan	0.773	0.801	-	-	-	-
	boat	0.717	0.989	0.91	0.8	0.718	nan	-	-	-	-
	all	0.771	0.996	0.941	0.8	0.733	0.814	0.819	0.8	0.77	0.832
b2ub-g25	victim	0.812	1	0.951	nan	0.647	0.817	-	-	-	-
	plane	0.738	1	0.929	nan	0.74	0.7	-	-	-	-
	boat	0.592	0.98	0.653	0.7	0.592	nan	-	-	-	-
	all	0.714	0.993	0.844	0.7	0.66	0.758	0.758	0.7	0.7	0.825
b2ub-g5-50	victim	0.831	1	0.963	nan	0.769	0.833	-	-	-	-
	plane	0.777	1	0.965	nan	0.778	0.75	-	-	-	-
	boat	0.716	0.99	0.913	0.8	0.716	nan	-	-	-	-
	all	0.775	0.997	0.947	0.8	0.754	0.792	0.818	0.8	0.788	0.807
b2ub-p30	victim	0.778	0.999	0.921	nan	0.565	0.784	-	-	-	-
	plane	0.7	0.989	0.944	nan	0.7	0.767	-	-	-	-
	boat	0.59	0.989	0.655	0.8	0.589	nan	-	-	-	-
	all	0.689	0.993	0.84	0.8	0.618	0.775	0.737	0.8	0.657	0.809
b2ub-p5-50	victim	0.807	1	0.936	nan	0.653	0.809	-	-	-	-
	plane	0.742	1	0.942	nan	0.744	0.759	-	-	-	-
	boat	0.669	0.99	0.823	0.7	0.668	nan	-	-	-	-
	all	0.739	0.997	0.901	0.7	0.688	0.784	0.787	0.7	0.74	0.846
nei-g25	victim	0.809	1	0.967	nan	0.671	0.813	-	-	-	-
	plane	0.725	1	0.918	nan	0.731	0.683	-	-	-	-
	boat	0.58	0.989	0.688	0.5	0.58	nan	-	-	-	-
	all	0.705	0.996	0.858	0.5	0.661	0.748	0.754	0.5	0.705	0.775
nei-g5-50	ship	0.516	0.783	0.603	0	0.466	0.55	-	-	-	-
	aircraft	0.368	0.739	0.347	nan	0.552	0.326	-	-	-	-
	human	0.35	0.487	0.446	0.8	0.314	0.303	-	-	-	-
	all	0.411	0.67	0.465	0.4	0.444	0.393	0.477	0.4	0.452	0.46
nei-p30	victim	0.751	0.989	0.899	nan	0.533	0.756	-	-	-	-
	plane	0.696	0.999	0.866	nan	0.695	0.701	-	-	-	-
	boat	0.539	0.988	0.526	0.2	0.54	nan	-	-	-	-
	all	0.662	0.992	0.764	0.2	0.59	0.728	0.712	0.2	0.665	0.745
nei-p5-50	victim	0.827	1	0.971	nan	0.681	0.832	-	-	-	-
	plane	0.796	1	0.968	nan	0.798	0.801	-	-	-	-
	boat	0.74	0.99	0.94	0.7	0.741	nan	-	-	-	-
	all	0.788	0.997	0.96	0.7	0.74	0.816	0.826	0.7	0.778	0.831

Table A.23: The FDD dataset is detected using the SSDMobileNetV2 algorithm. “noisy” represents the original noise dataset, and dspnet, b2ub, and nei represent the target detection after denoising using the DSPNet, Blind2Unblind, and Neighbor2Neighbor single-frame denoising algorithms, respectively. Bold fonts indicate data that is higher than the corresponding “noisy” dataset.

Denoising	Faster R-CNN										
	class	mAP	mAP@0.5	mAP@0.75	mAP_s	mAP_m	mAP_l	AR	AR_s	AR_m	AR_l
noisy	victim	0.807	0.99	0.935	nan	0.666	0.809	-	-	-	-
	plane	0.879	1	0.987	nan	0.88	0.725	-	-	-	-
	boat	0.849	0.987	0.987	0.9	0.849	nan	-	-	-	-
	all	0.845	0.992	0.969	0.9	0.798	0.767	0.887	0.9	0.827	0.803
dspnet	victim	0.802	1	0.928	nan	0.532	0.807	-	-	-	-
	plane	0.87	1	1	nan	0.873	0.801	-	-	-	-
	boat	0.833	0.987	0.987	0.9	0.833	nan	-	-	-	-
	all	0.835	0.996	0.972	0.9	0.746	0.804	0.876	0.9	0.795	0.825
b2ub-g25	victim	0.81	1	0.947	nan	0.641	0.815	-	-	-	-
	plane	0.88	1	0.986	nan	0.883	0.75	-	-	-	-
	boat	0.84	0.988	0.988	0.8	0.84	nan	-	-	-	-
	all	0.843	0.996	0.974	0.8	0.788	0.783	0.878	0.8	0.816	0.825
b2ub-g5-50	victim	0.815	1	0.942	nan	0.714	0.817	-	-	-	-
	plane	0.88	1	1	nan	0.881	0.75	-	-	-	-
	boat	0.855	0.987	0.987	0.9	0.855	nan	-	-	-	-
	all	0.85	0.996	0.977	0.9	0.817	0.784	0.89	0.9	0.843	0.83
b2ub-p30	victim	0.822	1	0.954	nan	0.661	0.825	-	-	-	-
	plane	0.885	1	0.987	nan	0.886	0.85	-	-	-	-
	boat	0.855	0.987	0.987	0.9	0.855	nan	-	-	-	-
	all	0.854	0.996	0.976	0.9	0.801	0.838	0.89	0.9	0.829	0.854
b2ub-p5-50	victim	0.804	0.99	0.947	nan	0.516	0.811	-	-	-	-
	plane	0.86	1	1	nan	0.861	0.8	-	-	-	-
	boat	0.836	0.988	0.978	0.9	0.836	nan	-	-	-	-
	all	0.833	0.993	0.975	0.9	0.737	0.806	0.87	0.9	0.768	0.822
nei-g25	victim	0.804	1	0.939	nan	0.638	0.809	-	-	-	-
	plane	0.875	1	0.986	nan	0.877	0.75	-	-	-	-
	boat	0.844	0.988	0.988	0.9	0.844	nan	-	-	-	-
	all	0.841	0.996	0.971	0.9	0.786	0.78	0.881	0.9	0.82	0.799
nei-g5-50	ship	0.822	1	0.954	nan	0.653	0.826	-	-	-	-
	aircraft	0.881	1	0.99	nan	0.882	0.75	-	-	-	-
	human	0.844	0.986	0.986	0.9	0.844	nan	-	-	-	-
	all	0.849	0.995	0.977	0.9	0.793	0.788	0.889	0.9	0.822	0.833
nei-p30	victim	0.797	0.99	0.927	nan	0.612	0.803	-	-	-	-
	plane	0.866	1	0.988	nan	0.867	0.75	-	-	-	-
	boat	0.839	0.986	0.986	0.9	0.839	nan	-	-	-	-
	all	0.834	0.992	0.967	0.9	0.773	0.777	0.873	0.9	0.8	0.795
nei-p5-50	victim	0.827	1	0.965	nan	0.599	0.834	-	-	-	-
	plane	0.891	1	0.987	nan	0.893	0.75	-	-	-	-
	boat	0.851	0.986	0.986	0.9	0.851	nan	-	-	-	-
	all	0.856	0.995	0.979	0.9	0.781	0.792	0.89	0.9	0.804	0.832

Table A.24: The FDD dataset is detected using the Faster R-CNN algorithm. “noisy” represents the original noise dataset, and dspnet, b2ub, and nei represent the target detection after denoising using the DSPNet, Blind2Unblind, and Neighbor2Neighbor single-frame denoising algorithms, respectively. Bold fonts indicate data that is higher than the corresponding “noisy” dataset.

Denoising	SSD300										
	class	mAP	mAP@0.5	mAP@0.75	mAP_s	mAP_m	mAP_l	AR	AR_s	AR_m	AR_l
noisy	victim	0.805	1	0.956	nan	0.634	0.81	-	-	-	-
	plane	0.842	1	0.975	nan	0.843	0.8	-	-	-	-
	boat	0.813	0.989	0.974	0.85	0.814	nan	-	-	-	-
	all	0.82	0.996	0.968	0.85	0.764	0.805	0.861	0.9	0.8	0.848
dspnet	victim	0.802	1	0.938	nan	0.66	0.806	-	-	-	-
	plane	0.833	1	0.973	nan	0.835	0.775	-	-	-	-
	boat	0.797	0.989	0.977	0.8	0.797	nan	-	-	-	-
	all	0.811	0.996	0.963	0.8	0.764	0.79	0.851	0.8	0.799	0.872
b2ub-g25	victim	0.805	1	0.956	nan	0.613	0.811	-	-	-	-
	plane	0.847	1	0.977	nan	0.85	0.767	-	-	-	-
	boat	0.811	0.99	0.978	0.9	0.811	nan	-	-	-	-
	all	0.821	0.997	0.97	0.9	0.758	0.789	0.863	0.9	0.795	0.851
b2ub-g5-50	victim	0.814	1	0.963	nan	0.678	0.817	-	-	-	-
	plane	0.85	1	0.987	nan	0.851	0.8	-	-	-	-
	boat	0.814	0.99	0.975	0.9	0.814	nan	-	-	-	-
	all	0.826	0.997	0.975	0.9	0.781	0.809	0.864	0.9	0.815	0.851
b2ub-p30	victim	0.807	1	0.947	nan	0.678	0.811	-	-	-	-
	plane	0.857	1	0.989	nan	0.859	0.725	-	-	-	-
	boat	0.817	0.989	0.976	0.9	0.817	nan	-	-	-	-
	all	0.827	0.996	0.971	0.9	0.785	0.768	0.866	0.9	0.813	0.801
b2ub-p5-50	victim	0.791	1	0.952	nan	0.626	0.796	-	-	-	-
	plane	0.805	1	0.974	nan	0.805	0.725	-	-	-	-
	boat	0.78	0.989	0.975	0.8	0.781	nan	-	-	-	-
	all	0.792	0.996	0.967	0.8	0.737	0.761	0.83	0.8	0.784	0.789
nei-g25	victim	0.811	1	0.966	nan	0.699	0.813	-	-	-	-
	plane	0.85	1	0.988	nan	0.853	0.719	-	-	-	-
	boat	0.814	0.989	0.974	0.7	0.815	nan	-	-	-	-
	all	0.825	0.996	0.976	0.7	0.789	0.766	0.864	0.7	0.823	0.827
nei-g5-50	ship	0.805	1	0.975	nan	0.616	0.81	-	-	-	-
	aircraft	0.845	1	0.989	nan	0.848	0.717	-	-	-	-
	human	0.809	0.99	0.975	0.9	0.809	nan	-	-	-	-
	all	0.82	0.997	0.979	0.9	0.758	0.764	0.86	0.9	0.794	0.8
nei-p30	victim	0.788	1	0.942	nan	0.63	0.792	-	-	-	-
	plane	0.838	1	0.988	nan	0.839	0.846	-	-	-	-
	boat	0.804	0.99	0.976	0.9	0.804	nan	-	-	-	-
	all	0.81	0.997	0.969	0.9	0.757	0.819	0.85	0.9	0.785	0.865
nei-p5-50	victim	0.812	1	0.961	nan	0.667	0.815	-	-	-	-
	plane	0.854	1	0.987	nan	0.856	0.742	-	-	-	-
	boat	0.815	0.989	0.963	0.8	0.815	nan	-	-	-	-
	all	0.827	0.996	0.97	0.8	0.779	0.864	0.8	0.811	0.825	0.825

Table A.25: The FDD dataset is detected using the SSD300 algorithm. “noisy” represents the original noise dataset, and dspnet, b2ub, and nei represent the target detection after denoising using the DSPNet, Blind2Unblind, and Neighbor2Neighbor single-frame denoising algorithms, respectively. Bold fonts indicate data that is higher than the corresponding “noisy” dataset.

Denoising	YOLOX										
	class	mAP	mAP@0.5	mAP@0.75	mAP_s	mAP_m	mAP_l	AR	AR_s	AR_m	AR_l
noisy	victim	0.83	1	0.964	nan	0.627	0.838	-	-	-	-
	plane	0.853	1	0.98	nan	0.853	0.817	-	-	-	-
	boat	0.825	0.99	0.979	0.8	0.825	nan	-	-	-	-
	all	0.836	0.997	0.974	0.8	0.768	0.827	0.863	0.8	0.788	0.855
dspnet	victim	0.811	1	0.967	nan	0.648	0.814	-	-	-	-
	plane	0.852	1	0.979	nan	0.852	0.783	-	-	-	-
	boat	0.816	0.989	0.989	0.9	0.817	nan	-	-	-	-
	all	0.826	0.996	0.978	0.9	0.772	0.799	0.855	0.9	0.796	0.82
b2ub-g25	victim	0.793	1	0.956	nan	0.585	0.798	-	-	-	-
	plane	0.832	1	0.978	nan	0.832	0.725	-	-	-	-
	boat	0.774	0.99	0.979	0.7	0.775	nan	-	-	-	-
	all	0.799	0.997	0.971	0.7	0.731	0.762	0.829	0.7	0.752	0.787
b2ub-g5-50	victim	0.818	1	0.968	nan	0.715	0.82	-	-	-	-
	plane	0.865	1	0.99	nan	0.866	0.723	-	-	-	-
	boat	0.816	0.99	0.99	0.7	0.816	nan	-	-	-	-
	all	0.833	0.997	0.983	0.7	0.799	0.771	0.861	0.7	0.823	0.824
b2ub-p30	victim	0.816	1	0.954	nan	0.628	0.821	-	-	-	-
	plane	0.866	1	0.98	nan	0.866	0.717	-	-	-	-
	boat	0.837	0.99	0.99	0.9	0.837	nan	-	-	-	-
	all	0.839	0.997	0.975	0.9	0.777	0.769	0.865	0.9	0.799	0.799
b2ub-p5-50	victim	0.843	1	0.975	nan	0.699	0.846	-	-	-	-
	plane	0.859	1	0.98	nan	0.86	0.8	-	-	-	-
	boat	0.847	0.99	0.99	0.9	0.847	nan	-	-	-	-
	all	0.85	0.997	0.982	0.9	0.802	0.823	0.875	0.9	0.82	0.834
nei-g25	victim	0.812	1	0.953	nan	0.687	0.815	-	-	-	-
	plane	0.833	1	0.98	nan	0.834	0.717	-	-	-	-
	boat	0.793	0.99	0.99	0.8	0.793	nan	-	-	-	-
	all	0.812	0.997	0.974	0.8	0.771	0.766	0.843	0.8	0.797	0.795
nei-g5-50	ship	0.819	1	0.974	nan	0.713	0.822	-	-	-	-
	aircraft	0.85	1	0.979	nan	0.852	0.723	-	-	-	-
	human	0.824	0.99	0.98	0.8	0.824	nan	-	-	-	-
	all	0.831	0.997	0.978	0.8	0.796	0.773	0.857	0.8	0.819	0.823
nei-p30	victim	0.821	1	0.977	nan	0.666	0.826	-	-	-	-
	plane	0.863	1	0.98	nan	0.864	0.7	-	-	-	-
	boat	0.83	0.989	0.989	0.8	0.831	nan	-	-	-	-
	all	0.838	0.996	0.982	0.8	0.787	0.763	0.866	0.8	0.808	0.825
nei-p5-50	victim	0.823	1	0.965	nan	0.718	0.825	-	-	-	-
	plane	0.856	1	0.98	nan	0.857	0.75	-	-	-	-
	boat	0.821	0.989	0.989	0.8	0.822	nan	-	-	-	-
	all	0.833	0.996	0.978	0.8	0.799	0.788	0.859	0.8	0.825	0.824

Table A.26: The FDD dataset is detected using the YOLOX algorithm. “noisy” represents the original noise dataset, and dspnet, b2ub, and nei represent the target detection after denoising using the DSPNet, Blind2Unblind, and Neighbor2Neighbor single-frame denoising algorithms, respectively. Bold fonts indicate data that is higher than the corresponding “noisy” dataset.

Denoising	class	SSDMobileNetV2									
		mAP	mAP@0.5	mAP@0.75	mAP_s	mAP_m	mAP_l	AR	AR_s	AR_m	AR_l
noisy	human body	0.475	0.972	0.345	0	0.471	0.552	-	-	-	-
	ball	0.436	0.934	0.313	nan	0.437	0.214	-	-	-	-
	circle cage	0.415	0.898	0.354	nan	0.412	0.474	-	-	-	-
	square cage	0.428	0.922	0.317	0	0.431	nan	-	-	-	-
	tyre	0.373	0.863	0.257	0	0.348	0.564	-	-	-	-
	cube	0.474	0.934	0.404	0.169	0.478	0.496	-	-	-	-
	cylinder	0.313	0.816	0.12	0.583	0.309	nan	-	-	-	-
	metal bucket	0.44	0.89	0.275	nan	0.443	0.363	-	-	-	-
	plane	0.562	0.974	0.586	nan	0.535	0.605	-	-	-	-
	rov	0.303	0.855	0.119	0	0.305	nan	-	-	-	-
dspnet	all	0.422	0.906	0.309	0.125	0.417	0.467	0.516	0.13	0.512	0.517
	human body	0.484	0.964	0.411	0	0.481	0.564	-	-	-	-
	ball	0.452	0.95	0.321	nan	0.451	0.327	-	-	-	-
	circle cage	0.433	0.858	0.341	nan	0.429	0.528	-	-	-	-
	square cage	0.447	0.933	0.356	0	0.45	nan	-	-	-	-
	tyre	0.372	0.896	0.234	0	0.355	0.507	-	-	-	-
	cube	0.462	0.917	0.38	0.348	0.462	0.524	-	-	-	-
	cylinder	0.329	0.795	0.219	0.288	0.331	nan	-	-	-	-
	metal bucket	0.456	0.906	0.37	nan	0.455	0.451	-	-	-	-
	plane	0.547	0.975	0.488	nan	0.502	0.622	-	-	-	-
b2ub-g25	rov	0.32	0.841	0.108	0.1	0.323	nan	-	-	-	-
	all	0.43	0.904	0.323	0.123	0.424	0.503	0.523	0.136	0.518	0.552
	human body	0.453	0.957	0.355	0	0.449	0.549	-	-	-	-
	ball	0.425	0.931	0.243	nan	0.425	0.277	-	-	-	-
	circle cage	0.404	0.876	0.243	nan	0.399	0.525	-	-	-	-
	square cage	0.404	0.906	0.282	0	0.408	nan	-	-	-	-
	tyre	0.333	0.833	0.192	0	0.314	0.499	-	-	-	-
	cube	0.439	0.931	0.281	0.283	0.439	0.543	-	-	-	-
	cylinder	0.284	0.767	0.161	0.222	0.288	nan	-	-	-	-
	metal bucket	0.391	0.832	0.248	nan	0.393	0.376	-	-	-	-
b2ub-g5-50	plane	0.551	0.987	0.545	nan	0.514	0.615	-	-	-	-
	rov	0.296	0.832	0.098	0	0.297	nan	-	-	-	-
	all	0.398	0.885	0.265	0.084	0.393	0.483	0.494	0.091	0.49	0.514

Table A.27: The UATD dataset is detected using the SSDMobileNetV2 algorithm (Part 1 of 3). “noisy” represents the original noise dataset, and dspnet, b2ub, and nei represent the target detection after denoising using the DSPNet, Blind2Unblind, and Neighbor2Neighbor single-frame denoising algorithms, respectively. Bold fonts indicate data that is higher than the corresponding “noisy” dataset.

		human body	0.469	0.974	0.312	0	0.464	0.579	-	-	-	-
b2ub-p30	ball	0.436	0.938	0.293	nan	0.437	0.277	-	-	-	-	-
	circle cage	0.419	0.888	0.317	nan	0.414	0.524	-	-	-	-	-
	square cage	0.426	0.951	0.248	0	0.428	nan	-	-	-	-	-
	tyre	0.373	0.857	0.254	0	0.357	0.506	-	-	-	-	-
	cube	0.462	0.923	0.402	0.223	0.465	0.498	-	-	-	-	-
	cylinder	0.301	0.801	0.153	0.417	0.3	nan	-	-	-	-	-
	metal bucket	0.41	0.894	0.284	nan	0.411	0.403	-	-	-	-	-
	plane	0.549	0.984	0.528	nan	0.51	0.61	-	-	-	-	-
	rov	0.304	0.832	0.135	0	0.306	nan	-	-	-	-	-
	all	0.415	0.904	0.292	0.107	0.409	0.485	0.512	0.121	0.506	0.534	-
b2ub-p5-50	human body	0.456	0.955	0.308	0	0.451	0.553	-	-	-	-	-
	ball	0.43	0.935	0.301	nan	0.43	0.218	-	-	-	-	-
	circle cage	0.43	0.882	0.363	nan	0.429	0.475	-	-	-	-	-
	square cage	0.422	0.936	0.27	0	0.426	nan	-	-	-	-	-
	tyre	0.372	0.889	0.252	0	0.35	0.542	-	-	-	-	-
	cube	0.468	0.941	0.379	0.362	0.468	0.493	-	-	-	-	-
	cylinder	0.312	0.791	0.143	0.32	0.314	nan	-	-	-	-	-
	metal bucket	0.44	0.917	0.271	nan	0.447	0.307	-	-	-	-	-
	plane	0.568	0.979	0.645	nan	0.547	0.597	-	-	-	-	-
	rov	0.294	0.84	0.115	0	0.296	nan	-	-	-	-	-
nei-g25	all	0.419	0.906	0.305	0.114	0.416	0.455	0.513	0.121	0.512	0.5	-
	human body	0.418	0.944	0.275	0	0.408	0.592	-	-	-	-	-
	ball	0.414	0.916	0.243	nan	0.414	0.202	-	-	-	-	-
	circle cage	0.381	0.827	0.315	nan	0.38	0.407	-	-	-	-	-
	square cage	0.413	0.932	0.247	0	0.416	nan	-	-	-	-	-
	tyre	0.328	0.814	0.197	0	0.307	0.474	-	-	-	-	-
	cube	0.439	0.919	0.31	0.23	0.44	0.509	-	-	-	-	-
	cylinder	0.315	0.807	0.13	0.5	0.312	nan	-	-	-	-	-
	metal bucket	0.444	0.906	0.32	nan	0.449	0.378	-	-	-	-	-
	plane	0.572	0.979	0.581	nan	0.534	0.633	-	-	-	-	-
nei-g5-50	rov	0.29	0.853	0.099	0	0.292	nan	-	-	-	-	-
	all	0.401	0.89	0.272	0.122	0.395	0.456	0.496	0.129	0.491	0.491	-
	human body	0.457	0.955	0.318	0	0.454	0.521	-	-	-	-	-
	ball	0.417	0.926	0.253	nan	0.417	0.235	-	-	-	-	-
	circle cage	0.419	0.895	0.295	nan	0.419	0.48	-	-	-	-	-
	square cage	0.434	0.935	0.267	0	0.435	nan	-	-	-	-	-
	tyre	0.318	0.844	0.122	0	0.313	0.372	-	-	-	-	-
	cube	0.439	0.915	0.339	0.244	0.441	0.508	-	-	-	-	-
	cylinder	0.306	0.776	0.174	0.466	0.304	nan	-	-	-	-	-
	metal bucket	0.418	0.855	0.265	nan	0.425	0.326	-	-	-	-	-
	plane	0.537	0.997	0.5	nan	0.515	0.579	-	-	-	-	-
	rov	0.27	0.8	0.075	0.2	0.271	nan	-	-	-	-	-
	all	0.401	0.89	0.261	0.152	0.399	0.432	0.495	0.16	0.494	0.471	-

Table A.28: The UATD dataset is detected using the SSDMobileNetV2 algorithm (Part 2 of 3). “noisy” represents the original noise dataset, and dspnet, b2ub, and nei represent the target detection after denoising using the DSPNet, Blind2Unblind, and Neighbor2Neighbor single-frame denoising algorithms, respectively. Bold fonts indicate data that is higher than the corresponding “noisy” dataset.

	human body	0.506	0.976	0.42	0	0.507	0.544	-	-	-	-
nei-p30	ball	0.535	0.968	0.521	nan	0.535	0.303	-	-	-	-
	circle cage	0.514	0.935	0.498	nan	0.518	0.524	-	-	-	-
	square cage	0.488	0.946	0.385	0	0.491	nan	-	-	-	-
	tyre	0.5	0.92	0.479	0	0.492	0.586	-	-	-	-
	cube	0.501	0.942	0.461	0.307	0.502	0.549	-	-	-	-
	cylinder	0.352	0.785	0.207	0.655	0.348	nan	-	-	-	-
	metal bucket	0.491	0.915	0.47	nan	0.5	0.295	-	-	-	-
	plane	0.573	0.997	0.604	nan	0.549	0.614	-	-	-	-
	rov	0.429	0.977	0.243	0	0.433	nan	-	-	-	-
	all	0.489	0.936	0.429	0.16	0.488	0.488	0.572	0.171	0.571	0.527
	human body	0.491	0.961	0.413	0	0.487	0.578	-	-	-	-
nei-p5-50	ball	0.461	0.948	0.35	nan	0.46	0.269	-	-	-	-
	circle cage	0.438	0.904	0.366	nan	0.437	0.479	-	-	-	-
	square cage	0.439	0.96	0.267	0	0.441	nan	-	-	-	-
	tyre	0.391	0.906	0.232	0	0.378	0.518	-	-	-	-
	cube	0.471	0.945	0.407	0.343	0.47	0.559	-	-	-	-
	cylinder	0.295	0.808	0.108	0.294	0.296	nan	-	-	-	-
	metal bucket	0.438	0.905	0.358	nan	0.436	0.467	-	-	-	-
	plane	0.56	0.974	0.576	nan	0.52	0.62	-	-	-	-
	rov	0.336	0.911	0.144	0	0.338	nan	-	-	-	-
	all	0.432	0.922	0.322	0.106	0.426	0.499	0.524	0.123	0.519	0.556

Table A.29: The UATD dataset is detected using the SSDMobileNetV2 algorithm (Part 3 of 3). “noisy” represents the original noise dataset, and dspnet, b2ub, and nei represent the target detection after denoising using the DSPNet, Blind2Unblind, and Neighbor2Neighbor single-frame denoising algorithms, respectively. Bold fonts indicate data that is higher than the corresponding “noisy” dataset.

Denoising	class	Faster R-CNN									
		mAP	mAP@0.5	mAP@0.75	mAP_s	mAP_m	mAP_l	AR	AR_s	AR_m	AR_l
noisy	human body	0.527	0.977	0.519	0	0.531	0.547	-	-	-	-
	ball	0.55	0.959	0.558	nan	0.551	0.252	-	-	-	-
	circle cage	0.527	0.904	0.552	nan	0.52	0.613	-	-	-	-
	square cage	0.528	0.962	0.502	0	0.53	nan	-	-	-	-
	tyre	0.54	0.957	0.532	0	0.53	0.638	-	-	-	-
	cube	0.537	0.955	0.574	0.343	0.538	0.578	-	-	-	-
	cylinder	0.446	0.895	0.411	0.734	0.437	nan	-	-	-	-
	metal bucket	0.523	0.932	0.509	nan	0.533	0.37	-	-	-	-
	plane	0.651	0.99	0.773	nan	0.606	0.702	-	-	-	-
	rov	0.504	0.968	0.398	0	0.507	nan	-	-	-	-
dspnet	all	0.533	0.95	0.533	0.179	0.529	0.528	0.605	0.182	0.603	0.563
	human body	0.531	0.978	0.501	0	0.536	0.549	-	-	-	-
	ball	0.549	0.955	0.555	nan	0.549	0.303	-	-	-	-
	circle cage	0.544	0.923	0.595	nan	0.544	0.574	-	-	-	-
	square cage	0.51	0.959	0.446	0	0.512	nan	-	-	-	-
	tyre	0.551	0.96	0.607	0	0.544	0.632	-	-	-	-
	cube	0.532	0.954	0.542	0.343	0.533	0.561	-	-	-	-
	cylinder	0.453	0.884	0.387	0.717	0.446	nan	-	-	-	-
	metal bucket	0.515	0.927	0.5	nan	0.528	0.334	-	-	-	-
	plane	0.638	0.999	0.68	nan	0.612	0.674	-	-	-	-
b2ub-g25	rov	0.53	0.986	0.443	0.1	0.533	nan	-	-	-	-
	all	0.535	0.952	0.526	0.193	0.534	0.518	0.606	0.196	0.604	0.554
	human body	0.484	0.946	0.421	0	0.486	0.499	-	-	-	-
	ball	0.523	0.953	0.503	nan	0.523	0.252	-	-	-	-
	circle cage	0.505	0.891	0.466	nan	0.497	0.59	-	-	-	-
	square cage	0.474	0.929	0.377	0	0.477	nan	-	-	-	-
	tyre	0.466	0.88	0.429	0	0.455	0.566	-	-	-	-
	cube	0.512	0.943	0.482	0.284	0.514	0.598	-	-	-	-
	cylinder	0.42	0.841	0.338	0.634	0.413	nan	-	-	-	-
	metal bucket	0.471	0.917	0.432	nan	0.488	0.127	-	-	-	-
	plane	0.643	0.998	0.745	nan	0.606	0.691	-	-	-	-
b2ub-g5-50	rov	0.508	0.963	0.438	0.3	0.507	nan	-	-	-	-
	all	0.5	0.926	0.463	0.203	0.497	0.475	0.577	0.236	0.575	0.506
	human body	0.537	0.968	0.525	0	0.535	0.591	-	-	-	-
	ball	0.555	0.96	0.571	nan	0.555	0.303	-	-	-	-
	circle cage	0.535	0.923	0.583	nan	0.537	0.53	-	-	-	-
	square cage	0.517	0.953	0.473	0	0.519	nan	-	-	-	-
	tyre	0.542	0.945	0.57	0	0.535	0.628	-	-	-	-
	cube	0.538	0.958	0.54	0.322	0.542	0.547	-	-	-	-
	cylinder	0.469	0.892	0.426	0.734	0.463	nan	-	-	-	-
	metal bucket	0.532	0.938	0.553	nan	0.537	0.452	-	-	-	-
nei	plane	0.635	0.99	0.741	nan	0.603	0.678	-	-	-	-
	rov	0.52	0.987	0.429	0	0.525	nan	-	-	-	-
	all	0.538	0.951	0.541	0.176	0.535	0.533	0.607	0.176	0.605	0.569

Table A.30: The UATD dataset is detected using the Faster R-CNN algorithm (Part 1 of 3). “noisy” represents the original noise dataset, and dspnet, b2ub, and nei represent the target detection after denoising using the DSPNet, Blind2Unblind, and Neighbor2Neighbor single-frame denoising algorithms, respectively. Bold fonts indicate data that is higher than the corresponding “noisy” dataset.

	human body	0.528	0.975	0.512	0	0.528	0.574	-	-	-	-
b2ub-p30	ball	0.555	0.955	0.593	nan	0.555	0.303	-	-	-	-
	circle cage	0.53	0.914	0.537	nan	0.532	0.538	-	-	-	-
	square cage	0.519	0.962	0.501	0	0.521	nan	-	-	-	-
	tyre	0.541	0.928	0.579	0	0.531	0.635	-	-	-	-
	cube	0.539	0.942	0.566	0.302	0.541	0.624	-	-	-	-
	cylinder	0.443	0.885	0.349	0.7	0.44	nan	-	-	-	-
	metal bucket	0.494	0.929	0.478	nan	0.498	0.427	-	-	-	-
	plane	0.629	0.999	0.739	nan	0.605	0.662	-	-	-	-
	rov	0.535	0.967	0.522	0.2	0.538	nan	-	-	-	-
	all	0.531	0.946	0.538	0.2	0.529	0.538	0.605	0.206	0.603	0.574
	human body	0.528	0.977	0.479	0	0.528	0.576	-	-	-	-
nei-g25	ball	0.554	0.967	0.593	nan	0.555	0.252	-	-	-	-
	circle cage	0.548	0.932	0.598	nan	0.548	0.55	-	-	-	-
	square cage	0.512	0.952	0.49	0	0.514	nan	-	-	-	-
	tyre	0.543	0.949	0.589	0	0.54	0.593	-	-	-	-
	cube	0.542	0.957	0.551	0.362	0.542	0.598	-	-	-	-
	cylinder	0.457	0.897	0.438	0.701	0.451	nan	-	-	-	-
	metal bucket	0.492	0.905	0.454	nan	0.5	0.33	-	-	-	-
	plane	0.634	0.989	0.741	nan	0.605	0.678	-	-	-	-
	rov	0.514	0.966	0.408	0	0.516	nan	-	-	-	-
	all	0.532	0.949	0.534	0.177	0.53	0.511	0.606	0.177	0.605	0.553
	human body	0.53	0.982	0.52	0	0.526	0.583	-	-	-	-
nei-g25	ball	0.541	0.957	0.558	nan	0.541	0.252	-	-	-	-
	circle cage	0.517	0.913	0.499	nan	0.519	0.525	-	-	-	-
	square cage	0.505	0.955	0.468	0	0.508	nan	-	-	-	-
	tyre	0.507	0.926	0.508	0	0.495	0.61	-	-	-	-
	cube	0.527	0.945	0.536	0.263	0.532	0.537	-	-	-	-
	cylinder	0.45	0.865	0.407	0.672	0.445	nan	-	-	-	-
	metal bucket	0.513	0.915	0.538	nan	0.522	0.326	-	-	-	-
	plane	0.654	0.99	0.777	nan	0.617	0.7	-	-	-	-
	rov	0.512	0.976	0.442	0.3	0.514	nan	-	-	-	-
	all	0.526	0.943	0.525	0.206	0.522	0.505	0.595	0.21	0.593	0.535
	human body	0.524	0.979	0.482	0	0.525	0.56	-	-	-	-
nei-g5-50	ball	0.556	0.966	0.588	nan	0.556	0.303	-	-	-	-
	circle cage	0.526	0.931	0.535	nan	0.526	0.551	-	-	-	-
	square cage	0.506	0.954	0.437	0	0.51	nan	-	-	-	-
	tyre	0.548	0.948	0.585	0	0.548	0.59	-	-	-	-
	cube	0.534	0.95	0.537	0.343	0.535	0.581	-	-	-	-
	cylinder	0.454	0.895	0.423	0.723	0.449	nan	-	-	-	-
	metal bucket	0.52	0.928	0.481	nan	0.524	0.478	-	-	-	-
	plane	0.649	0.98	0.709	nan	0.608	0.699	-	-	-	-
	rov	0.521	0.983	0.446	0.3	0.521	nan	-	-	-	-
	all	0.534	0.951	0.522	0.228	0.53	0.537	0.606	0.246	0.603	0.574

Table A.31: The UATD dataset is detected using the Faster R-CNN algorithm (Part 2 of 3). “noisy” represents the original noise dataset, and dspnet, b2ub, and nei represent the target detection after denoising using the DSPNet, Blind2Unblind, and Neighbor2Neighbor single-frame denoising algorithms, respectively. Bold fonts indicate data that is higher than the corresponding “noisy” dataset.

	human body	0.569	0.977	0.623	0	0.568	0.618	-	-	-	-
nei-p30	ball	0.587	0.973	0.663	nan	0.587	0.353	-	-	-	-
	circle cage	0.532	0.912	0.574	nan	0.531	0.57	-	-	-	-
	square cage	0.513	0.953	0.496	0	0.515	nan	-	-	-	-
	tyre	0.553	0.946	0.601	0	0.548	0.632	-	-	-	-
	cube	0.563	0.96	0.607	0.423	0.563	0.642	-	-	-	-
	cylinder	0.476	0.941	0.366	0.634	0.472	nan	-	-	-	-
	metal bucket	0.509	0.931	0.516	nan	0.522	0.251	-	-	-	-
	plane	0.658	1	0.742	nan	0.631	0.69	-	-	-	-
	rov	0.525	0.999	0.456	0.2	0.527	nan	-	-	-	-
	all	0.549	0.959	0.959	0.209	0.546	0.537	0.61	0.209	0.609	0.565
nei-p5-50	human body	0.537	0.978	0.538	0	0.536	0.581	-	-	-	-
	ball	0.554	0.969	0.577	nan	0.553	0.303	-	-	-	-
	circle cage	0.536	0.93	0.548	nan	0.538	0.535	-	-	-	-
	square cage	0.517	0.95	0.467	0	0.519	nan	-	-	-	-
	tyre	0.551	0.928	0.615	0	0.543	0.631	-	-	-	-
	cube	0.541	0.957	0.544	0.329	0.542	0.545	-	-	-	-
	cylinder	0.457	0.873	0.418	0.634	0.453	nan	-	-	-	-
	metal bucket	0.511	0.933	0.451	nan	0.523	0.326	-	-	-	-
	plane	0.653	0.999	0.708	nan	0.616	0.701	-	-	-	-
	rov	0.512	0.976	0.44	0.1	0.513	nan	-	-	-	-
	all	0.537	0.949	0.531	0.177	0.534	0.517	0.608	0.184	0.607	0.549

Table A.32: The UATD dataset is detected using the Faster R-CNN algorithm (Part 3 of 3). “noisy” represents the original noise dataset, and dspnet, b2ub, and nei represent the target detection after denoising using the DSPNet, Blind2Unblind, and Neighbor2Neighbor single-frame denoising algorithms, respectively. Bold fonts indicate data that is higher than the corresponding “noisy” dataset.

Denoising	SSD300											
	class	mAP	mAP@0.5	mAP@0.75	mAP_s	mAP_m	mAP_l	AR	AR_s	AR_m	AR_l	
noisy	human body	0.481	0.966	0.402	0	0.482	0.485	-	-	-	-	
	ball	0.517	0.963	0.497	nan	0.516	0.349	-	-	-	-	
	circle cage	0.496	0.92	0.504	nan	0.486	0.582	-	-	-	-	
	square cage	0.473	0.942	0.361	0	0.477	nan	-	-	-	-	
	tyre	0.463	0.908	0.425	0	0.451	0.574	-	-	-	-	
	cube	0.499	0.939	0.448	0.363	0.499	0.587	-	-	-	-	
	cylinder	0.355	0.823	0.19	0.666	0.352	nan	-	-	-	-	
	metal bucket	0.484	0.926	0.43	nan	0.492	0.337	-	-	-	-	
	plane	0.582	0.996	0.643	nan	0.542	0.644	-	-	-	-	
	rov	0.442	0.976	0.321	0	0.447	nan	-	-	-	-	
dspnet	all	0.479	0.936	0.422	0.172	0.474	0.508	0.561	0.171	0.558	0.586	
	human body	0.476	0.957	0.389	0	0.478	0.503	-	-	-	-	
	ball	0.512	0.962	0.443	nan	0.511	0.435	-	-	-	-	
	circle cage	0.494	0.931	0.434	nan	0.486	0.578	-	-	-	-	
	square cage	0.446	0.912	0.273	0	0.45	nan	-	-	-	-	
	tyre	0.457	0.864	0.424	0	0.443	0.582	-	-	-	-	
	cube	0.487	0.928	0.458	0.343	0.486	0.586	-	-	-	-	
	cylinder	0.379	0.838	0.24	0.623	0.375	nan	-	-	-	-	
	metal bucket	0.5	0.924	0.494	nan	0.51	0.327	-	-	-	-	
	plane	0.578	0.996	0.557	nan	0.55	0.617	-	-	-	-	
b2ub-g25	rov	0.426	0.946	0.257	0	0.437	nan	-	-	-	-	
	all	0.476	0.926	0.397	0.161	0.473	0.518	0.558	0.182	0.555	0.569	
	human body	0.454	0.974	0.312	0	0.455	0.498	-	-	-	-	
	ball	0.506	0.956	0.425	nan	0.507	0.384	-	-	-	-	
	circle cage	0.477	0.92	0.468	nan	0.469	0.546	-	-	-	-	
	square cage	0.458	0.929	0.351	0	0.461	nan	-	-	-	-	
	tyre	0.445	0.89	0.412	0	0.43	0.58	-	-	-	-	
	cube	0.486	0.939	0.412	0.261	0.484	0.596	-	-	-	-	
	cylinder	0.357	0.847	0.194	0.434	0.356	nan	-	-	-	-	
	metal bucket	0.458	0.922	0.316	nan	0.47	0.201	-	-	-	-	
b2ub-g5-50	plane	0.577	0.977	0.638	nan	0.559	0.606	-	-	-	-	
	rov	0.422	0.954	0.219	0	0.426	nan	-	-	-	-	
	all	0.464	0.931	0.375	0.116	0.462	0.487	0.546	0.116	0.545	0.538	
	human body	0.508	0.971	0.438	0	0.51	0.524	-	-	-	-	
	ball	0.534	0.967	0.519	nan	0.534	0.372	-	-	-	-	
	circle cage	0.495	0.934	0.408	nan	0.491	0.543	-	-	-	-	
	square cage	0.49	0.942	0.411	0	0.494	nan	-	-	-	-	
	tyre	0.48	0.913	0.464	0	0.469	0.59	-	-	-	-	
	cube	0.504	0.942	0.481	0.322	0.505	0.588	-	-	-	-	
	cylinder	0.364	0.839	0.201	0.655	0.359	nan	-	-	-	-	
b2ub-p30	metal bucket	0.492	0.928	0.487	nan	0.503	0.271	-	-	-	-	
	plane	0.58	0.979	0.612	nan	0.549	0.626	-	-	-	-	
	rov	0.428	0.958	0.262	0	0.435	nan	-	-	-	-	
	all	0.488	0.937	0.428	0.163	0.485	0.502	0.57	0.168	0.568	0.589	
	human body	0.501	0.97	0.456	0	0.504	0.522	-	-	-	-	
	ball	0.531	0.966	0.505	nan	0.531	0.382	-	-	-	-	
	circle cage	0.519	0.927	0.564	nan	0.514	0.57	-	-	-	-	
	square cage	0.495	0.948	0.452	0	0.497	nan	-	-	-	-	
	tyre	0.476	0.9	0.46	0	0.466	0.572	-	-	-	-	
	cube	0.505	0.936	0.484	0.236	0.506	0.599	-	-	-	-	
b2ub-p30	cylinder	0.375	0.803	0.253	0.578	0.371	nan	-	-	-	-	
	metal bucket	0.501	0.916	0.492	nan	0.508	0.35	-	-	-	-	
	plane	0.585	0.976	0.62	nan	0.547	0.647	-	-	-	-	
	rov	0.43	0.96	0.251	0	0.434	nan	-	-	-	-	
	all	0.492	0.93	0.454	0.136	0.488	0.521	0.575	0.156	0.573	0.596	

Table A.33: The UATD dataset is detected using the SSD300 algorithm (Part 1 of 3). “noisy” represents the original noise dataset, and dspnet, b2ub, and nei represent the target detection after denoising using the DSPNet, Blind2Unblind, and Neighbor2Neighbor single-frame denoising algorithms, respectively. Bold fonts indicate data that is higher than the corresponding “noisy” dataset.

	human body	0.501	0.97	0.456	0	0.504	0.522	-	-	-	-
b2ub-p30	ball	0.531	0.966	0.505	nan	0.531	0.382	-	-	-	-
	circle cage	0.519	0.927	0.564	nan	0.514	0.57	-	-	-	-
	square cage	0.495	0.948	0.452	0	0.497	nan	-	-	-	-
	tyre	0.476	0.9	0.46	0	0.466	0.572	-	-	-	-
	cube	0.505	0.936	0.484	0.236	0.506	0.599	-	-	-	-
	cylinder	0.375	0.803	0.253	0.578	0.371	nan	-	-	-	-
	metal bucket	0.501	0.916	0.492	nan	0.508	0.35	-	-	-	-
	plane	0.585	0.976	0.62	nan	0.547	0.647	-	-	-	-
	rov	0.43	0.96	0.251	0	0.434	nan	-	-	-	-
	all	0.492	0.93	0.454	0.136	0.488	0.521	0.575	0.156	0.573	0.596
	human body	0.509	0.974	0.431	0	0.512	0.522	-	-	-	-
b2ub-p5-50	ball	0.536	0.973	0.509	nan	0.535	0.468	-	-	-	-
	circle cage	0.512	0.924	0.515	nan	0.508	0.555	-	-	-	-
	square cage	0.487	0.931	0.4	0	0.49	nan	-	-	-	-
	tyre	0.483	0.917	0.404	0	0.472	0.593	-	-	-	-
	cube	0.497	0.944	0.442	0.323	0.497	0.57	-	-	-	-
	cylinder	0.383	0.837	0.225	0.7	0.378	nan	-	-	-	-
	metal bucket	0.501	0.929	0.518	nan	0.51	0.276	-	-	-	-
	plane	0.573	0.996	0.59	nan	0.559	0.598	-	-	-	-
	rov	0.44	0.97	0.289	0	0.444	nan	-	-	-	-
	all	0.492	0.94	0.432	0.17	0.49	0.512	0.572	0.17	0.571	0.568
	human body	0.47	0.971	0.333	0	0.471	0.513	-	-	-	-
nei-g25	ball	0.507	0.961	0.449	nan	0.507	0.252	-	-	-	-
	circle cage	0.495	0.921	0.494	nan	0.487	0.58	-	-	-	-
	square cage	0.465	0.939	0.344	0	0.468	nan	-	-	-	-
	tyre	0.446	0.879	0.387	0	0.433	0.564	-	-	-	-
	cube	0.489	0.935	0.449	0.323	0.487	0.666	-	-	-	-
	cylinder	0.392	0.863	0.322	0.634	0.388	nan	-	-	-	-
	metal bucket	0.475	0.937	0.391	nan	0.487	0.2	-	-	-	-
	plane	0.591	0.995	0.621	nan	0.568	0.63	-	-	-	-
	rov	0.46	0.965	0.35	0	0.465	nan	-	-	-	-
	all	0.479	0.937	0.414	0.159	0.476	0.486	0.558	0.159	0.556	0.532
	human body	0.505	0.96	0.474	0	0.508	0.508	-	-	-	-
nei-g5-50	ball	0.543	0.969	0.558	nan	0.543	0.329	-	-	-	-
	circle cage	0.511	0.934	0.526	nan	0.503	0.576	-	-	-	-
	square cage	0.486	0.946	0.394	0	0.489	nan	-	-	-	-
	tyre	0.505	0.926	0.446	0	0.498	0.594	-	-	-	-
	cube	0.508	0.946	0.505	0.343	0.507	0.603	-	-	-	-
	cylinder	0.389	0.845	0.287	0.606	0.386	nan	-	-	-	-
	metal bucket	0.496	0.925	0.508	nan	0.506	0.276	-	-	-	-
	plane	0.593	0.998	0.648	nan	0.564	0.634	-	-	-	-
	rov	0.438	0.975	0.289	0	0.444	nan	-	-	-	-
	all	0.498	0.942	0.464	0.158	0.495	0.503	0.575	0.173	0.573	0.573

Table A.34: The UATD dataset is detected using the SSD300 algorithm (Part 2 of 3). “noisy” represents the original noise dataset, and dspnet, b2ub, and nei represent the target detection after denoising using the DSPNet, Blind2Unblind, and Neighbor2Neighbor single-frame denoising algorithms, respectively. Bold fonts indicate data that is higher than the corresponding “noisy” dataset.

	human body	0.506	0.976	0.42	0	0.507	0.544	-	-	-	-
nei-p30	ball	0.535	0.968	0.521	nan	0.535	0.303	-	-	-	-
	circle cage	0.514	0.935	0.498	nan	0.518	0.524	-	-	-	-
	square cage	0.488	0.946	0.385	0	0.491	nan	-	-	-	-
	tyre	0.5	0.92	0.479	0	0.492	0.586	-	-	-	-
	cube	0.501	0.942	0.461	0.307	0.502	0.549	-	-	-	-
	cylinder	0.352	0.785	0.207	0.655	0.348	nan	-	-	-	-
	metal bucket	0.491	0.915	0.47	nan	0.5	0.295	-	-	-	-
	plane	0.573	0.997	0.604	nan	0.549	0.614	-	-	-	-
	rov	0.429	0.977	0.243	0	0.433	nan	-	-	-	-
	all	0.489	0.936	0.429	0.16	0.488	0.488	0.572	0.171	0.571	0.527
	human body	0.52	0.97	0.499	0	0.519	0.559	-	-	-	-
nei-p5-50	ball	0.534	0.965	0.512	nan	0.534	0.374	-	-	-	-
	circle cage	0.53	0.935	0.613	nan	0.524	0.593	-	-	-	-
	square cage	0.501	0.946	0.473	0	0.503	nan	-	-	-	-
	tyre	0.505	0.904	0.477	0	0.501	0.572	-	-	-	-
	cube	0.511	0.935	0.504	0.362	0.51	0.624	-	-	-	-
	cylinder	0.379	0.821	0.214	0.667	0.375	nan	-	-	-	-
	metal bucket	0.49	0.912	0.468	nan	0.497	0.435	-	-	-	-
	plane	0.581	0.997	0.654	nan	0.549	0.629	-	-	-	-
	rov	0.44	0.967	0.291	0	0.444	nan	-	-	-	-
	all	0.499	0.935	0.47	0.172	0.496	0.541	0.578	0.171	0.575	0.607

Table A.35: The UATD dataset is detected using the SSD300 algorithm (Part 3 of 3). “noisy” represents the original noise dataset, and dspnet, b2ub, and nei represent the target detection after denoising using the DSPNet, Blind2Unblind, and Neighbor2Neighbor single-frame denoising algorithms, respectively. Bold fonts indicate data that is higher than the corresponding “noisy” dataset.

Denoising	class	YOLOX									
		mAP	mAP@0.5	mAP@0.75	mAP_s	mAP_m	mAP_l	AR	AR_s	AR_m	AR_l
noisy	human body	0.563	0.977	0.562	0	0.56	0.639	-	-	-	-
	ball	0.571	0.968	0.639	nan	0.571	0.328	-	-	-	-
	circle cage	0.537	0.917	0.598	nan	0.529	0.63	-	-	-	-
	square cage	0.519	0.956	0.502	0	0.522	nan	-	-	-	-
	tyre	0.537	0.935	0.549	0	0.526	0.65	-	-	-	-
	cube	0.56	0.959	0.591	0.424	0.559	0.647	-	-	-	-
	cylinder	0.475	0.925	0.355	0.666	0.471	nan	-	-	-	-
	metal bucket	0.508	0.927	0.497	nan	0.522	0.201	-	-	-	-
	plane	0.663	1	0.783	nan	0.637	0.695	-	-	-	-
	rov	0.516	0.977	0.472	0.1	0.519	nan	-	-	-	-
dspnet	all	0.545	0.954	0.555	0.198	0.542	0.542	0.604	0.203	0.602	0.567
	human body	0.559	0.978	0.591	0	0.556	0.622	-	-	-	-
	ball	0.577	0.971	0.649	nan	0.577	0.353	-	-	-	-
	circle cage	0.528	0.923	0.567	nan	0.528	0.555	-	-	-	-
	square cage	0.514	0.953	0.504	0	0.515	nan	-	-	-	-
	tyre	0.539	0.942	0.589	0	0.531	0.63	-	-	-	-
	cube	0.553	0.961	0.584	0.362	0.554	0.634	-	-	-	-
	cylinder	0.473	0.927	0.415	0.55	0.471	nan	-	-	-	-
	metal bucket	0.508	0.918	0.479	nan	0.52	0.27	-	-	-	-
	plane	0.657	1	0.768	nan	0.637	0.684	-	-	-	-
b2ub-g25	rov	0.551	0.988	0.541	0	0.557	nan	-	-	-	-
	all	0.546	0.956	0.569	0.152	0.545	0.536	0.608	0.154	0.608	0.566
	human body	0.538	0.978	0.548	0	0.538	0.584	-	-	-	-
	ball	0.573	0.971	0.633	nan	0.573	0.303	-	-	-	-
	circle cage	0.531	0.905	0.565	nan	0.523	0.616	-	-	-	-
	square cage	0.502	0.96	0.419	0	0.505	nan	-	-	-	-
	tyre	0.498	0.928	0.509	0	0.493	0.588	-	-	-	-
	cube	0.543	0.957	0.566	0.363	0.539	0.695	-	-	-	-
	cylinder	0.481	0.926	0.401	0.699	0.476	nan	-	-	-	-
	metal bucket	0.481	0.917	0.401	nan	0.493	0.203	-	-	-	-
b2ub-g5-50	plane	0.65	0.99	0.738	nan	0.619	0.689	-	-	-	-
	rov	0.542	0.989	0.539	0	0.545	nan	-	-	-	-
	all	0.534	0.952	0.532	0.177	0.53	0.525	0.595	0.177	0.593	0.554
	human body	0.523	0.976	0.511	0	0.52	0.595	-	-	-	-
	ball	0.55	0.962	0.556	nan	0.55	0.303	-	-	-	-
	circle cage	0.507	0.892	0.492	nan	0.506	0.567	-	-	-	-
	square cage	0.479	0.947	0.396	0	0.482	nan	-	-	-	-
	tyre	0.484	0.899	0.459	0	0.47	0.596	-	-	-	-
	cube	0.533	0.963	0.477	0.363	0.533	0.625	-	-	-	-
	cylinder	0.442	0.91	0.332	0.6	0.439	nan	-	-	-	-
	metal bucket	0.484	0.924	0.357	nan	0.497	0.227	-	-	-	-
	plane	0.602	1	0.714	nan	0.583	0.627	-	-	-	-
	rov	0.488	0.969	0.449	0	0.491	nan	-	-	-	-
	all	0.509	0.944	0.474	0.161	0.507	0.506	0.575	0.16	0.574	0.544

Table A.36: The UATD dataset is detected using the YOLOX algorithm (Part 1 of 3). “noisy” represents the original noise dataset, and dspnet, b2ub, and nei represent the target detection after denoising using the DSPNet, Blind2Unblind, and Neighbor2Neighbor single-frame denoising algorithms, respectively. Bold fonts indicate data that is higher than the corresponding “noisy” dataset.

		human body	0.562	0.973	0.62	0	0.559	0.627	-	-	-	-
b2ub-p30	ball	0.579	0.97	0.679	nan	0.58	0.328	-	-	-	-	-
	circle cage	0.557	0.924	0.652	nan	0.556	0.599	-	-	-	-	-
	square cage	0.529	0.946	0.534	0	0.532	nan	-	-	-	-	-
	tyre	0.555	0.961	0.588	0	0.546	0.65	-	-	-	-	-
	cube	0.563	0.967	0.604	0.424	0.563	0.687	-	-	-	-	-
	cylinder	0.481	0.938	0.392	0.665	0.478	nan	-	-	-	-	-
	metal bucket	0.51	0.923	0.488	nan	0.523	0.251	-	-	-	-	-
	plane	0.645	0.99	0.777	nan	0.611	0.683	-	-	-	-	-
	rov	0.534	0.979	0.532	0	0.537	nan	-	-	-	-	-
	all	0.552	0.957	0.587	0.182	0.548	0.546	0.614	0.181	0.612	0.581	-
b2ub-p5-50	human body	0.569	0.977	0.623	0	0.568	0.618	-	-	-	-	-
	ball	0.587	0.973	0.663	nan	0.587	0.353	-	-	-	-	-
	circle cage	0.532	0.912	0.574	nan	0.531	0.57	-	-	-	-	-
	square cage	0.513	0.953	0.496	0	0.515	nan	-	-	-	-	-
	tyre	0.553	0.946	0.601	0	0.548	0.632	-	-	-	-	-
	cube	0.563	0.96	0.607	0.423	0.563	0.642	-	-	-	-	-
	cylinder	0.476	0.941	0.366	0.634	0.472	nan	-	-	-	-	-
	metal bucket	0.509	0.931	0.516	nan	0.522	0.251	-	-	-	-	-
	plane	0.658	1	0.742	nan	0.631	0.69	-	-	-	-	-
	rov	0.525	0.999	0.456	0.2	0.527	nan	-	-	-	-	-
nei-g25	all	0.549	0.959	0.564	0.209	0.546	0.537	0.61	0.209	0.609	0.565	-
	human body	0.43	0.917	0.353	0	0.421	0.565	-	-	-	-	-
	ball	0.505	0.936	0.455	nan	0.505	0.303	-	-	-	-	-
	circle cage	0.451	0.877	0.393	nan	0.442	0.565	-	-	-	-	-
	square cage	0.438	0.93	0.337	0	0.44	nan	-	-	-	-	-
	tyre	0.422	0.816	0.392	0	0.412	0.528	-	-	-	-	-
	cube	0.491	0.944	0.422	0.283	0.493	0.579	-	-	-	-	-
	cylinder	0.422	0.896	0.317	0.6	0.417	nan	-	-	-	-	-
	metal bucket	0.424	0.857	0.376	nan	0.43	0.277	-	-	-	-	-
	plane	0.649	1	0.736	nan	0.606	0.697	-	-	-	-	-
nei-g5-50	rov	0.511	0.978	0.387	0	0.515	nan	-	-	-	-	-
	all	0.474	0.915	0.417	0.147	0.468	0.502	0.541	0.152	0.537	0.539	-
	human body	0.554	0.986	0.577	0	0.552	0.601	-	-	-	-	-
	ball	0.581	0.972	0.687	nan	0.582	0.353	-	-	-	-	-
	circle cage	0.537	0.928	0.594	nan	0.536	0.578	-	-	-	-	-
	square cage	0.522	0.947	0.48	0	0.524	nan	-	-	-	-	-
	tyre	0.541	0.952	0.546	0	0.534	0.615	-	-	-	-	-
	cube	0.553	0.967	0.578	0.379	0.553	0.657	-	-	-	-	-
	cylinder	0.468	0.939	0.358	0.601	0.465	nan	-	-	-	-	-
	metal bucket	0.512	0.935	0.45	nan	0.524	0.276	-	-	-	-	-
nei-g5-50	plane	0.655	1	0.756	nan	0.623	0.695	-	-	-	-	-
	rov	0.521	0.968	0.448	0	0.524	nan	-	-	-	-	-
	all	0.544	0.959	0.547	0.163	0.542	0.539	0.608	0.167	0.606	0.572	-

Table A.37: The UATD dataset is detected using the YOLOX algorithm (Part 2 of 3). “noisy” represents the original noise dataset, and dspnet, b2ub, and nei represent the target detection after denoising using the DSPNet, Blind2Unblind, and Neighbor2Neighbor single-frame denoising algorithms, respectively. Bold fonts indicate data that is higher than the corresponding “noisy” dataset.

	human body	0.557	0.975	0.603	0	0.556	0.615	-	-	-	-
nei-p30	ball	0.593	0.971	0.683	nan	0.593	0.353	-	-	-	-
	circle cage	0.556	0.935	0.642	nan	0.555	0.582	-	-	-	-
	square cage	0.525	0.956	0.497	0	0.527	nan	-	-	-	-
	tyre	0.547	0.946	0.587	0	0.545	0.624	-	-	-	-
	cube	0.565	0.972	0.568	0.423	0.563	0.662	-	-	-	-
	cylinder	0.471	0.933	0.36	0.566	0.469	nan	-	-	-	-
	metal bucket	0.51	0.926	0.48	nan	0.524	0.227	-	-	-	-
	plane	0.651	1	0.746	nan	0.635	0.675	-	-	-	-
	rov	0.538	0.99	0.537	0.1	0.542	nan	-	-	-	-
	all	0.551	0.96	0.57	0.182	0.551	0.534	0.612	0.187	0.612	0.567
nei-p5-50	human body	0.559	0.989	0.582	0	0.564	0.569	-	-	-	-
	ball	0.585	0.966	0.687	nan	0.586	0.353	-	-	-	-
	circle cage	0.53	0.911	0.578	nan	0.529	0.561	-	-	-	-
	square cage	0.517	0.945	0.474	0	0.52	nan	-	-	-	-
	tyre	0.556	0.965	0.61	0	0.551	0.636	-	-	-	-
	cube	0.56	0.968	0.607	0.412	0.559	0.645	-	-	-	-
	cylinder	0.487	0.933	0.432	0.633	0.485	nan	-	-	-	-
	metal bucket	0.51	0.923	0.43	nan	0.517	0.351	-	-	-	-
	plane	0.658	0.989	0.785	nan	0.627	0.693	-	-	-	-
	rov	0.546	0.978	0.571	0	0.55	nan	-	-	-	-
	all	0.551	0.957	0.576	0.174	0.549	0.544	0.614	0.181	0.613	0.575

Table A.38: The UATD dataset is detected using the YOLOX algorithm (Part 3 of 3). “noisy” represents the original noise dataset, and dspnet, b2ub, and nei represent the target detection after denoising using the DSPNet, Blind2Unblind, and Neighbor2Neighbor single-frame denoising algorithms, respectively. Bold fonts indicate data that is higher than the corresponding “noisy” dataset.